FACTORS AFFECTING EARTHQUAKE BEHAVIOR OF MECHANICALLY STABILIZED EARTH WALLS

by

Berk Türkel

B.S., Civil Engineering, Istanbul Technical University, 2016

Submitted to the Institute for Graduate Studies in
Science and Engineering in partial fulfillment of
the requirements for the degree of
Master of Science

Graduate Program in Civil Engineering

Boğaziçi University

2019

FACTORS AFFECTING EARTHQUAKE BEHAVIOR OF MECHANICALLY STABILIZED EARTH WALLS

APPROVED BY:

Prof. Erol Güler (Thesis Supervisor)	. . . . .
Assist. Prof. İrem Zeynep Yıldırım (Thesis Co-supervisor)	. . . . .
Assoc. Prof. Özer Çinicioğlu	. . . . .
Assist. Prof. Berrak Teymür	. . . . .
Assist. Prof. Gökçe Tönük	. . . . .

DATE OF APPROVAL: 21.06.2019

ACKNOWLEDGEMENTS

I am deeply indebted to my advisor Prof. Erol Güler and my co-advisor Asst. Prof. İrem Zeynep Yıldırım for their competent advice and endless support, and guidance throughout my thesis study.

I would also like to express my gratitude to my thesis committee members Assoc. Prof. Özer Çinicoğlu, Asst. Prof. Berrak Teymür, and Asst. Prof. Gökçe Tönük for providing valuable insights into my thesis and their kind attitude towards me.

I would like to express my deepest appreciation to Dr. Ömer Tuğrul Turan for acquainting me with academic life and showing me the joy of intellectual pursuit.

I would also like to acknowledge all my friends who helped me during my studies, especially my engineer friends Ercan Tekin, Ozan Terzi, Berkay Aldırmaz for the sincere support they have given over the years.

Most of all, I dedicate my thesis to my loving family. I would like to thank my grandmother, my aunts, and my cousin for believing in my abilities, supporting me and giving me encouragement. I would like to express my special thanks to my brother and my colleague Dr. Enver Burak Türkel for his endless support in whole of my life. I am very grateful to my parents Dr. Zerrin Türkel and Dr. Ercan Türkel who have always enlightened me with their wisdom, encouraged me to strive for the best and stood by me to overcome difficulties.

ABSTRACT

FACTORS AFFECTING EARTHQUAKE BEHAVIOR OF MECHANICALLY STABILIZED EARTH WALLS

Mechanically Stabilized Earth (MSE) Walls are flexible retaining systems and their use in various applications has become very popular in recent years. Reliable design of MSE Walls requires an understanding of their behavior under earthquake loading conditions. Recent developments in software utilizing numerical methods such as the Finite Element Method (FEM) have made it possible to analyze the seismic behavior of these types of complex structures. The main goal of this study is to understand the behavior of MSE Walls under earthquake loading conditions. A parametric study was conducted using the FEM computer program PLAXIS v8.6 utilizing Hardening-Soil model. Frequency-dependent harmonic loading with a peak ground acceleration of 0.2g was applied on models with a constant damping ratio of 10%. For the harmonic loading, seven frequencies were selected around the estimated natural frequency of the MSE Wall. 8 m high MSE Walls were modeled with 12 different reinforcement design configurations and each model was excited with seven (7) different input ground motions. A matrix consisting of 84 analyses was generated in order to investigate the effect of the reinforcement length to wall height ratio (L/H), reinforcement stiffness (EA), vertical spacing of reinforcements (S_v), and frequency of the input ground motion on the overall MSE Wall response. Based on the results of the analysis, bulging behavior was observed at the end of the construction phase and outward movement of the top of the wall after the seismic loading. At the end of both stages, the horizontal displacement of the uppermost (top) reinforcement decreased by an increase in L/H ratio and EA, it also decreased by a decrease in S_v. Axial forces showed a similar trend with displacements, and they were mostly influenced by the change in S_v. The maximum amplification in the MSE Wall occurred for the seismic frequency at the estimated natural frequency of the MSE Wall indicating the significance of natural frequency of the structure in seismic analysis.

ÖZET

DONATILI ZEMİN DUVARLARIN DEPREM DAVRANIŞINA ETKİYEN FAKTÖRLER

Donatılı zemin (toprak istinat) duvarları, esnek istinat sistemleri olup yıldan yıla popüler hale gelmiş ve uygulamaları artmıştır. Güvenilir ve kararlı tasarımların yapılması, bu duvarların deprem yükü altındaki davranışlarının anlaşılmasıyla mümkündür. Sonlu Elemanlar Yöntemi gibi sayısal yöntemler kullanan yazılımlardaki son gelişmeler, bu tip karmaşık yapıların sismik davranışlarını analiz etme imkanı sunmaktadır. Bu çalışmanın temel amacı, donatılı zemin duvarlarının deprem yükleri altındaki davranışını daha iyi anlamaktır. Bilgisayar programı PLAXIS v8.6' da zeminler için "Hardening-Soil" isimli malzeme modeli kullanılarak parametrik bir çalışma yapılmıştır. 0.2g'lik maksimum yer ivmesine sahip ve frekansa bağlı değişen genlikte harmonik yükleme, %10'luk sabit bir sönümleme oranıyla modellerde uygulanmıştır. Harmonik yüklemeler için donatılı zemin duvarının doğal frekansı göz önüne alınarak yedi (7) farklı frekans değeri seçilmiştir. 8 m yüksekliğinde 12 farklı konfigürasyon ile tasarlanmış modellerden her birine, 7 farklı yer hareketi etkidiğinde, 84 analiz içeren bir matris oluşturularak her durum için analizler tamamlanmıştır. Donatı boyunun duvar yüksekliğine oranının (L/H), donatı rijitliğinin (EA), donatıların düşey aralıklarının (S_v) ve uygulanan yer hareketinin duvarın genel davranışına, etkisi araştırılmıştır. Analiz sonuçlarına dayanarak, inşaat aşamasının sonunda orta yükseklikte kabarma gözlenirken dinamik analizlerde duvarın üst kısmının dışa doğru hareket ettiği görülmüştür. Her iki aşamanın sonunda da en üst donatıdaki yatay yer değiştirmenin, L/H oranı ve EA'daki artış ve S_v'deki düşüş ile azaldığı gözlenmiştir. Eksenel kuvvetlerin yer değiştirmelerdeki değişimlere benzer bir eğilim gösterdiği ve en çok S_v değişiminden etkilendiği görülmüştür. Dinamik analizlerde maksimum büyütme, sismik yükleme frekansının donatılı zemin duvarın tahmin edilen doğal frekansı değerinde gözlenmiştir, bu sonuç da sismik yüklemelerde yapının doğal frekansının önemini göstermiştir.

TABLE OF CONTENTS

ACKNOWLEDGEMENTS iii
ABSTRACT iv
ÖZET v
TABLE OF CONTENTS vi
LIST OF FIGURES ix
LIST OF TABLES xvii
LIST OF SYMBOLS xix
LIST OF ACRONYMS/ ABBREVIATONS xxii
1. INTRODUCTION 1
1.1. General 1
1.2. Objectives 1
1.3. Scope 2
2. GEOSYNTHETICS 3
2.1. Introduction 3
2.2. History of Geosynthetics 4
2.3. Properties 5
2.4. Types of Geosynthetics 8
2.4.1. Geotextiles 12
2.4.2. Geogrids 14
2.4.3. Geonets 16
2.4.4. Geomembranes 16
2.4.5. Geocomposites 16
2.4.6. Geo- others and Applications 17
3. MECHANICALLY STABILIZED EARTH (MSE) WALLS 20
3.1. Introduction 20
3.2. Historical Development of MSE Walls 22
3.3. The Elements of MSE Walls 23
3.3.1. Soil Reinforcement 23
3.3.2. Reinforced Fill 24
3.3.3. Facing Unit 26

3.3.4. Retained Soil & Foundation Soil 28
3.4. Advantages and Potential Disadvantages of MSE Wall 29
4. MSE WALL DESIGN AND SEISMIC STUDIES 30
4.1. Introduction 30
4.2. Earth Pressures Acting on MSE Wall 30
4.3. External Stability of MSE Wall 32
4.3.1. Base Sliding 33
4.3.2. Limiting Eccentricity (Base Overturning) 34
4.3.3. Bearing Capacity 34
4.4. Internal Stability of MSE Wall 35
4.4.1. Sizing for Internal Stability 38
4.5. Design Requirements 40
4.6. Static Stability of the MSE Wall Model 42
4.6.1. External Stability Check 42
4.6.2. Internal Stability Check 44
4.7. Previous Studies on MSE Walls 45
5. NUMERICAL MODELING OF AN 8- M HEIGHT MSE WALL USING PLAXIS 48
5.1. Introduction 48
5.2. PLAXIS Version and Units 49
5.3. Model Dimensions 50
5.4. Material Modeling 51
5.4.1. Modeling of Soils 51
5.4.2. Modeling of Reinforcement 56
5.4.3. Modeling of the Facing Unit 58
5.4.4. Modeling of Interfaces 59
5.5. Boundary Modeling 61
5.6. Mesh Generation 62
5.7. Determining the Initial Conditions 63
5.8. Staged Construction 64
5.9. Dynamic Analysis 65
5.9.1. Natural Frequency of the Wall 65
5.9.2. Damping 69
5.9.3. Seismic Loading 74

5.9.4. Accelerogram 75
5.10. Configurations & FEM Analysis Cases 78
6. RESULTS AND DISCUSSIONS 80
6.1. Results of FEM Analysis 80
6.2. Results of FEM Analysis for Static (End of Construction) Case 82
6.3. Results of FEM Analysis for Seismic Case 89
6.4. Effect of Loading Frequency on Acceleration, Displacements and Axial Stresses 94
6.4.1. Effect of Frequency on Amplification 94
6.4.2. Effect of Frequency on Displacements 96
6.4.3. Effect of Frequency on Axial Stresses 97
6.5. Effect of Reinforcement Stiffness (EA) on Displacements and Axial Stresses 98
6.5.1. Effect of EA on Displacements 98
6.5.2. Effect of EA on Axial Stresses 100
6.6. Effect of L/ H on Displacements and Axial Stresses 102
6.6.1. Effect of L/ H on Displacements 102
6.6.2. Effect of L/ H on Axial Stresses 105
6.7. Effect of S_v on Displacements and Axial Stresses 107
6.7.1. Effect of S_v on Displacements 107
6.7.2. Effect of S_v on Axial Stresses 109
6.8. Effect of Overall Stiffness on Maximum Acceleration 111
6.9. Summary of Seismic Results 112
7. CONCLUSIONS 116
REFERENCES 120

LIST OF FIGURES

Figure 2.1. The process of polymerization: (a) An ethylene monomer; (b) A polyethylene molecule (Shukla & Yin, 2006). 6

Figure 2.2. Polyethylene (Ergul, 2012). 8

Figure 2.3. The eight types of geosynthetics (Koerner, 2012; Wikipedia, 2019). 9

Figure 2.4. Various functions of geosynthetics: (a) Separation (b) Filtration (c) Drainage (d) Reinforcement (e) Containment (f) Erosion control (Bathurst, 2019). 10

Figure 2.5. (a) Woven geotextiles; (b) Non- Woven geotextiles (Shukla, 2016). 13

Figure 2.6. Various polymeric fibers used in geotextile manufacturing (Koerner, 2005). . 14

Figure 2.7. Geogrids: (a) Bonded (Shukla & Yin, 2006) (b) Woven (ACE Geosynthetics, 2019a). 15

Figure 2.8. Extruded geogrids (a) Uniaxial (Tensar Earth Technologies, 2019), (b) Biaxial (Tensar, 2019b) (c) Triaxial (Tensar, 2019a). 15

Figure 2.9. Typical geosynthetic applications: (a) Retaining wall (b) Steep- sided embankment (c) Embankment on soft foundation soil (d) Bridge pier (e) Unpaved road (f) Paved road (g) Railway track (h) Slope- erosion control (i) Slope- stabilization (j) Landfill (k) Dam (l) Liquid reservoir (m) Water channel (n) Trench drain (Shukla & Yin, 2006). 17

Figure 3.1. Schematic diagram of an MSE Wall with precast concrete facing (Kavazanjian *et al.*, 2011) 21

Figure 3.2. Representative MSE Wall applications: (a) Retaining wall, (b) Access ramp, (c) Waterfront structure, (d) Bridge abutment (Berg *et al.*, 2009).....21

Figure 3.3. Retaining wall constructed with York method (Jones, 1996). 22

Figure 3.4. 45.7 m high MSE Wall (Reinforced Earth, 2015).....23

Figure 3.5. Reinforced fill extension beyond the reinforced zone (Berg *et al.*, 2009). 25

Figure 3.6. Various types of modular blocks (Tensar Earth Technologies, 2005). 26

Figure 3.7. Main facing types: (a) Segmental precast concrete panels (b) Dry cast modular block wall (MBW) units (c) Welded wire mesh (WWM) (d) Gabion facing (e) Geosynthetic facing (f) Post-construction facing (ACE Geosynthetics, 2019b).....27

Figure 4.1. An MSE Wall cross-section with seismic forces (Kavazanjian *et al.*, 2011)...32

Figure 4.2. External failure mechanisms for MSE Walls: (a) Sliding (b) Limiting eccentricity (c) Bearing (d) Deep seated failure (Kavazanjian *et al.*, 2011).....33

Figure 4.3. Potential failure surface for internal stability design of MSE Walls (Bilgin, 2009). 36

Figure 4.4. Internal failure mechanisms for MSE Walls: (a) Geosynthetic rupture (b) Geosynthetic pullout (c) Connection (and/or facing elements) failure (Shukla & Yin, 2006). 37

Figure 4.5. Stresses and strains in (a) an unreinforced and (b) reinforced soil element (Enunlu, 2007). 38

Figure 4.6. Stress transfer mechanisms for soil reinforcement (a) Frictional stress transfer (b) Bearing and frictional resistance (Berg *et al.*, 2009). 38

Figure 5.1. Nodes and stress distribution: (a) 6- node (b) 15- node soil elements (Brinkgreve, 2019b). 49

Figure 5.2. Preliminary design of 8 meters high MSE Wall. 50

Figure 5.3. The relation of hyperbolic stress-strain in primary loading for a standard drained triaxial test (Brinkgreve, 2019a). 53

Figure 5.4. Definition of E_{50}^{ref} and E_{ur}^{ref} for drained triaxial test results. 54

Figure 5.5. Definition of E_{oed}^{ref} in oedometer test results. 55

Figure 5.6. Close-up cross section view of the modular block (S_v= 0.4 m case). 58

Figure 5.7. Distribution of nodes and stress points in interface elements and their connection to: (a) 6- node (b) 15- node soil elements (Brinkgreve, 2019b). 59

Figure 5.8. Connectivity plot of 8m high wall: L/ H ratio= 0.7 (Scale: 1.0). 62

Figure 5.9. Reinforced fill area- connectivity plot of 8m high wall: L/ H ratio= 0.7 (Scale: 1.0). 63

Figure 5.10. Initial effective stress state of the 8m high wall: L/ H= 0.7 (Scale: 0.005). 64

Figure 5.11. Stiffness strain behavior (Laera & Brinkgreve, 2015). 66

Figure 5.12. Variation of Rayleigh damping parameters (Brinkgreve, 2019b; Tsai, Park, & Chen, 2014). 70

Figure 5.13. Damping ratio (ξ) as a function of cyclic shear strain (γ_c) (Brinkgreve *et al.*, 2007). 71

Figure 5.14. Modulus reduction curve (G/ G_0) and variation of damping ratio (D%) with the shear strain ($\gamma(\%)$) (Amorosi *et al.*, 2010).....72

Figure 5.15. Accelerogram using Bathurst & Hatami (1998): f= 3 Hz. 76

Figure 5.16. Accelerogram using Bathurst & Hatami (1998): (a) f= 1 Hz (b) f= 8Hz. 77

Figure 5.17. Models' input screen (a) Sv=0.4 m, L/ H=0.5 (b) Sv=0.4 m, L/ H=1 (c) Sv=0.6 m, L/ H=0.7. 79

Figure 6.1. Selected nodes for load/displacement curves on the connectivity plot. 81

Figure 6.2. Horizontal displacement distribution along reinforcements at various depths: Configuration 1, Static case (Scaled to 20.0).....83

Figure 6.3. Axial force (envelope) distribution along reinforcements at various depths: Configuration 1, Static case (Scaled to 1.0).....84

Figure 6.4. Deformed mesh: Configuration 1, Static case (Scaled to 10.0) (Zoom-in view). 85

Figure 6.5. Total displacements distribution for Configuration 1, Static case (with shadings). 85

Figure 6.6. Extreme horizontal displacement (abs.) versus wall elevation: 86

Figure 6.7. Axial force (env.) versus wall elevation:.....86

Figure 6.8. Extreme horizontal displacements (abs.) versus wall elevation:.....87

Figure 6.9. Axial force (env.) versus wall elevation:.....87

Figure 6.10. Extreme horziontal displacements (abs.) versus wall elevation:.....88

Figure 6.11. Axial force (env.) versus wall elevation:.....88

Figure 6.12. Deformed mesh: Configuration 1, SL=1.5 Hz (Scaled to 10.0).....90

Figure 6.13. Configuration 1 for SL=1.5 Hz: shear strain distribution. 90

Figure 6.14. Distribution of horizontal displacements: Configuration 1, L/H=0.7, for SL=1.5 Hz (Scaled to 20.0) (zoom-in view) (with arrows). 91

Figure 6.15. Configuration 1 for SL=4 Hz: shear strain distribution. 91

Figure 6.16. Horizontal displacement distribution along reinforcements at various depths: Configuration 1 for SL=1.5 (Scaled to 10.0).....92

Figure 6.17. Axial force (envelope) distribution along reinforcements at various depths: Configuration 1 for SL=1.5 (Scaled to 1.0). 93

Figure 6.18. Effective mean stress for Configuration 1 SL= 1.5 Hz (with shading).....94

Figure 6.19. Acceleration amplification factor versus height from base excitation level: Configuration 1, SL= 1, 1.5, 2, 3, 4, 6, & 8 Hz. 95

Figure 6.20. Configuration 1, Amplification factor versus height from the base level for SL= 1.5 & 4 Hz.....96

Figure 6.21. Extreme horizontal displacement (abs.) versus wall elevation: Configuration 1, SL= 1, 1.5, 2, 3, 4, 6, & 8 Hz. 97

Figure 6.22. Axial force (envelope) versus wall elevation: Configuration 1 (S_v= 0.4m, EA= 600kN/m, L/H= 0.7), for SL= 1, 1.5, 2, 3, 4, 6, & 8 Hz. 97

Figure 6.23. Ext. hor. (abs.) displacement versus wall elevation: Configuration 1-2 (Sv=0.4m, L/H=0.7), for SL=1.5 Hz. 98

Figure 6.24. Frequency versus extreme (abs.) horizontal displacement at uppermost reinforcement: Configuration 1-2 (Sv=0.4m, L/H=0.7), SL= 1, 1.5, 2, 3, 4, 6, & 8 Hz. 99

Figure 6.25. Reinforcement stiffness (EA) versus extreme horizontal displacement (abs.) of top most reinforcement, SL=1.5 Hz. 99

Figure 6.26. Extreme axial force (env.) for for the uppermost reinforcement: Configuration 1-2 (Sv=0.4m, L/H=0.7). 100

Figure 6.27. Axial force (env.) at the uppermost reinforcement versus reinforcement stiffness variation for SL=1.5 Hz. 101

Figure 6.28. Axial force (env.) versus wall elevation: Configuration 1-2 (Sv=0.4m, L/H=0.7) for SL=1.5 Hz. 101

Figure 6.29. Ext. hor. displacement (abs.) versus wall elevation: Configuration 1-3-5 (S_v= 0.4m, EA= 600kN/m), SL=1.5. 102

Figure 6.30. Frequency versus extreme horizontal displacement (abs.) at uppermost reinf.: Configuration 1-3-5 (S_v= 0.4m, EA= 600kN/m). 103

Figure 6.31. Frequency versus ext. hor. disp. (abs.) difference (from L/H=0.5 values, L/H=0.7 values subtracted) at the uppermost reinforcement. 103

Figure 6.32. Frequency versus extreme hor. disp. (abs.) difference (from L/H=0.7 values, L/H=1.0 values subtracted) at the uppermost reinforcement. 104

Figure 6.33. L/H versus extreme hor. disp. (abs.) at uppermost reinforcement for each frequency: Configuration 1-3-5 (Sv=0.4m, EA=600kN/m). 105

Figure 6.34. Frequency versus extreme axial force (env.) at the uppermost reinforcement: Configurations 1-3-5 (S_v= 0.4m, EA= 600kN/m). 106

Figure 6.35. Frequency versus extreme axial force (envelope) difference (From L/H=0.5 values, L/H=0.7 subtracted) at the uppermost reinforcement. 106

Figure 6.36. L/H: Configurations 1-3-5 (S_v=0.4m, EA=600kN/m) versus extreme axial forces (env.) at uppermost reinforcement. 107

Figure 6.37. Frequency versus extreme horizontal displacements (abs.) at the uppermost reinforcement: Configurations 1-7 (EA=600kN/m, L/H= 0.7).....108

Figure 6.38. Extreme horizontal displacement (abs.) versus wall elevation: reinforcement spacing comparison, Configuration 1-7 (Sv=0.4m, L/H=0.7), for SL=1.5 Hz. 108

Figure 6.39. S_v versus extreme horizontal displacement (abs.) at uppermost reinforcement versus variation for SL=1.5. 109

Figure 6.40. Extreme axial force (env.) at uppermost reinforcement versus frequencies: Configurations 1-7 (EA=600kN/m, L/H= 0.7). 110

Figure 6.41. Frequency versus extreme axial force (env.) difference (from S_v=0.4 values, S_v=0.6 values subtracted) at the uppermost reinforcement. 110

Figure 6.42. S_v versus extreme axial force (envelope) at the uppermost reinforcement, SL=1.5 Hz. 111

Figure 6.43. Frequency versus max. acc. difference (a_x) in terms of g=10m/s^2 at Point J (from L/H= 1.0 value, L/H= 0.5 subtracted). 112

Figure 6.44. Frequency versus maximum absolute acceleration at Point J. 113

Figure 6.45. Frequency versus maximum displacements (abs.) at Point J at the end of the 5th second. 114

Figure 6.46. Frequency versus extreme horizontal displacement (abs.) at the uppermost reinforcement. 114

Figure 6.47. Frequency versus extreme axial force values (env.) at the uppermost reinforcement. 115

LIST OF TABLES

Table 2.1. Polymers and the repeating units of geosynthetics (Koerner, 2005; Shukla & Yin, 2006). 7

Table 2.2. Abbreviations and graphical symbols for geosynthetic products (IGS, 2009). . 11

Table 2.3. Identification of the typical functions for each type of geosynthetic (Koerner, 2005). 12

Table 3.1. Reinforced fill requirements (Berg *et al.*, 2009)..... 25

Table 4.1. Bearing capacity factors: N_c, N_q, and N_γ (Berg *et al.*, 2009)..... 35

Table 4.2. Resistance factors for internal resistance for MSE Walls (Berg *et al.*, 2009). .. 40

Table 4.3. External stability resistance factors (Berg *et al.*, 2009). 41

Table 4.4. Minimum design requirements for Segmental Retaining Walls (National Concrete Masonry Association (NCMA), 2016). 41

Table 4.5. Earth pressures on the model. 43

Table 4.6. The factor of safety against sliding. 43

Table 4.7. The factor of safety against overturning. 43

Table 4.8. The factor of safety against bearing capacity failure. 43

Table 4.9. Design of reinforcement spacing. 44

Table 4.10. Design of reinforcement length 45

Table 5.1. Units used. 49

Table 5.2. Material properties of soils in PLAXIS model. 56

Table 5.3. Geogrid properties (Tensar, 2013). 57

Table 5.4. Reinforcement length. 57

Table 5.5. Facing properties. 59

Table 5.6. Strength reduction factors. 61

Table 5.7. Fixities and boundaries. 61

Table 5.8. Number of elements, nodes, and stress points. 63

Table 5.9. Typical shear modulus values (AASHTO, 1998). 66

Table 5.10. Natural frequency calculation of the MSE Wall 69

Table 5.11. Rayleigh α and β coefficients. 74

Table 5.12. MSE Wall configurations for reinforcement design parameters. 78

Table 6.1. Max. acc. (abs.) (a_x) in terms of g=10m/s^2 at Point J (for L/H= 0.5 and 1.0). 112

LIST OF SYMBOLS

a	Acceleration
a_h	Horizontal acceleration
a_v	Vertical acceleration
B	Width
B'	Effective length of the foundation
C	Damping correlation
c	Cohesive strength of the soil
C_1	Relaxation coefficient
C_2	Relaxation coefficient
C_c	Critical damping coefficient
e	Eccentricity
E_{50}	Triaxial loading stiffness
E_{50}^{ref}	Secant stiffness in standard drained triaxial test
E_{oed}	Oedometer loading stiffness
E_{oed}^{ref}	Tangent stiffness for primary oedometer loading
E_{ur}	Triaxial unloading stiffness
E_{ur}^{ref}	Unloading/ reloading stiffness
EA	Reinforcement stiffness
f	Frequency
f_1	Frequency of infinite long uniform soil
F_d	Driving forces
F_R	Resisting forces
$FS_{sliding}$	Factor of safety against base sliding
$FS_{overturning}$	Factor of safety against overturning
FS_{bc}	Factor of safety against bearing capacity
G	Shear modulus
g	Gravitational acceleration
G_0	Maximal small-strain shear modulus
G_{ur}	Unload- reload shear modulus

GF	Geometric factor
H	Wall height
Hz	Hertz
I_a	Arias Intensity
K	Stiffness
K_0	Coefficient of lateral earth pressure at rest
K_0^{nc}	Ko- value for normal consolidation
K_A	Coefficient of active earth pressure
k_h	Horizontal pseudostatic seismic coefficient
k_v	Vertical pseudostatic seismic coefficient
L	Reinforcement length
L_e	Effective reinforcement length
L_r	Reinforcement length within the Rankine failure zone
M	Mass
m	Power for stress-level dependency of stiffness
M_D	Driving moment
M_R	Resisting moment
M_{net}	Difference of the resisting and driving moments
N_c	Bearing capacity factor
N_q	Bearing capacity factor
N_γ	Bearing capacity factor
P_A	The active earth pressure resultant
P_{AE}	Dynamic active earth pressure resultant
p^{ref}	Reference stress for stiffnesses
q	Stress
q_f	Deviatoric stress
q_{ult}	Ultimate bearing capacity of the foundation soil
R_f	Failure ratio
R_{inter}	Interface strength
S_v	Reinforcement spacing
T	Natural period
t	Time

T_a	Allowable tensile force per unit width of reinforcement
T_{max}	Maximum load
u_x	Horizontal displacement
u_y	Vertical displacement
V_p	Longitudinal wave velocity
V_s	Shear wave velocity
z	Depth
α	Rayleigh alpha coefficient
β	Rayleigh beta coefficient
γ	Unit weight of soil
γ_c	Cyclic shear strain
ΔP_{AE}	Dynamic active earth pressure resultant
δ	Interface friction angle
ϵ	Strain
ϵ_1	Vertical axial strain
ϵ_h	Horizontal deformation
ν	Poisson's ratio
ξ	Damping ratio
ρ	Density
σ_3'	Minor principal stress
σ_h	Horizontal stress
σ_n	Normal stress
σ^t	Tension cut- off and tensile strength
σ_v'	Vertical effective stress
τ	Shear stress
ϕ	Internal friction angle
ψ	Dilatancy angle
ω	Angular frequency

LIST OF ACRONYMS/ ABBREVIATONS

AASHTO	American Association of State Highway and Transportation Officials
ASTM	American Society of Testing Materials
BSI	British Standards Institution
EPS	Expanded Polystyrene
FEM	Finite Element Method
FHWA	Federal Highway Administration
GCL	Geosynthetic Clay Liner
GRS- RW	Geosynthetic Reinforced Soil Retaining Wall
HDPE	High- Density Polyethylene
ISO	International Organization for Standardization
LDPE	Low- Density Polyethylene
LRFD	Load Resistance Factor Design
MBW	Modular Block Wall
MSE	Mechanically Stabilized Earth
NCMA	National Concrete Masonry Association
PA	Polyamide
PE	Polyethylene
PET	Polyester
PGA	Peak Ground Acceleration
PP	Polypropylene
PVC	Polyvinyl Chloride
PVD	Prefabricated Vertical Drain
UV	Ultra- Violet
WWM	Welded Wire Mesh

1. INTRODUCTION

1.1. General

Reinforced soil walls have become very popular worldwide and these earth-wall systems have been replacing traditional retaining walls rapidly in the last decades. Due to the fact that soils can only bear low tensile stresses, in Mechanically Stabilized Earth (MSE) Walls, soils are coupled with materials (e.g., geosynthetics, steel bars) that possess higher tensile strength. This combination resembles the reinforced concrete approach in which concrete, a material that has lower tensile strength, is combined with steel. MSE Walls generally satisfy this need by a facing wall that is connected with reinforcements that retain the backfill material (soil).

Our earth is struck with many major earthquakes every year and earthquake-resistant design is one of the main challenges of engineers face today and an extremely important problem. For geotechnical engineers, this problem is even more difficult because a deep understanding of soil-structure interaction is essential for earthquake-resistant design. One of these geotechnical structures is retaining walls. Regardless of their type (conventional or MSE Walls), retaining wall design should encompass both static and dynamic loading conditions. It is important to understand the seismic behavior of MSE Walls. In the last decades, numerical analysis utilizing the Finite Element Method (FEM) is the most preferred analysis method. Especially for MSE Walls, modeling staged construction becomes essential and hence, FEM software that is capable of modeling this feature is typically selected for this purpose. FEM analysis can be used to better understand the MSE Walls' resistance under earthquake loads.

1.2. Objectives

The main goal of this study is to better evaluate the dynamic behavior of an 8- m high MSE Wall under earthquake loading. The main objectives of this thesis are to:

- To compare MSE Wall deformed shape in static and dynamic cases,

- To determine the effects of reinforcement stiffness (600 and 1200 kN/m), reinforcement length to wall height ratio (0.5, 0.7, 1.0), and vertical reinforcement spacing (0.4 and 0.6 m) on wall deformations and tensile loads,
- To determine the effect of characteristics of the harmonic earthquake loading on the wall response,
- To evaluate the effect of the natural frequency of the MSE Wall on its' earthquake behavior, and
- To determine the input ground motion acceleration change (i.e., amplification and de-amplification) within the MSE models.

1.3. Scope

This thesis is organized into seven main chapters and presented in the following order. Chapter 1 introduces the thesis and gives the objectives and the scope of the study. Chapter 2 provides background information on geosynthetics focusing on their history, general properties and types. Chapter 3 is on MSE Walls that present their historical development and the elements used in their construction. Additionally, their advantages and potential disadvantages are given with their basic working mechanism in this chapter. Chapter 4 provides the general design principles (external and internal stability checks) of the model. Furthermore, literature review on studies of MSE Walls and the basic information for Finite Element Method (FEM) is presented in Chapter 4. Chapter 5 consists of modeling details of the MSE Wall PLAXIS 2D v8.6, together with the details of the parametric study and the application of the seismic loading. Results and discussions of numerical analyses are presented in Chapter 6, providing the results of the separate effect of each parameter in different subheadings. Chapter 7 summarizes the findings of the research study and recommendations for future studies.

2. GEOSYNTHETICS

2.1. Introduction

Geosynthetics are polymeric elements that are used within or together with soils in civil engineering projects. The name “Geosynthetic” consists of two parts: geo and synthetic. “Geo” part refers to earth/ground/soil and “synthetic” refers to man-made products. Geosynthetics are generally obtained from crude petroleum oils, and they are mainly produced by polymeric products such as polyester (PET), polypropylene (PP), high-density polyethylene (HDPE), low-density polyethylene (LDPE), and nylon. These products have become useful in time because it is possible to adjust their property according to the desired needs. In order to satisfy the wide range of the desired needs, today geosynthetics are available in a wide horizon with mainly eight types: geogrids, geotextiles, geonets, geomembranes, geosynthetic clay liners, geopipe, geofoam, and geocomposites (Koerner, 2005; Shukla, 2002).

Geosynthetics have been considered as a civil engineering construction material for a while now. Engineering solutions that include geosynthetics offer many advantages when they are compared with traditional solutions. Firstly, geosynthetics solutions are typically cheaper than conventional solutions and it is also possible to eject and reuse them in other application areas which makes its use very convenient. Secondly, the use of geosynthetics as a construction material generally improve field performance and thirdly, they can be efficiently produced to the specific application demand. Because of these main reasons, geosynthetics are preferred in a wide range of applications in, geotechnical, environmental, hydraulics, transportation engineering. They are also preferred in marine, and private development engineering including roads, railroads, embankment, retaining walls, canals, erosion control, waste landfill, land reclamation, breakwaters, jetties, groins, revetments, aquaculture, agriculture, and mining applications. In these fields, these various types of geosynthetics have the functions of separation, reinforcement, filtration, drainage, containment. They can also be used as a barrier, for surface erosion control, and protection (Koerner, 2005; Shukla & Yin, 2006).

2.2. History of Geosynthetics

Before Casagrande suggested the idea of using membranes for soil reinforcement, a similar concept was already used by ancient Romans who used fabrics for road construction. In the second period of the 1920s, road construction field tests were applied by the South Carolina Highway Department and in these tests, primitive woven cotton fabrics were firstly tried. The results indicated that cracking was reduced with this application. While some research on the petrochemical industry was carried out, the first synthetic products were found, and they were started being used in the industry. Polymers', the main constituent of geosynthetics', commercial usage started with polyvinyl chloride (PVC) in 1933 and continued with low density polyethylene (LDPE) and polyamide (PA) (a.k.a. nylon) in 1939, expanded polystyrene (EPS) in 1950, polyester (PET) in 1953, and high density polyethylene (HDPE) and polypropylene (PP) in 1955 (Shukla, 2011).

Towards 1960, for the construction industry, there was a need for a material, which can be used in the production of railroads and asphalt, that is durable and does not quickly degrade like silk and cotton in 5 to 10 years when it is placed on soil. To satisfy this need, synthetic products were utilized in the construction industry and this man-made products' durability made its use very beneficial. At that time, Terzaghi obtained the flexible fabrics with filter functionality and a range of fabrics, now they are called as "Geo-textiles", started to be used as separation and filter layers between granular fills and unsteady subsoils. It is claimed that after the first application of polymer-based woven industrial geotextiles, PVC monofilament woven geotextile was used in 1958. In the 1960s, geotextiles started to be applied in highway and railway beds. Rhone-Poulence Textiles started working on non-woven needle-punched geotextiles in France, ICI in the UK, Chemie Linz in Austria and DuPont in the USA also started producing non-woven geotextiles. In the 1970s, a non-woven geotextile was used in an earth dam, and also filter fabrics were developed in Japan. Furthermore, first woven geotextile was used as essential reinforcement beneath embankments and for the first time geotextile was used in reinforced soil walls. In 1977 the precursor conference about geotextiles named "International Conference on the Use of Fabrics in Geotechnics" was launched. Additionally, in the 1970s, the first composite geotextiles began to be used and they were specifically developed for their use as vertical drains for consolidations of clays. Moreover, in 1972 geofoam was firstly introduced in

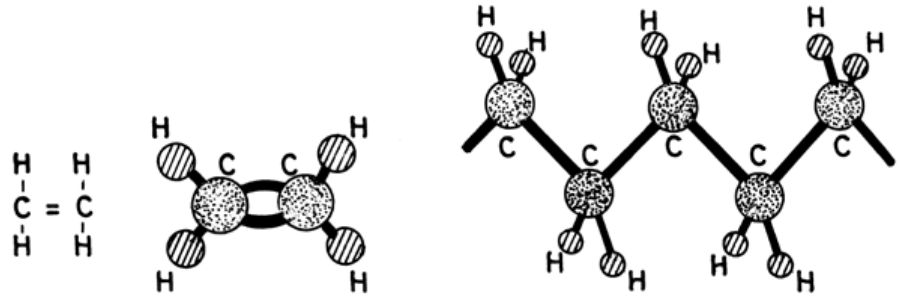
Norway. The invention of geonets in 1958, later on, led to the production of Tensar grids by Netlon Ltd in the UK in 1978 (Shukla, 2011).

In the 1980s, the soil confinement systems related to geotextile nets were developed to control surface erosion. Afterward, Netlon developed Tensar Geocell Mattress which had a similar concept with geotextile nets. In time, different types of synthetic products were started to be used; thus, a family name was needed to comprise the diversity of the categorized names. Therefore, since the end of the 1980s and the beginning of 1990s, the term "Geosynthetics" has been used. In 1980 Koerner and Welsh wrote the first book on geosynthetics. After 1983 with the establishment of International Geosynthetics Society, two international journals, which are Geotextiles and Geomembranes and Geosynthetics International, were initiated in time respectively. In the 1990s, many geosynthetics standards were declared, American Society of Testing Materials (ASTM) in USA, the International Organization for Standardization (ISO) in Switzerland, the British Standards Institution (BSI) in the UK, the Bureau of Indian Standards (BIS) in India, etc. (Koerner, 2005; Shukla, 2011).

2.3. Properties

Geosynthetics' raw materials are polymeric materials. Thermoplastics, which are amorphous or semi-crystalline, are generally for their manufacture. Monomers, which are mostly hydrocarbon molecules constitute long chains by covalent bonds. This process is called polymerization. The molecular weight of the polymer chain is determined by the number of monomers which also defines the length of the polymer chain. The physical and mechanical properties of polymers are affected by molecular weight, but also by the bonds within and between chains, the chain branching and the degree of crystallinity (Shukla & Yin, 2006).

Figure 2.1 shows the polymerization process of a long polyethylene (PE) chain molecule. Polymerization occurs with the transformation of a double carbon bond into the covalent bond between adjacent monomers. Polymers' crystalline and amorphous structure changes according to chains' form and order. When they are highly ordered and have a regular form, then they have a crystalline configuration (Shukla & Yin, 2006).



(a) (b)

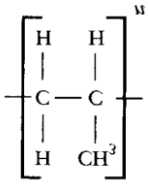
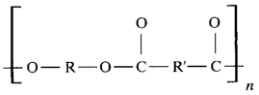
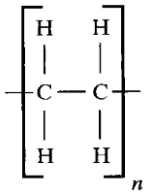
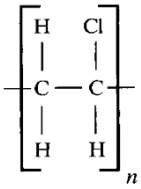
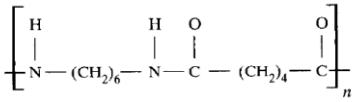
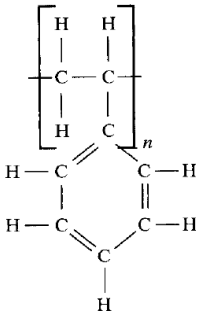
Figure 2.1. The process of polymerization: (a) An ethylene monomer; (b) A polyethylene molecule (Shukla & Yin, 2006).

The increase in molecular weight, which can also be thought as a degree of polymerization, results in an increase in strength, elongation, impact strength, stress crack resistance, and heat resistance, but a decrease in the ability to process of the material (Shukla & Yin, 2006).

The most common polymers used in the geosynthetic manufacturing; polypropylene (PP), high density polyethylene (HDPE) and polyester (polyethylene terephthalate (PET)), and other ones are given with their names and abbreviations in Table 2.1 (Shukla et al., 2006).

Figure 2.2 shows the polyethylene (PE), one of the most common thermoplastic polymers. Polyethylene has three types according to their production processes. The first one developed is Linear Low Density Polyethylene (LDPE) which has a density of about 920-930 kg/m^3. The flexibility of LDPE comes from the at high pressures used at its production. In contrast to LDPE, HDPE with a density of 940-960 kg/m^3, is produced at low pressures and temperatures which make it inert. The third group is linear low density polyethylene (LLDPE) with a density in 925-945 kg/m^3 range, which is produced by co-polymerizing ethylene with a small amount of alpha-olefins. Another raw material is polypropylene (PP) which is the most common manufacturing raw material for geotextiles and known for its' durability against chemical degradation, and sensitivity to Ultra Violet (UV) light. Last but not least, polyester (PET) is the one which is obtained by polymerization of petroleum derivates (Yardimci, 2013).

Table 2.1. Polymers and the repeating units of geosynthetics (Koerner, 2005; Shukla & Yin, 2006).

	Types of polymer	Abbreviations	Repeating Unit
	Polypropylene	PP	
	Polyester (polyethylene terephthalate)	PET	
Polyethylene	Low density	LDPE	
	Very low density	VLDPE	
	Linear low density	LLDPE	
	Medium density	MDPE	
	High density	HDPE	
	Chlorinated	CPE	
	Chlorosulfonated	CSPE	
	Polyvinyl chloride	PVC	
	Polyamide	PA	
	Polystyrene	PS	

The important characteristics of geosynthetics facilitate their widespread use. Geosynthetics are:

- Durable against biological and chemical degradation,
- Durable under soil cover for a long-time span,
- Non-corrosive,
- Highly flexible,
- Lightweight,
- Compact in volume,
- Easy to store, transport & install,
- Constructed fast,
- Economical,
- Aesthetic, and
- Environmentally friendly (Shukla & Yin, 2006).



Figure 2.2. Polyethylene (Ergul, 2012).

2.4. Types of Geosynthetics

In the 1970s, there were only five (5) or six (6) types of geosynthetics available, but now it is possible to find hundreds of geosynthetic products with various functionalities, application areas, and names. Because of this reason, they are mainly classified according to

their material properties (e.g., permeability) or their application purposes (e.g., reinforcement, separation). Several classification systems are available for material properties. Koerner grouped geosynthetics into eight (8) major types and the related images of these geosynthetics are provided in Figure 2.3. The abbreviations and graphical symbols declared by International Geosynthetics Society are shown in Table 2.2.

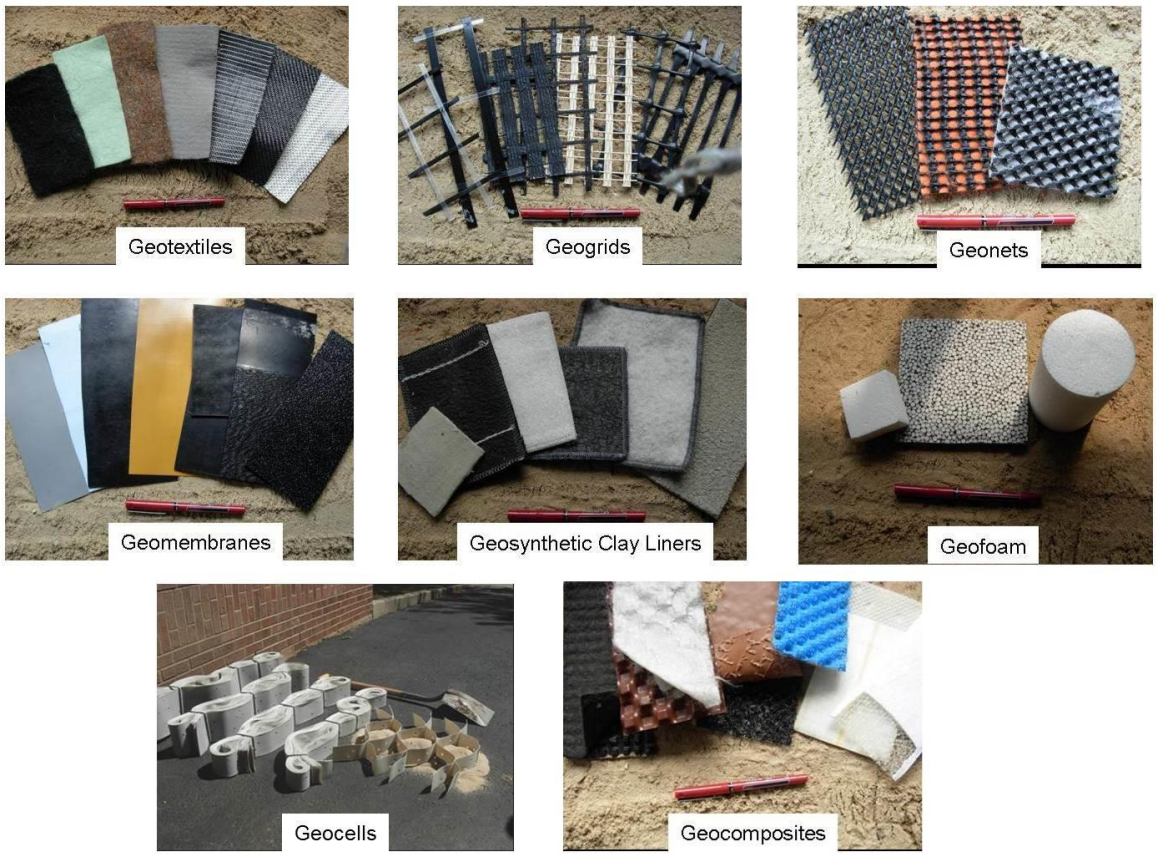


Figure 2.3. The eight types of geosynthetics (Koerner, 2012; Wikipedia, 2019).

Geosynthetics have various functions in different engineering fields as mentioned in the Introduction section, these are shown in Figure 2.4a through 2.4f. When two soil layers having different particle sizes, geosynthetics can prevent the mixing of the two different types of soils, in this way (see Figure 2.4a), it acts as a separator. Geosynthetics are placed against the flow direction of the water and in this way, they act as a filter to keep the fine-grained material. When the excess water is to be drained through less permeable soils, geosynthetics with drainage functions are preferred. Additionally, as it is illustrated in Figure

2.4c, to speed up the consolidation of cohesive foundations, prefabricated vertical drains (PVDs) are used (Koerner, 2005).

Another primary function of geosynthetics is their use as reinforcement. Geosynthetics are mainly used to spread loads and hence, increasing soils resistance against tensile and shear stresses. Geosynthetics are also used for containment. Geosynthetics with this function, prevent soils from penetration of fluids or gases. Geosynthetic clay liners (GCLs) are mostly used to supply this function (Koerner, 2005).

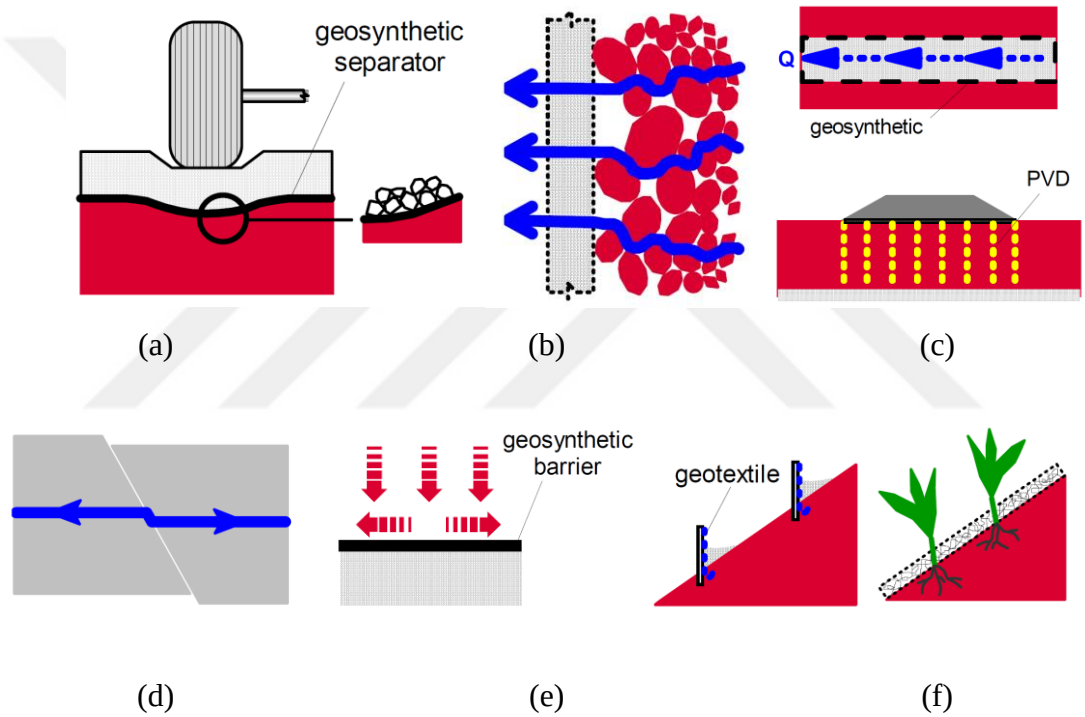


Figure 2.4. Various functions of geosynthetics: (a) Separation (b) Filtration (c) Drainage (d) Reinforcement (e) Containment (f) Erosion control (Bathurst, 2019).

The final primary function for geosynthetics is their use for erosion control, and geosynthetics with this function act to prevent soil erosion which is generally triggered by rainfall and surface water runoff. (Bathurst, 2019; Berg, Christopher, & Samtani, 2009; Ergul, 2012). For each type of geosynthetics' typical functions are illustrated in Table 2.3. It is also possible to benefit their dual functions at the same time as seen in Table 2.3 (Koerner, 2005).

Table 2.2. Abbreviations and graphical symbols for geosynthetic products (IGS, 2009).

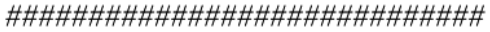
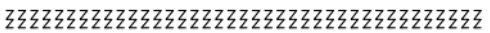
Abbreviations	Graphical Symbols	Geosynthetic Products (generic)
GTX		Geotextile
GMB		Geomembrane
GBA		Geobar
GBL		Geoblanket
GCD		Geocomposite drain – with geotextile on both sides
GCE		Geocell
GCL		Geocomposite clay liner
GEC		Surficial geosynthetic erosion control
GEK		Electrokinetic geosynthetic
GGR		Geogrid
GMA		Geomat
GMT		Geomattress
GNT		Geonet
GSP		Geospacer
GST		Geostrip

Table 2.3. Identification of the typical functions for each type of geosynthetic (Koerner, 2005).

Type of Geosynthetic	Primary Function				
	Separation	Reinforcement	Filtration	Drainage	Containment
Geotextile	✓	✓	✓	✓	
Geogrid		✓			
Geonet				✓	
Geomembrane					✓
Geosynthetic Clay Liner					✓
Geopipe				✓	
Geofoam	✓				
Geocomposite	✓	✓	✓	✓	✓

In the following section, the most common geosynthetics which are geotextiles, geogrids, geomembranes, geonets, and geocomposites are briefly explained.

2.4.1. Geotextiles

Nowadays, geotextiles are among the most preferred geosynthetic materials which are planar, permeable and polymeric textile products that can be used in separation, filtration, drainage, reinforcement, and protection (Das, 2010). Geotextiles are generally sub-grouped based on their fiber type and manufacturing processes. According to geotextile manufacturing methods, geotextiles can be grouped into the following categories:

- Woven geotextiles,
- Non-woven geotextiles,
- Knitted geotextiles, and

- Stitch-bonded geotextiles (Shukla & Yin, 2006).

Woven geotextiles have regular textile structure and are produced from yarns, one or several fibers, by conventional weaving methods. Monofilament, multifilament, slit-film are used to fabricate woven geotextiles, while non-woven geotextiles are manufactured from the continuous filament and staple fiber which are shown in Figure 2.5. Woven geotextiles are manufactured with a conventional method from yarns with a regular textile structure. For non-woven geotextile fibers, there are certain main techniques which are needle punching, thermal bonding, chemical bonding, and spun bonding. Knitted geotextiles are manufactured by interlooping one or more yarns jointly. Finally, in the last manufacturing method, stitch-bonded geotextiles come together by sewing (Das, 2010; Shukla & Yin, 2006).



(a) (b)

Figure 2.5. (a) Woven geotextiles; (b) Non- Woven geotextiles (Shukla, 2016).

Five different types of fibers are used to manufacture the geotextiles (See Figure 2.6). These are monofilament, multifilament, staple fiber yarn, slit film monofilament, and slit-film multifilament. Firstly, polymers are transformed into fibers and by mostly melting and stretching, monofilaments are produced. When these monofilaments are twisted together, a multifilament is obtained. Staple fibers are produced by continuous filaments gathered in a large rope-like bundle. For fabric manufacturing, these staples are opened and twisted or spun into long yarns. The final one is the slit-film monofilament that is manufactured from a continuous sheet of polymers by cutting into fibers. When they are twisted, slit-film multifilament can be obtained. (Koerner, 2005).

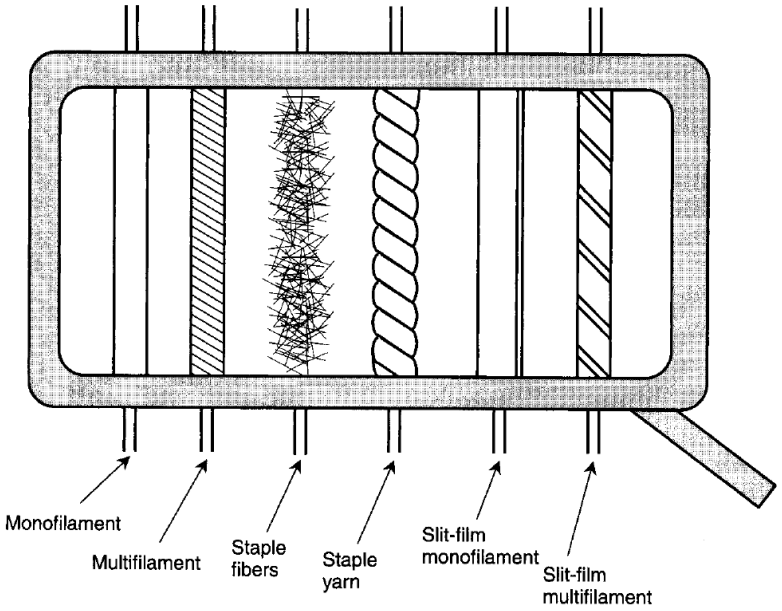
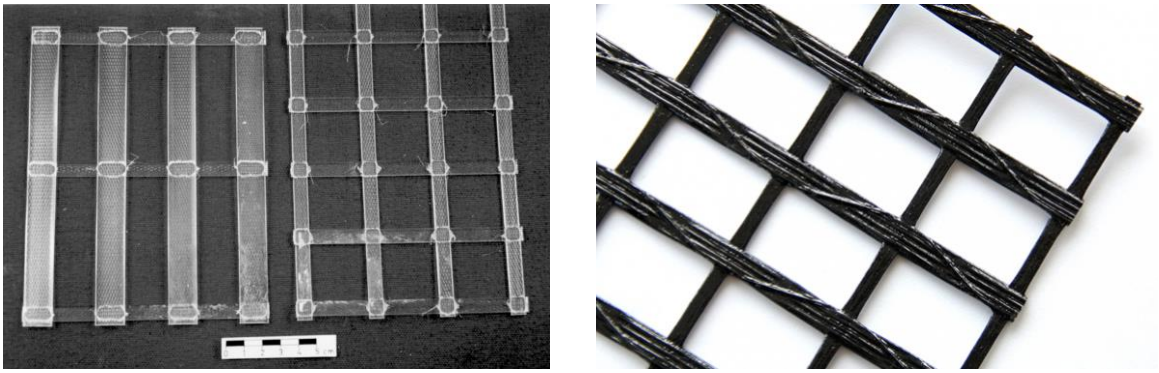


Figure 2.6. Various polymeric fibers used in geotextile manufacturing (Koerner, 2005).

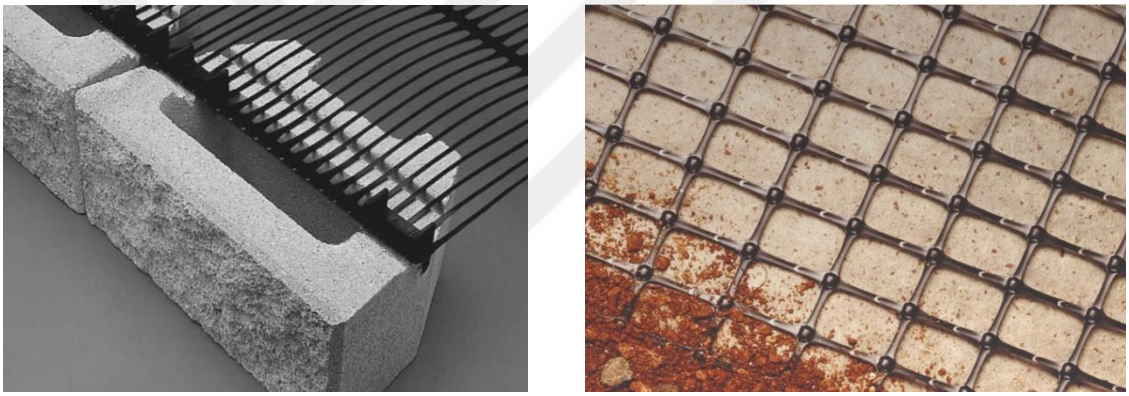
2.4.2. Geogrids

Geogrids are high strength geosynthetic reinforcements made of a variety of polymers engineered to carry the tensile stresses. They consist of a mesh with large open spaces which are also called as apertures. The elements, known as ribs form the network by joining at intersections. This structure provides geogrids extra strength because of its interlocking mechanism. When the granular materials are placed over the geogrid, this geogrid interlocking with the granular soil providing additional strength. There are three main methods for the linking of the ribs: extrusion, bonding, and interlacing. According to these methods, the manufactured geogrids can be grouped into: Extruded geogrids, bonded geogrids, and woven geogrids. The bonded and woven geogrids are shown in Figure 2.7a and Figure 2.7b. Types of extruded geogrids: uniaxial, biaxial and triaxial are provided in Figure 2.8a through 2.8c. According to the direction of the stretching extruded geogrids, are classified as uniaxial, biaxial and triaxial (Shukla, 2011; Tensar, 2016).



(a) (b)

Figure 2.7. Geogrids: (a) Bonded (Shukla & Yin, 2006) (b) Woven (ACE Geosynthetics, 2019a).



(a) (b)



(c)

Figure 2.8. Extruded geogrids (a) Uniaxial (Tensar Earth Technologies, 2019), (b) Biaxial (Tensar, 2019b) (c) Triaxial (Tensar, 2019a).

2.4.3. Geonets

Geonets and geogrids look like each other when their physical configuration is only considered, although, they show different functionality. The outstanding feature of geonets comes from their structure. Geonets are principally obtained with the extrusion method and their ribs intersect at $60^{o}$to 80^{o}range which allows them to create a structure with depth, so they have 5-10 mm thickness. Because of geonets' geometrical properties, it is possible to differ them from geogrids as geonets are able to drain liquids or gases in the axis of the plane (Shukla & Yin, 2006).

2.4.4. Geomembranes

In contrast to geotextiles and geogrids' that have a porous structure, geomembranes are relatively nonporous materials. They are mostly obtained using three methods: extrusion, calendaring, and spread coating, consecutively. In these methods, mostly polyethylene and polyvinyl chloride are used to manufacture this relatively thin, impervious sheets which are primarily used for linings and to cover liquid or solid storage facilities such as landfills, reservoirs, canals, and other containment facilities. In the extrusion process, a molten polymer is extruded into a non-reinforced sheet using an extruder. Then the sheet can be reinforced by laminating geotextiles, and the reinforced geomembrane is obtained. Afterward, they are coated in a geotextile by spreading a polymer. Finally, the heated polymeric compound is passed through heated rollers of the calendar under mechanical or hydraulic pressure (Das, 2010; Koerner, 2005; Shukla & Yin, 2006).

2.4.5. Geocomposites

A geocomposite is composed of two or more materials such that at least of one them is a geosynthetic product (e.g.; geotextile, geogrid, geonet, geomembrane, etc.). By combining the functional properties of various materials, geocomposites are manufactured to function effectively for the desired needs (Shukla & Yin, 2006). Considering the five primary functions, the following composites are obtained for specific applications:

- Geotextile- geonet composites,

- Geotextile- geomembrane composites,
- Geomembrane-geogrid composites,
- Geotextile- geogrid composites,
- Geotextile- polymer core composites, and
- Geosynthetic- soil composites (Koerner, 2005).

2.4.6. Geo- others and Applications

Today there are many applications of geosynthetics (see Figure 2.9). Many other types and corresponding terms of geosynthetics are also used such as: geosynthetic clay liner (GCL), geocell, geopipe, geomat, geomesh, geospacer, geostrip, geotube. geocell, geoblanket, geobar, geomattress, electrokinetic geosynthetic (EKG) geoproducts, geonatural, geofabric (IGS, 2009; Shukla & Yin, 2006).

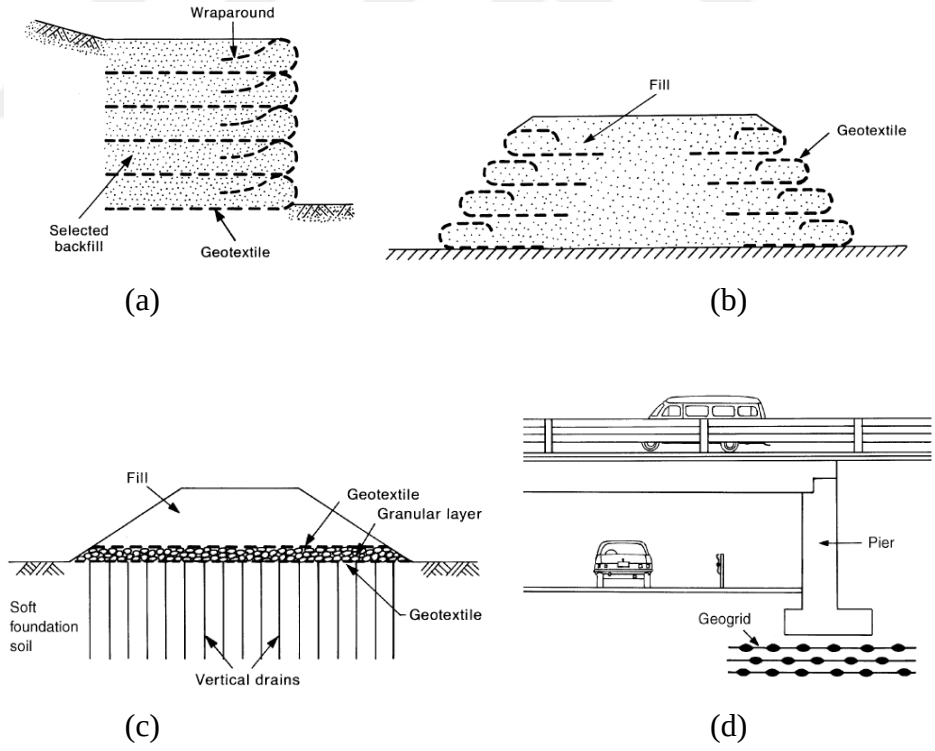
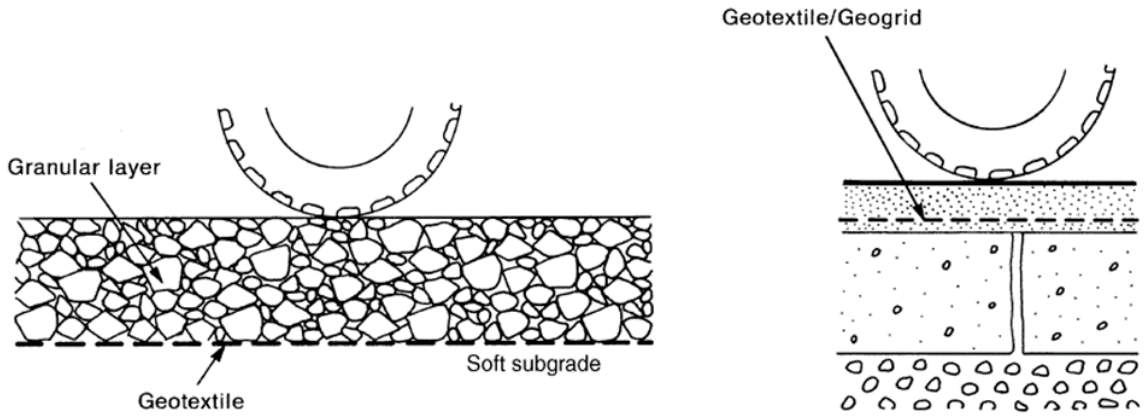
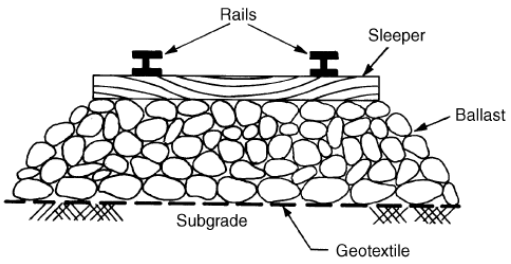


Figure 2.9. Typical geosynthetic applications: (a) Retaining wall (b) Steep- sided embankment (c) Embankment on soft foundation soil (d) Bridge pier (e) Unpaved road (f) Paved road (g) Railway track (h) Slope- erosion control (i) Slope- stabilization (j) Landfill (k) Dam (l) Liquid reservoir (m) Water channel (n) Trench drain (Shukla & Yin, 2006).

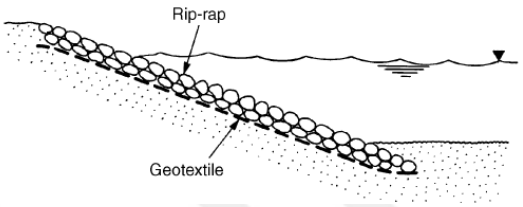


(e)

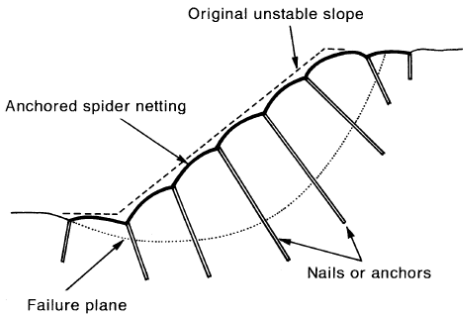
(f)



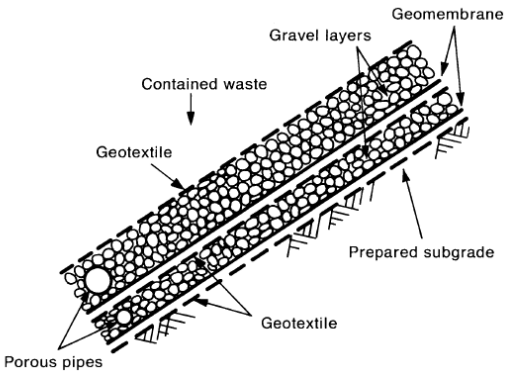
(g)



(h)

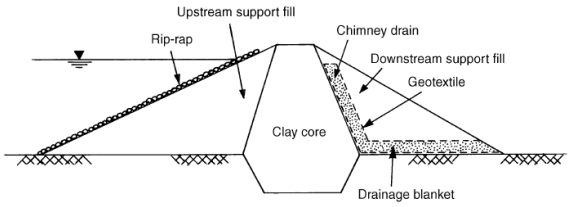


(i)

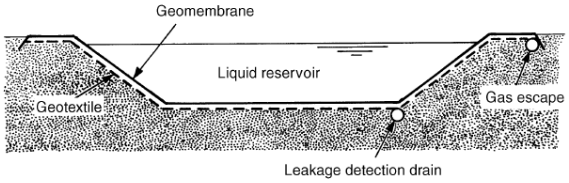


(j)

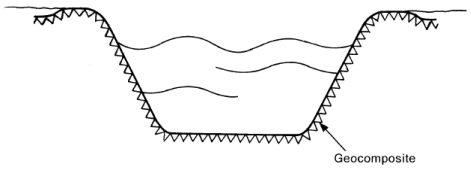
Figure 2.9. Typical geosynthetic applications: (a) Retaining wall (b) Steep- sided embankment (c) Embankment on soft foundation soil (d) Bridge pier (e) Unpaved road (f) Paved road (g) Railway track (h) Slope- erosion control (i) Slope- stabilization (j) Landfill (k) Dam (l) Liquid reservoir (m) Water channel (n) Trench drain (Shukla & Yin, 2006) (cont.).



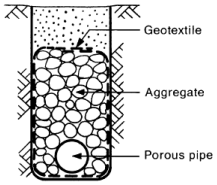
(k)



(l)



(m)



(n)

Figure 2.9. Typical geosynthetic applications: (a) Retaining wall (b) Steep- sided embankment (c) Embankment on soft foundation soil (d) Bridge pier (e) Unpaved road (f) Paved road (g) Railway track (h) Slope- erosion control (i) Slope- stabilization (j) Landfill (k) Dam (l) Liquid reservoir (m) Water channel (n) Trench drain (Shukla & Yin, 2006) (cont.).

3. MECHANICALLY STABILIZED EARTH (MSE) WALLS

3.1. Introduction

Reinforced earth walls essentially function as flexible retaining walls that are used to retain the soils behind them. The reinforcement can be made of various materials such as steel strips, fabric or geosynthetics. In FHWA, Mechanically Stabilized Earth (MSE) Wall is defined as a generic term for reinforced soils, which is known as a soil system that acts in company with multiple soil layers which includes reinforcements (see Figure 3.1). MSE Walls are generally constructed with reinforcement spacing of 0.3 to 1.0 m. As reinforcement, metallic or high strength geosynthetics are typically preferred and as a facing material, heavy concrete blocks are preferred for MSE structures. When the spacing between the reinforcement material is reduced to 0.2- 0.3 m, it becomes possible to use reinforcement with a lower strength (such as geotextiles) as a quasi-tiebacks, then the wall is considered as "reinforced soil" and this type of wall is typically referred to as Geosynthetic Reinforced Soil Retaining Wall (GRS-RW). As GRS-RWs have minimal facing blocks with tightly placed geosynthetics, it is considered as an enhancement of as they enhance the overall engineering features of the soil, whereas widely spaced reinforcements in MSE Walls are more helpful for the stabilization against a potential failure wedge (Barrett & Ruckman, 2007; Berg *et al.*, 2009; Wu & Payeur, 2015).

MSE Walls are mostly designed for long service life (typically 75 years). For this reason, long-term environmental effects such as material deterioration should be considered. When MSE Walls are considered as permanent structures, proper safety factors should be incorporated in design for their longer service life. Their sustainability and lower cost make them widely spread. Currently, the use of MSE Walls increases year by year. Based on the information provided by FHWA (2009), approximately more than 850,000 m^2 (9,000,000 ft^2) of MSE Walls with precast facing, and more than 280,000 m^2 (3,000,000 ft^2) MSE Walls with modular block wall are built each year in the United States. MSE Walls have many applications. The illustrations in Figure 3.2 demonstrates their typical applications such as their use in bridge abutments, waterfront structures, areas where the right-of-way is restricted, steep-sided terrain and sites where foundation soils are poor (Berg *et al.*, 2009).

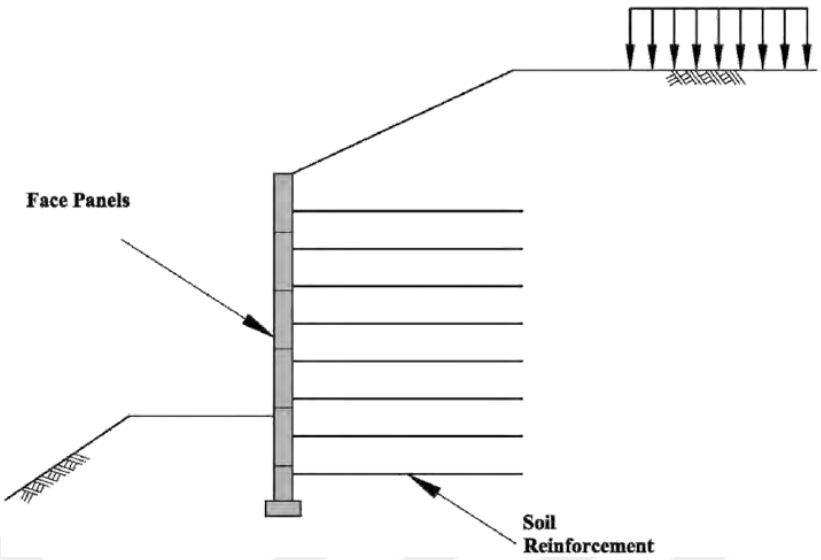


Figure 3.1. Schematic diagram of an MSE Wall with precast concrete facing (Kavazanjian *et al.*, 2011)

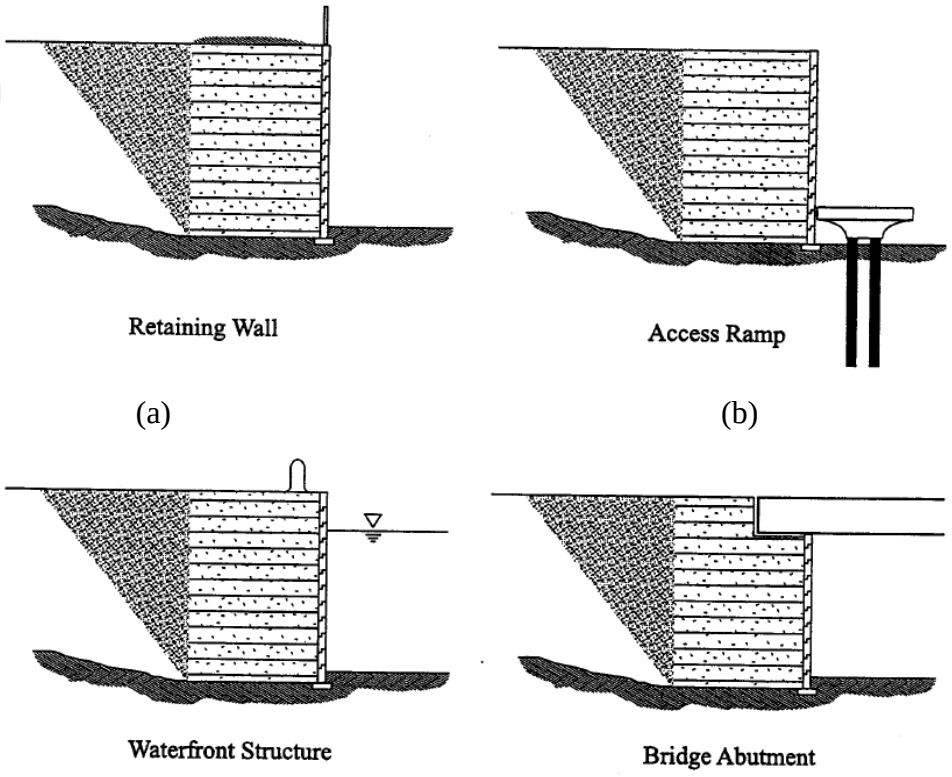


Figure 3.2. Representative MSE Wall applications: (a) Retaining wall, (b) Access ramp, (c) Waterfront structure, (d) Bridge abutment (Berg *et al.*, 2009).

3.2. Historical Development of MSE Walls

The oldest utilization of inclusions in the soil dates to the prehistoric times, people used straws to enhance the quality of adobes bricks and sticks to mud dwellings. According to literature, this method was used in 5th and 4th millenniums B.C. The 3000 years old ziggurat of the ancient city of Dur-Kurigatzu, now known as Agar-Quf, is one of the oldest remaining examples of soil reinforcement with 45m height, despite the belief that it was once over 80 m. Another important remaining example of reinforced soil system is The Great Wall of China, which still stands with mixtures of clay and gravel reinforced with branches from circa 200 B.C. (Jones, 1996).

In 1925, Munster took a remarkable step to the modern concept of reinforced soil structures. He modeled earth retaining wall with wooden reinforcing members and a light facing. In 1930, Coyne, the French developer, launched a retaining wall with a mass of granular fill unified by ties with anchors (Jones, 1996). Casagrande proposed the modern concept of earth reinforcement and soil structures with the idea of reinforcing weak soils by high-strength membranes laid horizontally. In the early 1960s, the modern form of soil reinforcement for retaining walls was developed by French architect and engineer Henry Vidal who invented a Reinforced Earth® system with steel strip inclusion. In 1964 he started building these structures. In 1968 in France and in 1972 in the United States, first major retaining walls using this method were constructed and afterward, Henry Vidal's concept pioneered the world (Berg *et al.*, 2009; Jones, 1996). The first reinforced earth structure in the UK was introduced in 1973 and in the same year the York method, illustrated in Figure 3.3, which have similarities with the Munster technique was introduced (Jones, 1996).

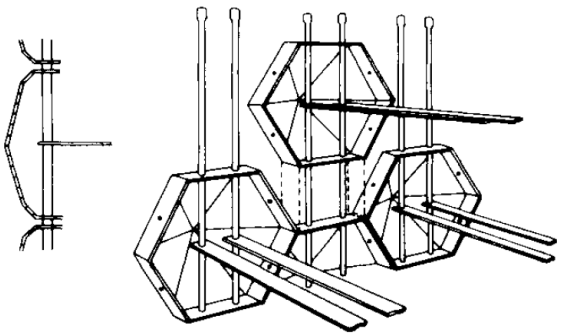


Figure 3.3. Retaining wall constructed with York method (Jones, 1996).

After the 1960s, the use of synthetic products in civil engineering started, and since the end of the 1960s, the implementations of these products into the reinforced soil structures. At first, there were only two options. Geogrids were firstly implemented in civil engineering applications in the early 1960s and geotextile applications followed it and increased significantly. Since then, the use of geosynthetics spread in the world (Jones, 1996). With the advancements in geosynthetics used as reinforcement, there are many examples of tall MSE Walls throughout the world. One of the tallest MSE Walls in the United States (see Figure 3.4) has a height of 45.7 m (150-ft) and was built for the expansion of the Seattle-Tacoma International Airport. One of the world's tallest reinforced earth wall was built in India and had a height of 74 m (Berg *et al.*, 2009).

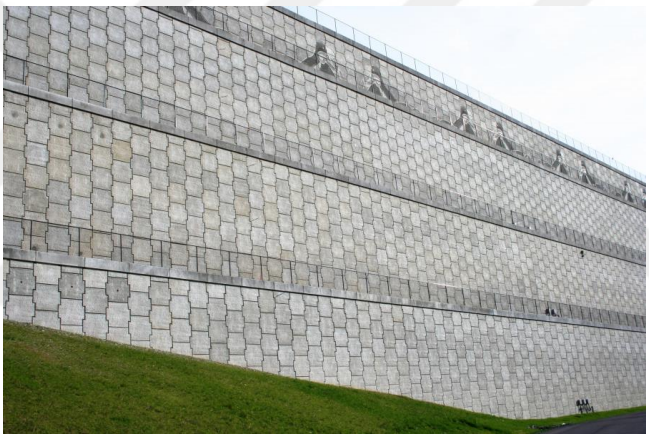


Figure 3.4. 45.7 m high MSE Wall (Reinforced Earth, 2015).

3.3. The Elements of MSE Walls

MSE Walls are constructed on the foundation soil and they are composed of three main elements: (i) soil reinforcement, (ii) reinforced fill and (iii) facing units as shown in Figure 3.5 (Das, 2010):

3.3.1. Soil Reinforcement

Reinforcements used in MSE Walls are grouped according to their geometry, material, and extensibility. According to reinforcement geometry, they are classified into 3 groups. Firstly, linear unidirectional reinforcements are generally steel or coated geosynthetic strips.

Secondly, grids or bar mats with having grid spacing greater than 150 mm are categorized as composite unidirectional. Thirdly, reinforcements that are continuous sheets of geosynthetics, welded wire mesh, and woven wire mesh with mesh element spacing of less than 150 mm are classified as planar bi-directional. In terms of reinforcement material, reinforcements are categorized as metallic and nonmetallic reinforcements. Metallic reinforcements are generally mild steel, and nonmetallic ones are made up of polymeric materials. When the flexibility of the reinforcements is considered, two main groups exist: (i) inextensible, and (ii) extensible. Inextensible reinforcements (e.g., steel strips and bar mats) deforms less than the soil at failure. The deformation on extensible reinforcements occurs comparable to or greater than the soils at failure. Examples of them are geogrid, geotextile, and woven steel wire mesh (Berg *et al.*, 2009).

3.3.2. Reinforced Fill

Reinforced backfill is sometimes also called as mechanically stabilized soil mass but in fact, mechanically stabilized soil mass is the family name of reinforced fill and multi-anchored soil mass. Reinforced fill is used for the cases in which multiple reinforced layers act. Well graded, granular material constitutes a high quality fill which is needed for MSE Walls to supply durability, good drainage, and constructability. Selecting the appropriate material for reinforced fill has great importance for the walls' long-term performance. It is typically recommended to use granular materials that are free from organics as reinforced fill material. According to FHWA, the fill material should not confront with the gradation limits, PI and soundness criteria provided in Table 3.1. Furthermore, compaction has a significant impact on the properties of the reinforced soil. Compaction should be performed with lighter equipment close to 1 m beyond the facing. In terms of design strength parameters, based on the knowledge and experience of the engineering community, typically that peak shear strength parameters and a maximum effective friction angle of 34 degrees are usually preferred (Berg *et al.*, 2009).

The length of the reinforced fill needs to be considered carefully in many applications. The length of the reinforced zone is typically about 0.8 H (Bowles, 1996). However, the reinforced fill is sometimes extended beyond the reinforcement length. In most applications apart from back-to-back walls it is preferred to extend the fill 0.3 m beyond the reinforcement

length, and in some of the applications, a wedge behind the reinforced zone is filled (see Figure 3.5) (Berg *et al.*, 2009).

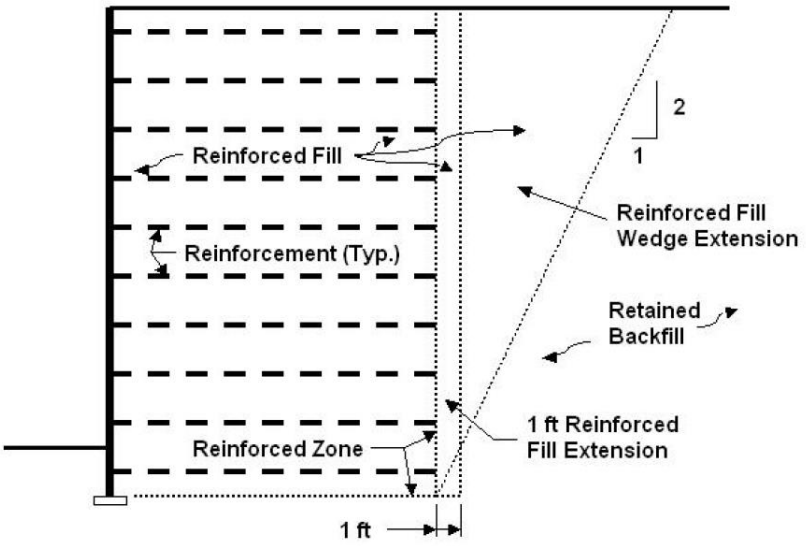


Figure 3.5. Reinforced fill extension beyond the reinforced zone (Berg *et al.*, 2009).

Table 3.1. Reinforced fill requirements (Berg *et al.*, 2009).

Gradation: (AASHTO T-27)	**U.S. Sieve Size**	**Percent Passing** [a]
	4 in. (102 mm) [a,b]	100
	No.40 (0.425 mm)	0-60
	No.200 (0.075 mm)	0-15
Plasticity Index, PI (AASHTO T-90)	PI ≤ 6	
Soundness: (AASHTO T-104)	The materials shall be substantially free of shale or other soft, poor durability particles. The material shall have a magnesium sulfate soundness loss of less than 30 percent after four cycles (or a sodium sulfate value less than 15 percent after five cycles).	
Notes: (a) To apply default F* values, Cu, should be greater than or equal to 4. (b) As a result of recent research on construction survivability of geosynthetics and epoxy coated reinforcements, it is recommended that the maximum particle size for these materials be reduced to ¾-in. (19 mm) for geosynthetics, and epoxy and PVC coated steel reinforcements unless construction damage assessment tests are or have been performed on the reinforcement combination with the specific or similarly graded large size granular fill. Prequalification tests on reinforcements using standard agency fill materials should be considered.		

3.3.3. Facing Unit

The wall facing is very commonly comprised of precast concrete modular blocks as seen in Figure 3.6. It can also be made of steel plates, wooden planks, and concrete interlocking panels. It is possible to find many types and colors of facing units as seen in Figure 3.7. Besides the aesthetics side, the facing unit also has important design implications, as an example, it can impact the settlement of the wall. According to the design criteria, facing units can be either flexible or rigid. Both of these are accepted as long as they are designed properly for the reinforcement connection and they are stiff enough to retain the soil. One should note that the modular block units also provide stability with their dead weight. In addition to providing protection against erosion, they can also supply paths to the drainage (Berg *et al.*, 2009; Das, 2010).

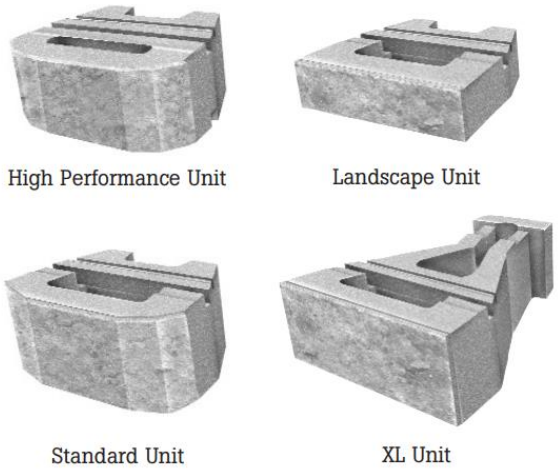
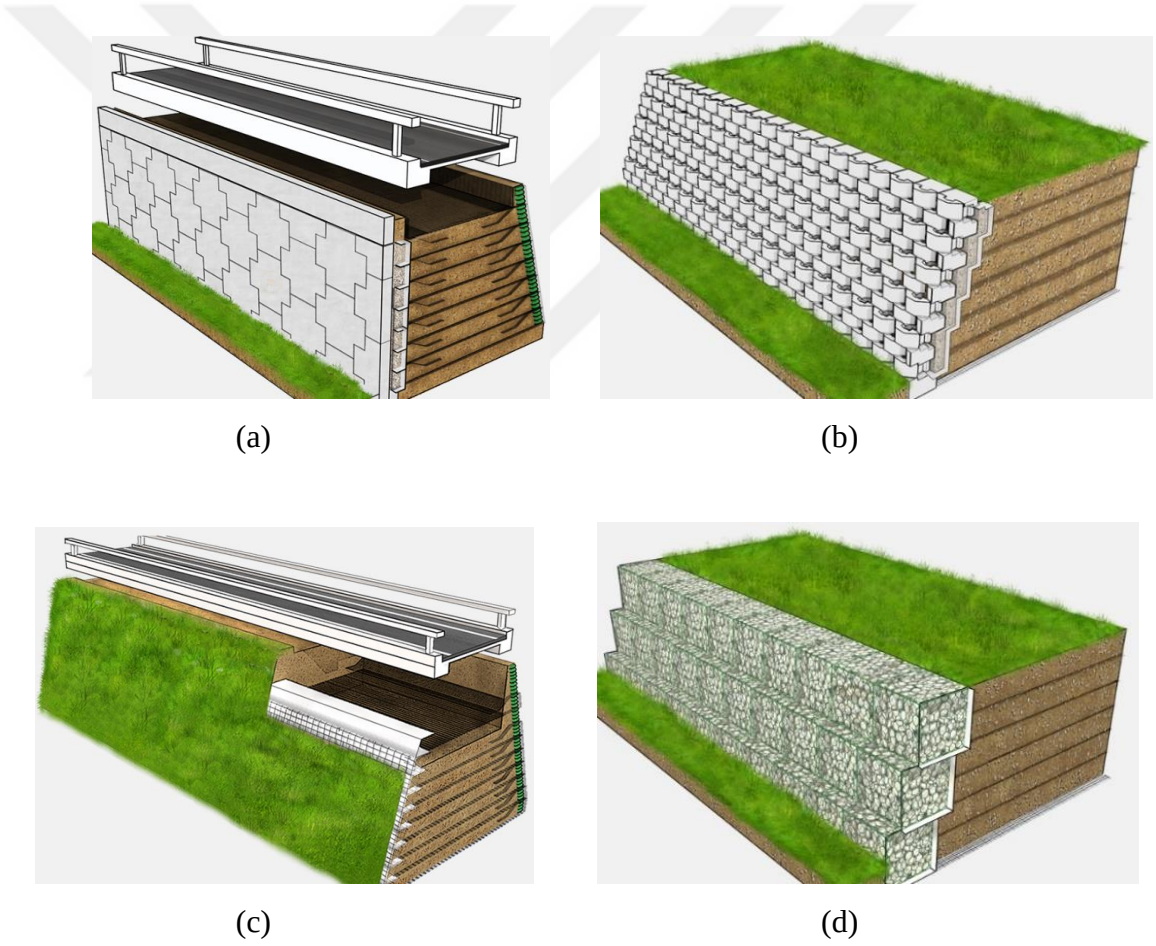


Figure 3.6. Various types of modular blocks (Tensar Earth Technologies, 2005).

Major six (6) facing types preferred for various applications are provided below with some information about each:

- *Segmental precast concrete panels* need relatively less construction time and they are stiff with less concrete.
- *Dry cast modular block wall (MBW) units* are small, square concrete which is given in Figure 3.7. They have different types, although, common ones weigh 15 to 50kg. Their heights range from 10 to 30 cm and their face length from 20 cm 45 cm.

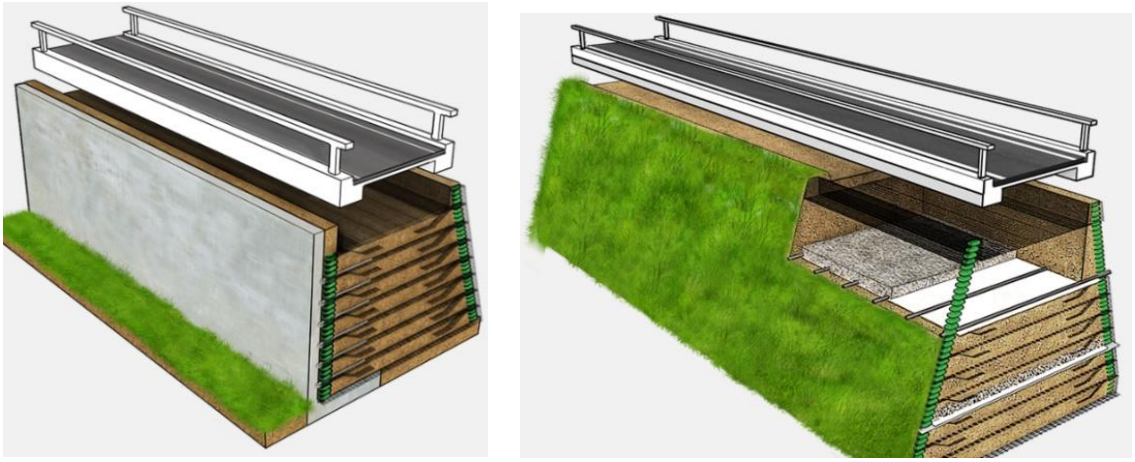
- *Welded wire mesh (WWM)* is used to shape the wall facing by bending up at the face of the wall.
- *Gabion facing* provides stability to the structure also with providing extra permeability.
- *Geosynthetic facing* is constituted by looping the reinforcement to form the face. Vegetation is important to prevent ultraviolet exposure to the reinforcement.
- *Post-construction facing* is the method in which the facing is constructed with shotcreting, cast-in-place concrete, guniting, or a similar procedure (Berg *et al.*, 2009).



(a) (b)

(c) (d)

Figure 3.7. Main facing types: (a) Segmental precast concrete panels (b) Dry cast modular block wall (MBW) units (c) Welded wire mesh (WWM) (d) Gabion facing (e) Geosynthetic facing (f) Post-construction facing (ACE Geosynthetics, 2019b).



(e) (f)

Figure 3.7. Main facing types: (a) Segmental precast concrete panels (b) Dry cast modular block wall (MBW) units (c) Welded wire mesh (WWM) (d) Gabion facing (e) Geosynthetic facing (f) Post-construction facing (ACE Geosynthetics, 2019b) (cont.).

3.3.4. Retained Soil & Foundation Soil

Retained backfill is the natural or artificial soils located behind the mechanically stabilized soil zone. The strength and unit weight parameters of the retained soils are required for the analyses and the design of MSE Walls. The potential performance problems such as settlements between the reinforced and retained fill should also be evaluated (Berg *et al.*, 2009).

Foundation soil is the soil underneath the reinforced fill and the retained backfill. Foundation soils play an important role in bearing capacity, settlement, and global stability calculations. The engineering properties have to be determined before the design and construction phase. Obviously, to calculate bearing conditions, frictional and cohesive parameters ($\emptyset$, c), unit weights (γ), and groundwater table should also be determined. In the case of the presence of weak foundation soil, soil improvement should be performed to satisfy the bearing capacity requirements (Berg *et al.*, 2009).

3.4. Advantages and Potential Disadvantages of MSE Wall

MSE Walls have many advantages when their features are compared with conventional reinforced or gravity types of walls. They are alternatives to traditional methods basically because of being cost-effective and their technical superiorities. The advantages of MSE Walls can be listed as follows (Enunlu, 2007):

- Construction procedure is simple and does not require an extensive scope of equipment, qualified and skilled operator is not required.
- They do not require much space in front of the structure.
- Site preparation procedure does not take much time.
- Construction is relatively cheap and cost-effective
- They have flexibility and capability to tolerate deformations even under poor subsoil foundation conditions.
- They have a higher resistance to seismic activity.
- They provide aesthetics with various facing units (Berg *et al.*, 2009).

In spite of having many advantages, MSE Walls may have the following disadvantages which can change according to project conditions:

- To ensure the internal and external stability, a large area is demanded behind the wall.
- To fulfill the need for granular fill, in some cases it can be difficult and expensive to provide required fill materials.
- A design responsibility may be required between material suppliers and owners.
- To prevent potential degradation of polymer reinforcement, extra precautions may be required against ultraviolet rays (Berg *et al.*, 2009).

4. MSE WALL DESIGN AND SEISMIC STUDIES

4.1. Introduction

Basic design principles of Mechanically Stabilized Earth (MSE) Walls and use of Finite Element Method (FEM) in MSE Wall deformation analysis under static and dynamic loads are explained in this Chapter. An 8 m high MSE Wall model was planned for FEM analysis. Prior to conducting the FEM analysis, preliminary static stability checks were performed following the basic MSE Wall design principles. Additionally, a literature review on the previous studies utilizing FEM for the analysis of MSE Walls is presented in this Chapter.

MSE Walls have to be designed to resist both external and internal modes of failure. In external stability calculations, the reinforced soil and the facing are considered as a monolithic structure and factor of safety values are calculated for base sliding, overturning and the bearing capacity. In internal stability calculations, the structure is checked against a possible pullout and bond breakage (over-stressing) of reinforcements.

4.2. Earth Pressures Acting on MSE Wall

Earth pressures and loads acting on MSE Walls have to be determined carefully to perform a reliable design. Like conventional retaining walls, total lateral earth pressures have a remarkable effect on MSE Walls' behavior. When the earthquake loading condition is considered, the total lateral earth pressures consist of both static and dynamic loads.

In static conditions, lateral earth pressures can be calculated for active, passive or at rest earth conditions. To estimate the active lateral earth pressures on MSE Walls, two commonly used theories are: Coulomb (1776) and Rankine (1857) (Kramer, 1996).

Equation 4.1 shows the active earth pressure (K_A) coefficient for a horizontal backfill. The horizontal active earth pressure is provided in Equation 4.2), in which σ_v' is the vertical effective stress. For dry cohesionless backfill soils, the triangular active stress distribution is

proposed. The force generated from this triangular stress distribution is P_A (see Equation 4.3.) which acts at the one third of the wall height (Das, 2010).

$$K_A = \frac{1 - sin\phi}{1 + sin\phi} = \tan^2(45 - \frac{\phi}{2}) \quad (4.1)$$

$$P_A = K_A \sigma_v' - \sqrt{2c(K_A)} \quad (4.2)$$

$$P_A = \frac{1}{2} K_A \gamma H^2 \quad (4.3)$$

Besides static stability, the reinforced zone also experiences a dynamic soil thrust at the back additionally inertial forces within the fill are generated during seismic activity. P_{AE} can be calculated using the dynamic earth pressure coefficient (K_{AE}) (see Equation 4.4 and Equation 4.5). The total active trust (P_{AE}) consists of the static (P_A), and dynamic (ΔP_{AE}) components (see Equation 4.6). The effect of the inertia is reflected by horizontal and vertical components: $a_h = k_{h.}g$, $a_v = k_{v.}g$ in pseudostatic-analysis. k_h and k_v are the horizontal and vertical pseudostatic seismic coefficients respectively and g is the gravitational acceleration. The effect of the vertical acceleration on the seismic earth pressure is usually ignored and the P_{AE} can be written as (Kramer, 1996):

$$\mathrm{K_{AE}} = \frac{\cos^2(\phi - \theta - \psi)}{cos\psi \cos^2\theta \cos(\delta + \phi + \psi \left[1 + \sqrt{\frac{\sin(\delta + \phi)\sin(\phi - \beta - \psi)}{\cos(\delta + \phi + \psi)\cos(\beta - \phi)}}\right]^2} \quad (4.4)$$

$$P_{EA} = \frac{1}{2} K_{AE} \gamma H^2 (1 - k_v) \quad (4.5)$$

$$P_{AE} = \mathrm{P_A} + \Delta P_{AE} \quad (4.6)$$

This static component acts at about a distance of H/3 from the bottom of the wall and the dynamic component acts about 0.6 H from the bottom of the wall, and hence the total active thrust acts about mid-height of the wall. The forces acting on the MSE wall in the dynamic case is shown in Figure 4.1.

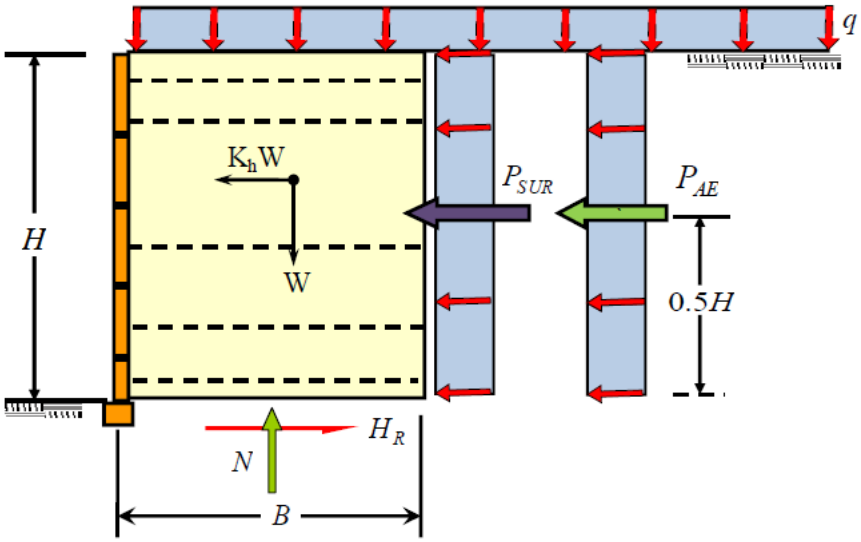


Figure 4.1. An MSE Wall cross-section with seismic forces (Kavazanjian *et al.*, 2011).

MSE Walls have to be designed to sustain both external and internal stability against static and seismic loading conditions (Kramer, 1996).

4.3. External Stability of MSE Wall

Reinforced walls' external stability evaluation is similar to gravity walls. The factor of safety against sliding, limiting eccentricity (base overturning), and bearing is needed to be calculated to obtain external stability (see Figure 4.2). It is assumed that MSE Walls' facing and reinforced soil behave coherently as a rigid body (Berg *et al.*, 2009).

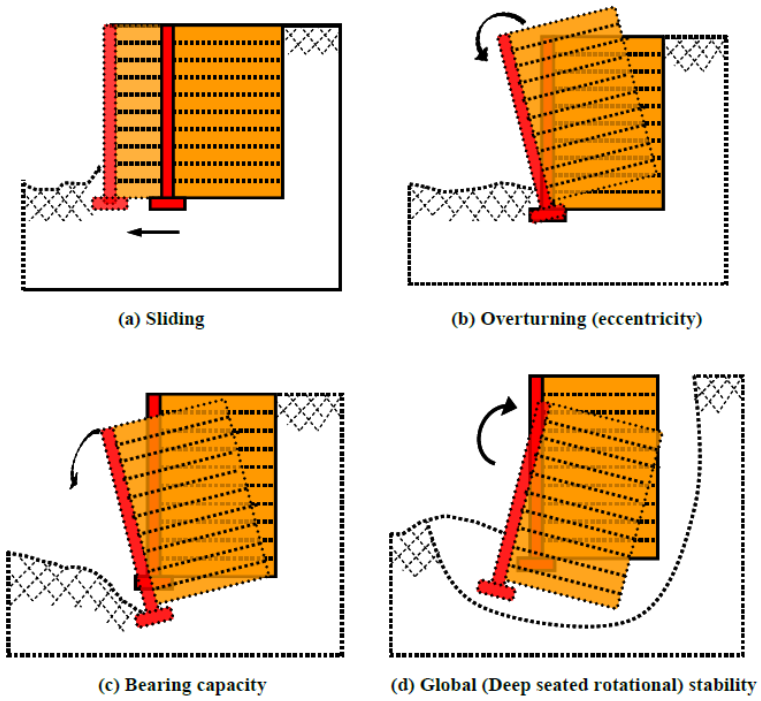


Figure 4.2. External failure mechanisms for MSE Walls: (a) Sliding (b) Limiting eccentricity (c) Bearing (d) Deep seated failure (Kavazanjian *et al.*, 2011).

4.3.1. Base Sliding

The factor of safety (FS) against base sliding is defined as the ratio of the sum of resisting forces (vertical) (ΣF_R) to sum of the driving forces (horizontal) (ΣF_d) (see Equation 4.7) (Das, 2007).

$$FS_{sliding} = \frac{\Sigma F_R}{\Sigma F_d} \qquad (4.7)$$

In addition to the weight of the backfill soil, it is significant to consider the adhesion between the foundation soil and the bottommost reinforcement placed in MSE Wall as one of the resisting forces. Driving forces are considered as the horizontal component of the active earth pressure and horizontal effect of surcharge load.

4.3.2. Limiting Eccentricity (Base Overturning)

Base overturning's factor of safety is expressed as the ratio of the sum of resisting moments (ΣM_R) to the sum of driving moments (ΣM_D). Moments are taken about the toe of the wall to calculate the FS (see Equation 4.8) (Das, 2007).

$$FS_{overturning} = \frac{\Sigma M_R}{\Sigma M_D} \quad (4.8)$$

4.3.3. Bearing Capacity

Bearing capacity of an MSE Wall can be calculated using the traditional bearing capacity equations used for foundations. The factor of safety for bearing capacity is expressed as the ratio of ultimate bearing capacity (q_{ult}) to the stresses acting at the foundation level, (q), that is the base of the MSE Wall in this case (see Equation 4.9). Equations for q_{ult} and q are shown in Equation 4.10 and Equation 4.11. B' value used in Equation 4.10 is the effective length of the foundation (see Equation 4.12). In Equation 4.13, B stands for the foundation width, M_{net} stands for net moment which is the difference of the resisting moments ($\Sigma(M_R)$) and driving moments ($\Sigma(M_D)$), e stands for eccentricity, ΣV stands for total of the vertical forces which is the sum of the vertical weight and the vertical component of the P_A. Table 4.1 shows bearing capacity factors (N_c, N_q, N_γ) for the calculation of q_{ult}; however, N_q is the embedment term and it is naturally eliminated for MSE Walls (Berg *et al.*, 2009; Das, 2007).

$$FS_{bc} = \frac{q_{ult}}{q} \quad (4.9)$$

$$q_{ult} = c * N_c + q * N_q + 0.5 * \gamma * B' * N_\gamma \quad (4.10)$$

$$q = \gamma_{backfill} * H + c_{foundation} \quad (4.11)$$

$$B' = L - 2 * e \quad (4.12)$$

$$e = \frac{B}{2} - \frac{Mnet}{\Sigma V} \quad (4.13)$$

Table 4.1. Bearing capacity factors: N_c, N_q, and N_γ (Berg *et al.*, 2009)

∅	N_c	N_q	N_γ	∅	N_c	N_q	N_γ
0	5.14	1.0	0.0	23	18.1	8.7	8.2
1	5.4	1.1	0.1	24	19.3	9.6	9.4
2	5.6	1.2	0.2	25	20.7	10.7	10.9
3	5.9	1.3	0.2	26	22.3	11.9	12.5
4	6.2	1.4	0.3	27	23.9	13.2	14.5
5	6.5	1.6	0.5	28	25.8	14.7	16.7
6	6.8	1.7	0.6	29	27.9	16.4	19.3
7	7.2	1.9	0.7	30	30.1	18.4	22.4
8	7.5	2.1	0.9	31	32.7	20.6	25.9
9	7.9	2.3	1.0	32	35.5	23.2	30.2
10	8.4	2.5	1.2	33	38.6	26.1	35.2
11	8.8	2.7	1.4	34	42.2	29.4	41.1
12	9.3	3.0	1.7	35	46.1	33.3	48.0
13	9.8	3.3	2.0	36	50.6	37.8	56.3
14	10.4	3.6	2.3	37	55.6	42.9	66.2
15	11.0	3.9	2.7	38	61.4	48.9	78.0
16	11.6	4.3	3.1	39	37.9	56.0	92.3
17	12.3	4.8	3.5	40	75.3	64.2	109.4
18	13.1	5.3	4.1	41	83.9	73.9	130.2
19	13.9	5.8	4.7	42	93.7	85.4	155.6
20	14.8	6.4	5.4	43	105.1	99.0	186.5
21	15.8	7.1	6.2	44	118.4	115.3	224.6
22	16.9	7.8	7.1	45	133.9	134.9	271.8

4.4. Internal Stability of MSE Wall

To perform the internal stability of the MSE Wall, it is sufficient to determine the reinforcement length in addition to the engineering properties of backfill and foundation soils. Internal (also known as local) stability checks are related to the tension and pull-out

resistance in the reinforcements, and therefore it is important to determine other properties of reinforcements such as stiffness, tensile strength, and spacing. Completeness of internal stability also involves ensuring the integrity of the facing elements. Rankine failure surface is considered for the internal stability check for extensible reinforcements (such as geogrid used in this study) as they are capable of elongating more than soils (see Figure 4.3) (Berg *et al.*, 2009).

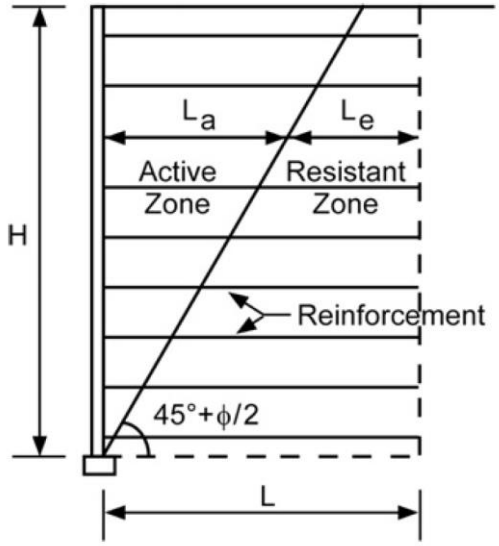


Figure 4.3. Potential failure surface for internal stability design of MSE Walls (Bilgin, 2009).

Two important mechanisms are considered for the internal failure modes of MSE Walls (see Figure 4.4). The first failure is named as "failure by elongation or breakage of the reinforcements" which occurs when the tensile forces in the reinforcements arise more than their capacity. This generally results in elongation or breakage of reinforcements. The second failure is named as "failure by pullout". In this type of failure, the tensile forces in the reinforcement are greater than the pullout resistance, which is related to the friction between the reinforcement and the soils. Both failures can result in large deformations of the wall and possible failure of the structure (Berg *et al.*, 2009). In addition to pullout and bond breakage failure of the facing elements can also be considered as an internal failure type as it involves connections. Especially for seismic conditions, the integrity of the facing elements is also checked. The failure shape and movement of the wall will be different for each (see Figure 4.4) (Berg *et al.*, 2009).

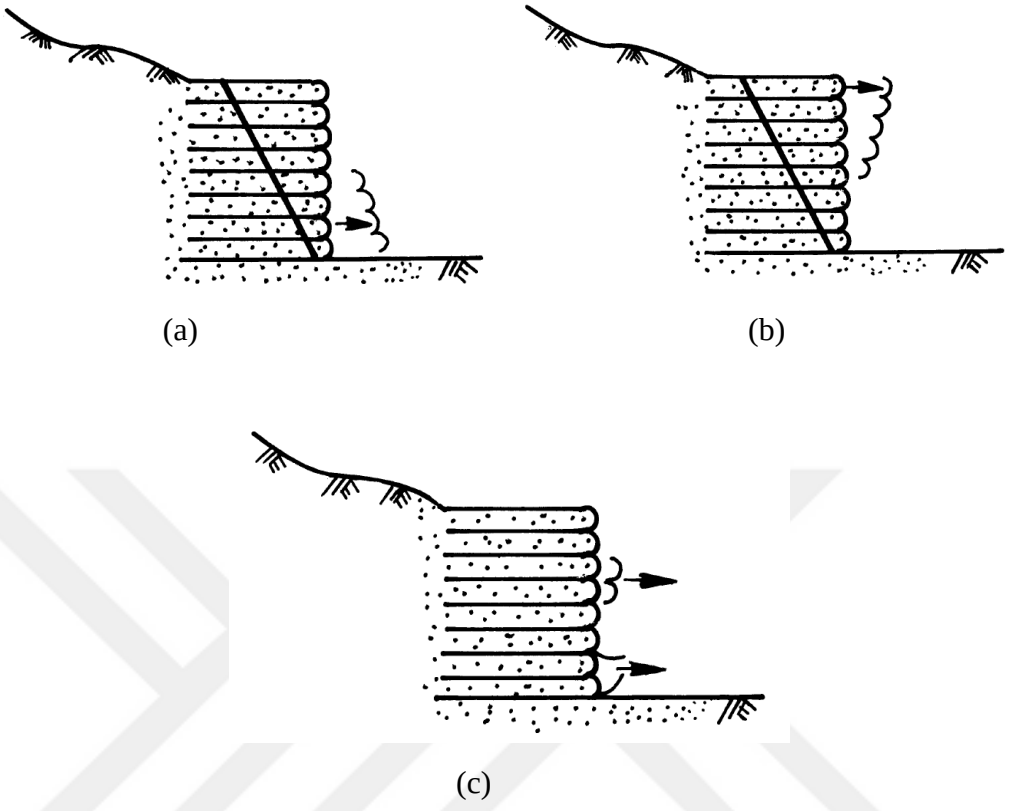
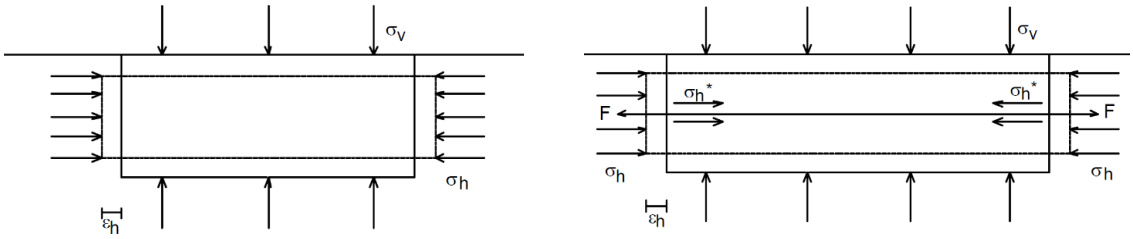


Figure 4.4. Internal failure mechanisms for MSE Walls: (a) Geosynthetic rupture (b) Geosynthetic pullout (c) Connection (and/or facing elements) failure (Shukla & Yin, 2006).

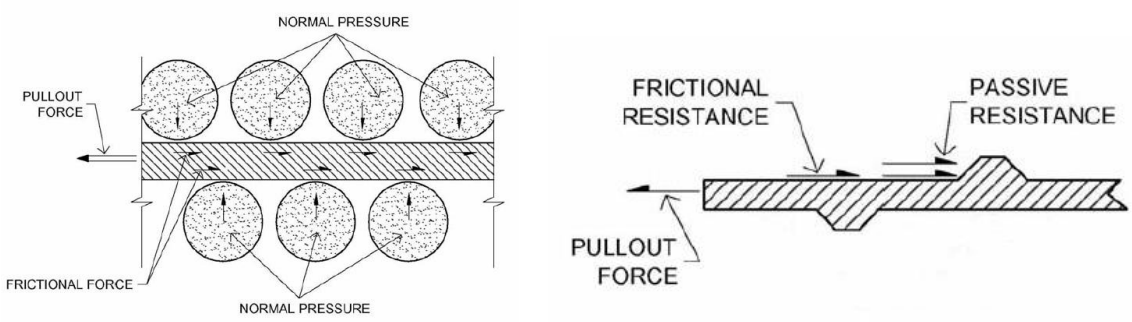
On the other hand, understanding of basic principles of MSE Wall has a significance to estimate the wall behavior. Figure 4.5 shows an illustration of soil element undergoing a horizontal deformation ε_h under horizontal stress σ_h. The weight of everything above the soil element and all of the external vertical loads causes the vertical effective stress σ'_v. As a result of it σ'_h and ε_h is generated. This deformation does not occur only at soil in MSE Walls, geosynthetic materials laid in soil also deforms. This formation prevents the structure from further failures by creating horizontal confinement that can resist the horizontal forces. As it is illustrated in Figure 4.5, geosynthetic materials undergo tensile deformations and the tensile strength in the reinforcement produces horizontal stress σ_h^*. Thus, reinforcements take the stresses and strains on the soil (Enunlu, 2007).



(a) (b)

Figure 4.5. Stresses and strains in (a) an unreinforced and (b) reinforced soil element (Enunlu, 2007).

Two stress transfer mechanism exists between soil and reinforcement (See Figure 4.6). The first mechanism is the friction that develops between soil and the reinforcement surface at the points when the shear displacement and the corresponding shear stress occur. Since uniaxial reinforcing elements can mostly bear stress in one direction, they should be placed according to their bearing direction. Secondly, on transverse reinforcement surfaces, the bearing type stresses generate passive resistance (Berg *et al.*, 2009).



(a) (b)

Figure 4.6. Stress transfer mechanisms for soil reinforcement (a) Frictional stress transfer (b) Bearing and frictional resistance (Berg *et al.*, 2009).

4.4.1. Sizing for Internal Stability

Preliminary design of the reinforcement mainly consists of the reinforcement length and spacing determination. It can be performed considering the possible internal failure mechanisms. Evaluating the location of the critical surface and the maximum tension forces

both along the reinforcements and at the connection points are important (Berg *et al.*, 2009). For internal stability calculations, coefficient of at-rest earth pressure (K_0) is used. K_0 can be calculated using the relation for normally consolidated soils (Jaky, 1944) (see Equation 4.14) (Das, 2007).

To check the internal stability against reinforcement breakage, the maximum load in the reinforcements (T_{max}) is calculated (see Equation 4.15). The horizontal stresses (σ_h) are calculated and surcharge load are also considered in the calculation. T_{max} in the reinforcements is compared with the allowable tensile force per unit width of reinforcement (T_a) to check against the reinforcement breakage (Berg *et al.*, 2009).

$$K_0 = 1 - sin\phi \quad (4.14)$$

$$T_{max} = \sigma_h \, S_v \quad (4.15)$$

To determine the reinforcement length, the formulation in Equation 4.16 is used. The formulation is the summation of the effective length (L_e) and length within the Rankine failure zone (L_r). Equations for L_r and L_e are given respectively in Equation 4.17 and Equation 4.18. The minimum value for L_e is generally considered as 1 m in the calculations (See Figure 4.2.) (Berg *et al.*, 2009; Das, 2007; Koerner, 2005).

$$L = L_r + L_e \quad (4.16)$$

$$L_r = (H - z) * \tan(45 - \frac{\phi}{2}) \quad (4.17)$$

$$L_e = \frac{S_v * \sigma_h * FS}{2 * (c + \gamma * z * tan\delta)} \quad (4.18)$$

In addition to the weight of the backfill soil, it is significant to consider the adhesion between the foundation soil and the bottommost reinforcement placed in MSE Wall as one of the resisting forces. Driving forces are considered as the horizontal component of the active earth pressure and horizontal effect of surcharge load.

4.5. Design Requirements

FHWA recommends external and internal stability LRFD (Load Resistance Factor Design) resistant factors which are provided by AASHTO (see Table 4.2 and Table 4.3). Minimum design requirements and the recommended factor of safety values for segmental retaining walls under static and dynamic loading conditions are published by the National Concrete Masonry Association (NCMA) (see Table 4.4). A 25% reduction of the static FS values are recommended for the dynamic cases.

Table 4.2. Resistance factors for internal resistance for MSE Walls (Berg *et al.*, 2009).

Reinforcement Type and Loading Condition			Resistance Factor
Metallic reinforcement and connectors	Strip reinforcements [A]		
		Static loading	0.75
		Combined static/earthquake loading	1.00
		Combined static/traffic barrier impact [B]	1.00
	Grid reinforcements [A, C]		
		Static loading	0.65
		Combined static/earthquake loading	0.85
		Combined static/traffic barrier impact [B]	0.85
Geosynthetic reinforcement and connectors		Static loading	0.90
		Combined static/earthquake loading	1.20
		Combined static/traffic barrier impact [B]	1.20
Pullout resistance of tensile reinforcement (metallic and geosynthetic)		Static loading	0.90
		Combined static/earthquake loading	1.20
		Combined static/traffic barrier impact [B]	1.00

Notes:

A. Apply to gross cross-section less sacrificial area. For sections with holes, reduce gross area in accordance with AASHTO (2007) Article 6.8.3 and apply to net section less sacrificial area.
B. Combined static/traffic barrier impact resistance factors are not presented in AASHTO.
C. Applies to grid reinforcements connected to rigid facing element, e.g., a concrete panel or block. For grid reinforcements connected to a flexible facing mat or which are continuous with the facing mat, use the resistance factor for strip reinforcements.

Table 4.3. External stability resistance factors (Berg *et al.*, 2009).

Stability Mode	Condition	Resistance Factor
Bearing Resistance	-	0.65
Sliding	-	1
Overall (global) Stability	Where geotechnical parameters are well defined, and the slope does not support or contain a structural element	0.75
	Where geotechnical parameters are based on limited information, or the slope contains or supports a structural element	0.65

Table 4.4. Minimum design requirements for Segmental Retaining Walls (National Concrete Masonry Association (NCMA), 2016).

Minimum Safety Factor	Static	Dynamic (Seismic)
Sliding (Base/Internal)	1.5	75% of Static
Overturning	2.0	75% of Static
Geogrid Overstress	1.5	75% of Static
Pullout from Soil/Block	1.5	75% of Static
Internal Compound Stability	1.3	1.1
Global Stability	1.3	1.1
Bearing Capacity	2.0	75% of Static
Additional Detailing Criteria		
Minimum Reinforced Zone Width	60% of Wall Height (H)	60% of Wall Height (H) for Bottom and Middle Layers; 90% of Wall Height (H) for Upper Layers
Minimum Wall Embedment	6 inches (152 mm)	6 inches (152 mm)
Minimum Anchorage Length	12 inches (305 mm)	12 inches (305 mm)
Maximum Wall Batter	20 degrees	16 inches (406 mm)

4.6. Static Stability of the MSE Wall Model

Preliminary stability analysis of the MSE model was performed prior to the FEM analyses. An Excel calculation spread sheet was prepared to obtain the factor of safety values for the external and internal stability of the wall.

The analysis was performed for the wall with height (H) of 8 m. The dry unit weight (γ_{dry}) was taken as 18 kN/m^3 for the backfill (granular) soil and 17 kN/m^3 for the natural (foundation) soil. Cohesion (c) was considered as 1 kN/m^2 for backfill, and 100 kN/m^2 for foundation soil. Friction angle (ϕ) was taken as 34° for backfill, and 20° for foundation soil. In addition, adhesion between the foundation soil and the reinforcement was estimated as 0.80 times of the cohesion of the foundation soil. Friction angle (δ) between the backfill soil and reinforcement was considered as 0.80 times of the backfill soil' s ϕ. δ between the foundation soil and reinforcement was taken as 0.95 times of foundation soil' s ϕ. Additionally, an external (dead) load (q) of 12 kN/m^2 was considered along the approximate reinforced soil zone (when L/H is 0.7, it is 5.6 m).

The external and internal stability checks of 8 m tall MSE Wall models with L/H ratios of 0.5, 0.7 and 1 were performed. The results of the external and internal stability of the L/H= 0.7 case is provided below:

4.6.1. External Stability Check

Rankine's lateral earth pressure theory was utilized to calculate the active earth pressures to perform external stability analysis for preliminary design. The calculated earth pressure loads, FS for sliding, overturning and bearing capacity failures are presented in Tables 4.5, Table 4.6, Table 4.7 and Table 4.8, respectively.

Table 4.5. Earth pressures on the model.

Name	Symbol	Unit	Value
Coefficient of Active Earth Pressure	K_A	-	0.283
Active Earth Pressure Resultant	P_A	kN/m	162.84
Vertical (Vert.) Component of P_A	P_A Vert.	kN/m	91.06
Horizontal (Hor.) Component of P_A	P_A Hor.	kN/m	135.00

Table 4.6. The factor of safety against sliding.

Name	Symbol	Unit	Value
Total Resisting (Vert.) Force	$\Sigma(F_R)$	kN/m	748.81
Total Driving (Hor.) Force	$\Sigma(F_D)$	kN/m	162.14
Factor of Safety	$FS_{sliding}$	-	4.62

Table 4.7. The factor of safety against overturning.

Name	Force	Unit	Moment Arm	Unit	Moment	Unit
Vertical Weight	806.40	kN/m	2.80	m	2257.92	kN
P_A Vertical Component	91.06	kN/m	5.60	m	509.94	kN
$\Sigma(M_R)$					2767.86	kN
Name	**Force**	**Unit**	**Moment Arm**	**Unit**	**Moment**	**Unit**
P_A Hor. Component	135.00	kN/m	2.67	m	360.01	kN
$\Sigma(M_D)$					360.01	kN
Name					**Value**	**Unit**
$FS_{overturning}$					7.69	-

Table 4.8. The factor of safety against bearing capacity failure.

Name	Symbol	Unit	Value
Ultimate Bearing Capacity	q_{ult}	kN/m^2	1726.30
Active Bearing Capacity	q	kN/m^2	180.36
Factor of Safety	FS_{bc}	-	9.57

4.6.2. Internal Stability Check

To carry out the internal stability checks for the preliminary model design, K_0 is calculated as 0.441 for the backfill soil (see Equation 4.11). To check the internal stability against reinforcement breakage, σ_h values are calculated to estimate the load in the reinforcements. By using the equation for T_{max} (see Equation 4.12) and considering the values obtained in Table 4.9 and Table 4.10, it is found that no reinforcement breakage occurs when allowable tensile force per unit width of reinforcement (T_a) is taken as 60 kN/m and factor of safety as 1.3 for the calculation.

Appropriate reinforcement spacing and length is required for pull-out calculation. Table 4.9 shows the reinforcement spacing selection corresponding to the layer depth (z) and Table 4.10 shows the reinforcement length calculation for the preliminary design (see Table 4.10).

Table 4.9. Design of reinforcement spacing.

z (m)	σ_h (kPa)	S_v (m)	Selected S_v (m)
8	68.77	0.67	0.4
7	60.83	0.76	0.4
6	52.90	0.87	0.4
5	44.96	1.03	0.4
4	37.03	1.25	0.4
3	29.09	1.59	0.4
2	21.16	2.18	0.4
1	13.22	3.49	0.4
Total Reinforcement			20

For pullout resistance, FS is taken as 1.3 in determining the reinforcement length. Based on the preliminary design, the appropriate reinforcement lengths are found in 1- 5.04 m range for the 8- m high wall which has 0.4 m vertical reinforcement spacing. For simplicity, in FEM analysis L/H ratio is taken as 0.5, 0.7 and 1.0.

Table 4.10. Design of reinforcement length

Layer Nr.	Selected S_v (m)	z (m)	σ_h (kPa)	L_e (m)	Le_{min} (m)	L_r (m)	L (m)	L_{used} (m)
20	0.4	0.40	8.46	0.47	1	4.04	5.04	5.6
19	0.4	0.8	11.64	0.36	1	3.83	4.83	5.6
18	0.4	1.2	14.81	0.32	1	3.62	4.62	5.6
17	0.4	1.6	17.98	0.30	1	3.40	4.40	5.6
16	0.4	2.0	21.16	0.28	1	3.19	4.19	5.6
15	0.4	2.4	24.33	0.27	1	2.98	3.98	5.6
14	0.4	2.8	27.51	0.27	1	2.76	3.76	5.6
13	0.4	3.2	30.68	0.26	1	2.55	3.55	5.6
12	0.4	3.6	33.85	0.26	1	2.34	3.34	5.6
11	0.4	4.0	37.03	0.25	1	2.13	3.13	5.6
10	0.4	4.4	40.20	0.25	1	1.91	2.91	5.6
9	0.4	4.8	43.38	0.25	1	1.70	2.70	5.6
8	0.4	5.2	46.55	0.25	1	1.49	2.49	5.6
7	0.4	5.6	49.72	0.24	1	1.28	2.28	5.6
6	0.4	6.0	52.90	0.24	1	1.06	2.06	5.6
5	0.4	6.4	56.07	0.24	1	0.85	1.85	5.6
4	0.4	6.8	59.24	0.24	1	0.64	1.64	5.6
3	0.4	7.2	62.42	0.24	1	0.43	1.43	5.6
2	0.4	7.6	65.59	0.24	1	0.21	1.21	5.6
1	0.4	8.0	68.77	0.24	1	0.00	1.00	5.6

4.7. Previous Studies on MSE Walls

Many numerical modeling studies were carried out on MSE Walls; however, only a few of them were verified with shaking table test results.

Since 2005, many researchers studied MSE Wall earthquake behavior using shaking tests. Latha & Santhanakumar (2015) indicated that the performance of modular block walls is better than rigid faced walls. Additionally, they showed that the acceleration amplification factor is not equal along the wall also mentioned that the frequency of the input ground motion may have an effect on the behavior of the wall (Latha & Santhanakumar, 2015). Panah *et al.* (2015) suggested the use of extensible reinforcements against the possible acceleration amplification through the wall (Panah, Yazdi, & Ghalandarzadeh, 2015). Wang

et al. (2015) suggested considering far or mid far-field earthquakes for the seismic design of MSE Walls (Wang, Chen, & Chen, 2015). Latha & Krishna (2008) observed that the walls constructed with backfills of higher relative density show fewer face deformations, but also higher acceleration amplifications at stronger seismic loading (Latha & Krishna, 2008). El-Emam & Bathurst (2007) indicated that an increase in the reinforcement length, stiffness, and decrease in the vertical spacing, decreases the horizontal displacements of the wall. Additionally, their study indicated that reinforcement connection loads are related inversely with reinforcement length and spacing; however directly with stiffness. This study also indicated that increasing the reinforcement length and vertical spacing, decreases the acceleration amplification and the critical acceleration value has an influence on the increase of the amplification factor (El-Emam & Bathurst, 2007). The study by Ling *et al.* (2005) showed that the maximum horizontal displacement is observed at the top of the MSE Wall under seismic loading and it is indicated that the design methods proposed by FHWA and NCMA are not adequate against seismic loading (Ling, Mohri, *et al.*, 2005). Anastasopoulos *et al.* (2010) performed a study comparing the results from the ABACUS model utilizing a modified kinematic hardening soil model with a shaking table test result. It is indicated that similar results are obtained in both shaking table and numerical test in terms of residual displacements which develop at larger intensity excitations and active failure wedge develops entirely only at greater excitations with strong cycles. (Anastasopoulos, Georgarakos, Georgiannou, Drosos, & Kourkoulis, 2010; Vieira, 2017).

A number of numerical studies on the analysis of MSE Walls performed in the last decade. El-Emam *et al.* (2004) deduced that a simple elastic-plastic soil model can be enough to conduct analysis for the seismic behavior MSE Walls' in FLAC (El-Emam, Bathurst, & Hatami, 2004). El-Emam *et al.* (2001) and Zarnani *et al.* (2011), conducted studies using FLAC and they mentioned that the size of soil failure zone and reinforcement anchorage lengths are not properly modeled using pseudo- static seismic methodologies (El-Emam, Bathurst, Hatami, & Mashhour, 2001; Zarnani, El-Emam, & Bathurst, 2011). Fakharian & Attar (2007) indicated that axial forces on the reinforcements are overestimated using active earth pressure theories (Fakharian & Attar, 2007). Bhattacharjee & Krishna (2015) observed that displacements at the backfill are related inversely with the stiffness of the wall (Bhattacharjee & Krishna, 2015). Krishna & Latha (2011) indicated that the seismic behavior of the MSE Wall is enhanced when the backfill has higher friction and dilation

angle. They also indicated that the soil- reinforcement interaction influences the seismic behavior of the wall more than the reinforcement stiffness does (Krishna & Latha, 2011). Burke (2003) indicated in the study that damping properties given in the numeric calculation is important to understand the seismic behavior of the walls (Burke, 2003). Ling *et al.* (2004) observed that acceleration amplification is not influenced significantly by the reinforcement layout; however, displacements of the reinforcements are affected by the reinforcement length and arrangement (Ling, Liu, Kaliakin, & Leshchinsky, 2004). In the research of Ling *et al.* (2005), it was observed that settlement of the wall crest is developed more on the rear end of the top reinforcement. It was also seen that vertical spacing influenced the acceleration amplification more than reinforcement length. However, this is affected mostly by soil behavior and earthquake motions (Ling, Liu, & Mohri, 2005). Ling *et al.* (2010) remarked the importance of Rayleigh parameters that the damping ratio of 15% is suggested for the models with a maximum acceleration of 0.4g, and 5% for 0.8g (Ling, Yang, Leshchinsky, Liu, & Burke, 2010; Vieira, 2017).

5. NUMERICAL MODELING OF AN 8- M HEIGHT MSE WALL USING PLAXIS

5.1. Introduction

Numerical modeling can be used for analyzing and understanding the seismic behavior of MSE Wall. One of the most preferred methods is the Finite Element Method (FEM) which provides approximate solutions to boundary value problems by iteration processes. It helps to analyze complex models to get approximate solutions by estimating the response of physical structures under external loads. As MSE Walls have a complex system of soil-structure interaction, FEM analysis of MSE Walls have also increased drastically with the development of more advanced FEM tools. FEM analysis provides more information related to deformations and axial forces developed on the reinforcements when it is compared with traditional limit equilibrium methods (Enunlu, 2007).

PLAXIS is one of the commercial computer programs utilizes FEM. It was developed in 1987 at Delft University of Technology. It is firstly used for the finite element analysis of river embankments. Now it has 2D and 3D versions and uses the FEM for the calculations of the plane strain and axisymmetric models. Since those times, it has been used widely in the academia and industry. PLAXIS is preferred for many analyses in the broad horizons of geotechnical engineering, especially for deformation analysis, stability checks and groundwater flow (Brinkgreve, Kumarswamy, Swolfs, Zampich, & Ragi Manoj, 2019).

With the recent versions, it is possible to model the material with various material models such as Linear Elastic, Mohr-Coulomb, Hardening Soil, and Modified Cam-Clay, etc. The material models are defined inside the areas which are bounded by lines. These areas are identified as clusters, and with the composition of clusters, finite element meshes are generated automatically. During the calculation, the mesh is created with many triangles and the mesh is identified with elements, nodes, and stress points. It is possible to generate the mesh either with 6 or 15 node-elements. 6 nodes define a 6-node element and 3 stress points (see Figure 5.1), on which stresses are calculated during FEM analyses. However, displacements are calculated by the second order interpolation (Aslan, 2007).

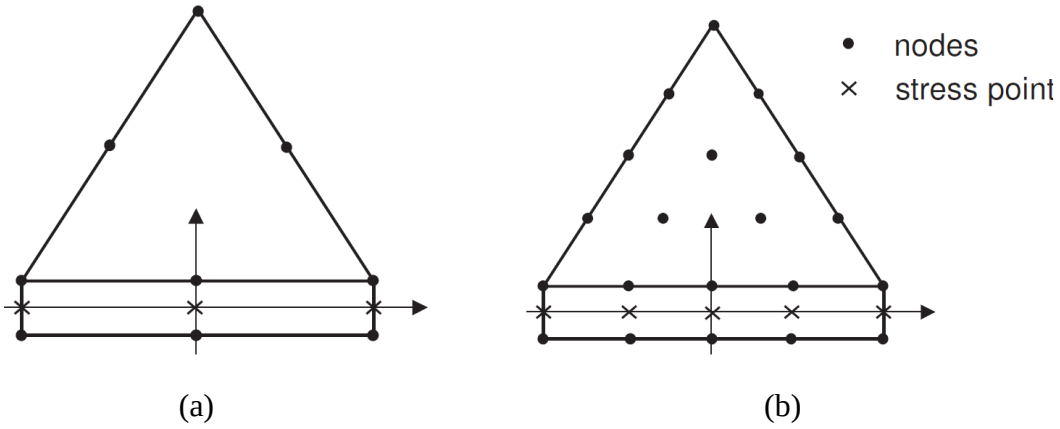


Figure 5.1. Nodes and stress distribution: (a) 6- node (b) 15- node soil elements (Brinkgreve, 2019b).

5.2. PLAXIS Version and Units

MSE Wall models were prepared in the well-known two-dimensional finite element program PLAXIS 2D version 8.6 for this study. The units used in the model study were presented in Table 5.1. Plane strain model was used due to the uniform cross-sectional geometry and loading scheme (with corresponding stress state) perpendicular to the cross-section (z-direction). Displacements and strains were estimated as zero in the z-direction. A satisfactory number of 6-noded triangular elements were used in this study. A sensitivity analysis was performed considering both 6-noded and 15-noded triangular elements. For this standard deformation analysis, the 6-noded elements provided similar results with 15-noded elements with minimal computation time. Therefore the parametric study was proceeded with 6-noded elements (Brinkgreve). The main goal of the parametric study was to determine the effects of the reinforcement length/ wall height (L/H) ratio, reinforcement stiffness (EA), and vertical spacing of reinforcement (S_v) under various harmonic earthquake input ground motions.

Table 5.1. Units used.

Type	**Length**	**Force**	**Time**
Unit	m	kN	day

5.3. Model Dimensions

MSE models had a foundation depth (F_d) of 15 m, and the distance in front of the reinforced fill (F_w) was about 40 m. Various MSE Walls were modeled with various reinforcement design parameters of reinforcement length, reinforcement stiffness, and reinforcement vertical spacing. Models were created with Reinforcement Length (L) / Wall Height (H) ratios (L/ H) of 0.5, 0.7 and 1.0. The models were created with two vertical spacing (S_v) values 0.4 m and 0.6 m. The model dimensions of 8-meter height MSE Wall with 5.6 m-long reinforcement (L/H= 0.7) are provided as an example in Figure 5.2.

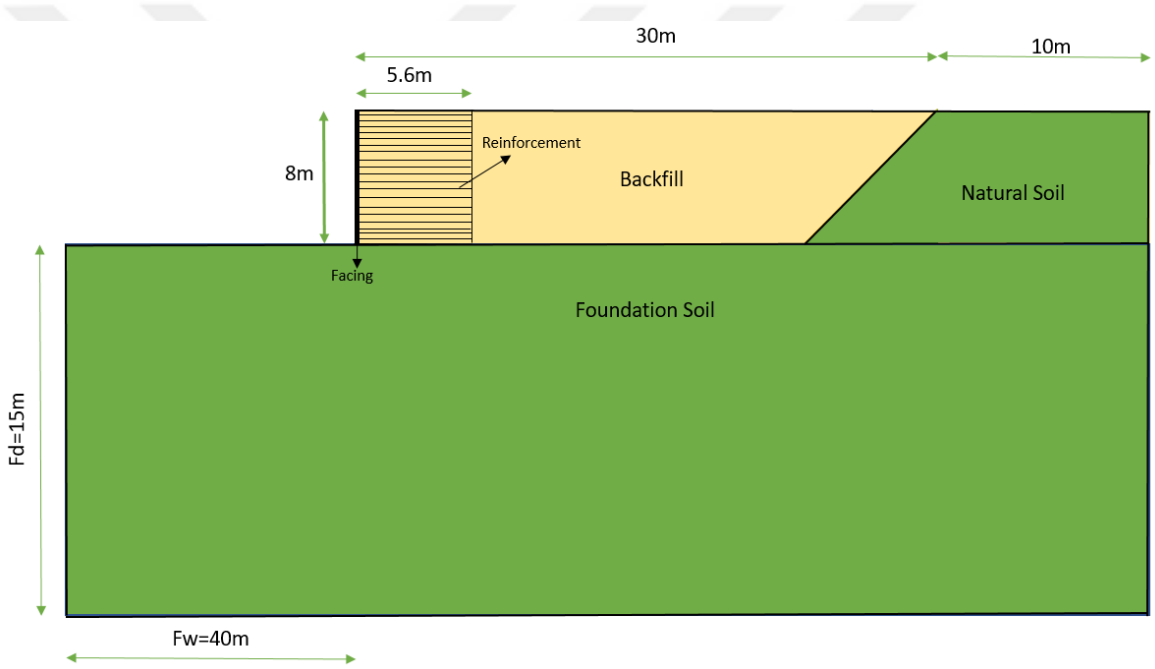


Figure 5.2. Preliminary design of 8 meters high MSE Wall.

Examples of other models analyzed are introduced later in detail. In addition to these geometric variations, two different reinforcement strength values (EA = 600 kN/ m and EA =1200 kN/ m) were used in the models. Each model was excited with, seven (7) different harmonic input ground motions. A total of 84 analyses were performed for this study for 8 meter- height MSE Wall.

During the constitution of the FEM models, the model's geometry is created first. The model is designed by defining points and lines. Clusters are automatically generated by the

program when a confined area is formed by the input points and lines. The next step is material modeling in which material properties are determined, and the clusters are assigned to the constituted soils. For each cluster, the soil is created as homogenous. Afterward, the structural elements such as geogrids and distributed loads are defined (Brinkgreve).

5.4. Material Modeling

5.4.1. Modeling of Soils

Soils and rocks' mechanical behavior can be modeled using various material models PLAXIS. Basic elastic parameters are Young's Modulus (E) and Poisson's ratio (ν). However, these are not sufficient to define soil behavior. Mohr- Coulomb model can be considered as the first order approximation of soil behavior. Properties like stress-dependency of stiffness, strain-hardening/softening, the memory of pre-consolidation, critical state, anisotropy, creep, swelling and shrinkage can only be defined with sophisticated material models. PLAXIS allows the user to choose among the linear elastic, Mohr- Coulomb, soft soil model, hardening soil model, HSsmall, modified Cam- clay, soft soil creep model, and jointed rock models. It is also possible to create more complex user-defined models using PLAIXS as well (Brinkgreve, 2019a).

The hardening soil material model was used for all soils defined in this study. Hardening soil model is a complex soil model in which it is possible to define three different stiffness parameters. In this regard, the hardening soil model is different from the Mohr-Coulomb material model as it allows more advanced definition of soil stiffness. These three stiffness parameters are: triaxial loading stiffness (E_{50}), the triaxial unloading stiffness (E_{ur}) and the oedometer loading stiffness (E_{oed}). It is suggested to take $E_{ur} \sim 3\ E_{50}$ and $E_{oed} \sim E_{50}$. Furthermore, the reference stress is determined as 100 kPa, which eliminates the stress-dependency of stiffness moduli (stiffnesses rise with effective stress increase). The equation regarding the oedometer conditions of stress and strain relationship is provided in Equation 5.1 (Brinkgreve, 2019a).

$$E_{oed} = E_{oed}^{ref}(\frac{-\sigma_1'}{p^{ref}})^m \quad (5.1)$$

There is a formulation of the Hardening Soil model that shows the hyperbolic relationship between the vertical axial strain (ε_1), and the deviatoric stress (q) in primary triaxial loading. Equation 5.2 illustrates the curves that are obtained from the standard drained triaxial tests. In this equation, q_a is the asymptotic value of the shear strength, E_i the initial stiffness which is related with E_{50} given in Equation 5.3 (Brinkgreve, 2019a).

Figure 5.3 shows the hyperbolic relationship between strains ε_1 and stresses q and the corresponding equation of the effective confining stress dependent stiffness modulus for primary loading parameter E_{50} is provided in Equation 5.4. In this equation, E_{50}^{ref} is reference stiffness modulus corresponding to the reference effective confining stress (p_{ref}). The minor principal stress, σ_3', is the confining pressure determines the actual stiffness, and is negative for compression. The power m indicates the degree of stress dependency. It is recommended that m is selected in the 0.5 to 1.0 range (Brinkgreve, 2019a).

$$\epsilon_1 = \frac{1}{E_i} \cdot \frac{q}{1 - \frac{q}{q_a}} \quad for\ q < q_f \quad (5.2)$$

$$E_i = \frac{2E_{50}}{2 - R_f} \quad (5.3)$$

$$E_{50} = E_{50}^{ref}(\frac{c\cos\varphi - \sigma_3'\sin\varphi}{c\cos\varphi - p_{ref}\sin\varphi})^m \quad (5.4)$$

The ultimate deviatoric stress (q_f) and the quantity (q_a) are defined in Equation 5.5 which is derived from the Mohr- Coulomb failure criterion and where σ_3' is generally negative. The plastic yielding occurs when the failure criterion, q=q_f is obtained. The failure ratio R_f is chosen as 0.9 (default setting).

$$q_f = (c\,\cot\varphi - \sigma_3')\frac{2\sin\varphi}{1-sin\varphi}\ and\ q_a = \frac{q_f}{R_f} \qquad (5.5)$$

Another stress-dependent stiffness modulus is defined for unloading-reloading stress paths given in Equation 5.6 in which E_{ur}^{ref} is the reference Young's modulus for unloading and reloading which corresponds to the p_{ref}. The default setting is $E_{ur}^{ref} \sim 3\ E_{50}^{ref}$.

$$E_{ur} = E_{ur}^{ref} = \left(\frac{c\cos\varphi - \sigma_3'\sin\varphi}{c\cos\varphi + p_{ref}\sin\varphi}\right)^m \qquad (5.6)$$

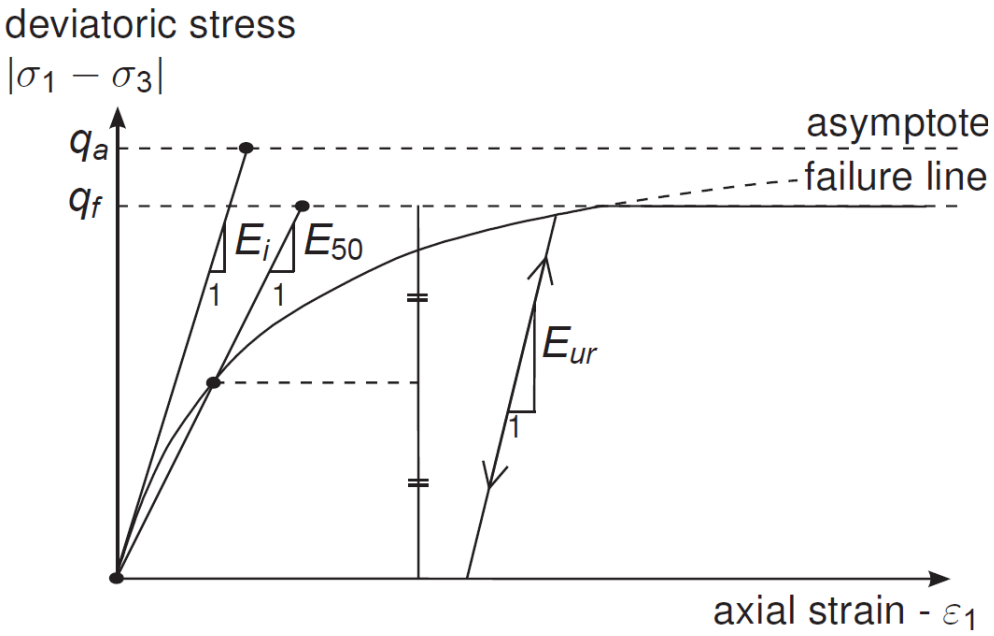


Figure 5.3. The relation of hyperbolic stress-strain in primary loading for a standard drained triaxial test (Brinkgreve, 2019a).

Besides using the hyperbolic stress-strain curve instead of a bi-linear curve, Hardening Soil model also has the superiority of the control of stress level dependency over Mohr-Coulomb model as the stiffness depends on the stress level for real soils. This also means that it is important to estimate stress levels. For a reference minor principal effective stress

of $-\sigma_3' = p_{ref}$, a stiffness modulus E_{50}^{ref}, is defined as the secant stiffness at 50 % of the maximum deviatoric stress, at a cell pressure equal to the reference stress p_{ref}, 100 kPa (see Figure 5.4) (Brinkgreve, 2019a).

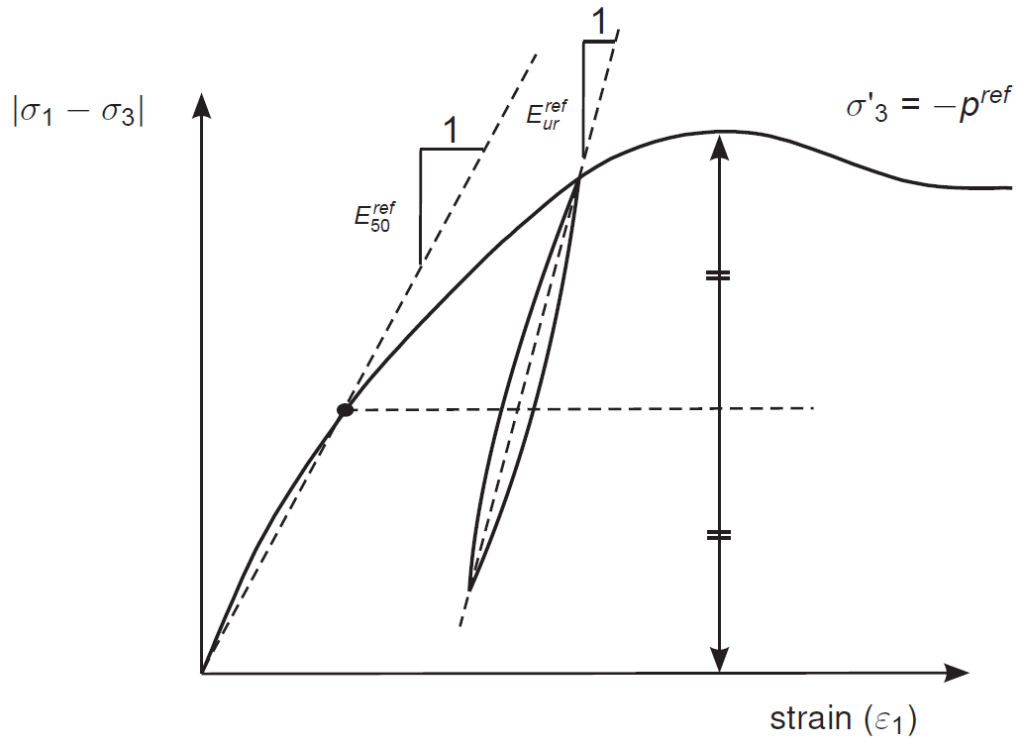


Figure 5.4. Definition of E_{50}^{ref} and E_{ur}^{ref} for drained triaxial test results.

In Hardening Soil model, it is possible to use E_{ur}, real elastic stiffness to obtain G_{ur}, elastic shear moduli from the Hooke's law of isotropic elasticity conversion, $E_{\mathrm{ur}} = 2\,(1+\nu)G_{ur}$. Despite the presence of this equation, the secant modulus E_{50} cannot be used for G_{50} calculation as E_{50} does not suit in an elasticity concept so there is not any conversion from E_{50} to G_{50} (Brinkgreve, 2019a).

For the elastoplastic Hardening Soil model, it is important to define E_{oed} (see Equation 5.7) as it is not possible to create a correlation between E_{oed} and E_{50} in contrast to elasticity based models. E_{oed} is a tangent stiffness modulus obtained from oedometer test, and E_{oed}^{ref} is a tangent stiffness at a vertical stress of $-\sigma_1' = \frac{-\sigma_3'}{K_0^{nc}} = p_{ref}$ where it is remarkable that as primary loading is considered σ_1' is used (see Figure 5.5) (Brinkgreve, 2019a).

$$E_{oed} = E_{oed}^{ref} = \left(\frac{c\cos\varphi - \sigma_1' \sin\varphi}{c\cos\varphi + p_{ref}\sin\varphi}\right)^m \quad (5.7)$$

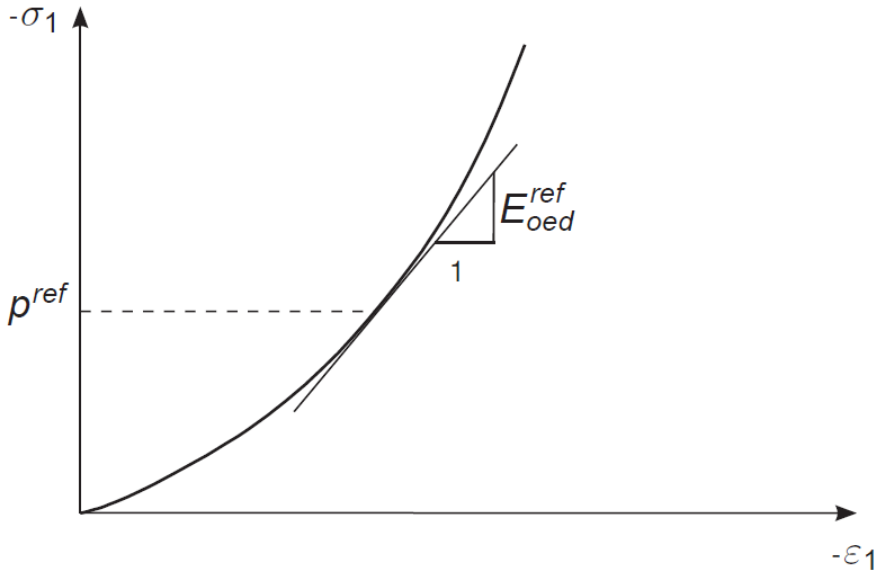


Figure 5.5. Definition of E_{oed}^{ref} in oedometer test results.

The input parameters for the hardening soil model are:

- m: Stress dependent stiffness according to a power law (Power for stress-level dependency of stiffness),
- E_{50}^{ref}: Plastic straining due to primary deviatoric loading (Secant stiffness in standard drained triaxial test),
- E_{oed}^{ref} : Plastic straining due to primary compression (Tangent stiffness for primary oedometer loading),
- E_{ur}^{ref} : Unloading/ reloading stiffness,
- ν_{ur}: Poisson's ratio for unloading- reloading,
- c, φ, and ψ: Failure according to the Mohr- Coulomb model,
- p_{ref}: Reference stress for stiffness,
- K_0^{nc} : Ko- value for normal consolidation.
- R_f : Failure ratio q_f / q_a,
- σ^t: Tension cut-off and tensile strength (Brinkgreve, 2019a).

In this study, two types of soils are defined: backfill soil, and natural soil. They are both modeled with Hardening Soil Material Model. In the Model, backfill soil is used in the reinforced zone and the backward area of the reinforced zone of the wall. FHWA recommends an upper limit of 34° for the internal friction of the reinforced zone unless there is a triaxial or direct shear test result. For his reason, 34° was selected for the internal friction angle of the reinforced zone. The soil parameters used in the model are provided in Table 5.2 (Berg *et al.*, 2009).

Table 5.2. Material properties of soils in PLAXIS model.

Title	**Material Properties**	**Symbol**	**Unit**	**Backfill Soil (Granular)**	**Natural Soil (Foundation)**
General	Model	-	-	Hardening Soil	Hardening Soil
	Unit Weight (dry)	γ_{dry}	kN/m^3	18	17
Strength	Cohesion	c_{ref}	kN/m^2	1	100
	Angle of Internal Friction	ϕ	°	34	20
	Dilatancy Angle	ψ	°	4	0
Stiffness	Secant Stiffness	E_{50}^{ref}	kN/m^2	60,000	30,000
	Tangent stiffness	E_{oed}^{ref}	kN/m^2	60,000	30,000
	Unloading/ Reloading Stiffness	E_{ur}^{ref}	kN/m^2	180,000	90,000

5.4.2. Modeling of Reinforcement

In PLAXIS, it is possible to model the reinforcement either as geogrid or metal strip. These reinforcing elements have slender properties that they only bolster tensile forces but not compressive forces. It is possible to assign elastic or elastoplastic material properties for geogrids. When the element's behavior is selected as elastic, then there is no need to define its' tensile strength which is N_p. The important parameter for elastic material is axial normal stiffness, which is denominated with EA, it can also be called "J". It is calculated by the product of modulus of elasticity and the reinforcement's thickness and therefore, its' unit is force per unit width.

In this study, soil reinforcements were modeled using the geogrid feature. The geogrid properties were based on the Tensar's Structural Geogrid elements as summarized in Table 5.3 (Tensar, 2013). Two parameters are considered to define the elastic behavior of the material: Tensile strength and strain. Tensile strength at 5% strain is taken into account and corresponding axial stiffness values were calculated based on (see Equation 5.8). (International Organization for Standardization (ISO), 2015):

$$E * A = \frac{T_{max}}{\varepsilon_{max}} \quad (5.8)$$

Table 5.3. Geogrid properties (Tensar, 2013).

	Material Properties	**Symbol**	**Unit**	**Value**
UX1100MSE	Tensile Strength	T	kN/m	27
	Strain	ε	-	5%
	Axial Stiffness	EA	kN/m	540
UX1600MSE	**Material Properties**	**Symbol**	**Unit**	**Value**
	Tensile Strength	T	kN/m	58
	Strain	ε	-	5%
	Axial Stiffness	EA	kN/m	1160

In order to investigate the effect of reinforcement length (L) on the MSE Wall behavior, L/ H ratios of 0.5, 0.7 and 1.0 were used. Corresponding reinforcement lengths are provided in Table 5.4. It is important to note that 0.5m of the reinforcements were between the modular blocks.

Table 5.4. Reinforcement length.

L/H Ratio	**0.5**	**0.7**	**1.0**
L for H=8 m (m)	4	5.6	8

5.4.3. Modeling of the Facing Unit

Facing unit was modeled with line elements and defined as concrete modular block type. Unlike soils that require more than E and ν, it is recommended to define concrete walls, intact rock formations or stiff volumes using soil with Linear Elastic Model (LE) as it is based on Hooke's law of isotropic elasticity (Brinkgreve, 2019a).

In this study, modular blocks were modeled as a soil element with 0.5 m width and 0.2 m height (see Figure 5.6). The model was selected as Linear Elastic, and the material type as non-porous. Material properties of the facing unit are given in Table 5.5.

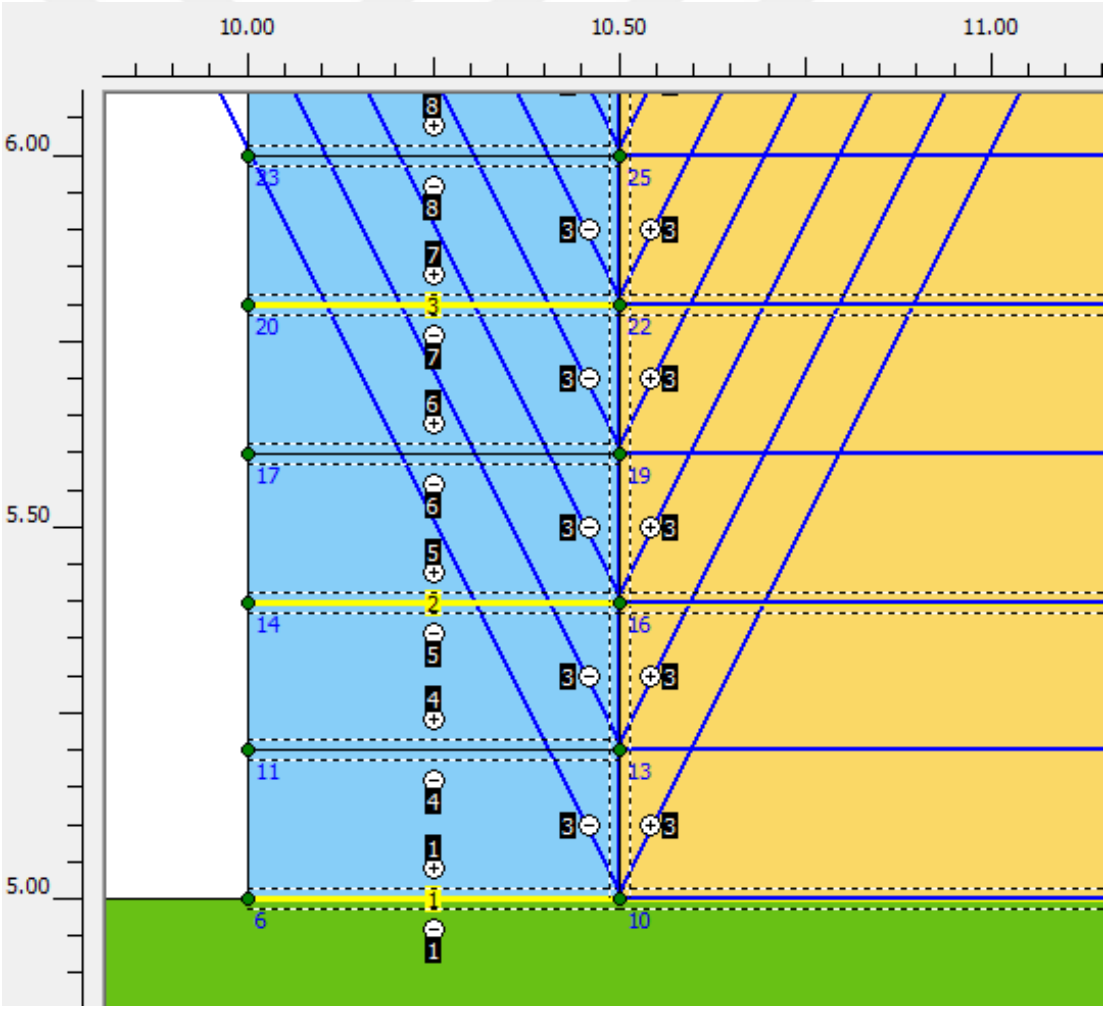


Figure 5.6. Close-up cross section view of the modular block (S_v= 0.4 m case).

Table 5.5. Facing properties.

	Material Properties	Symbol	Unit	Modular Block
General	Model	-	-	Linear Elastic
	Material Type	-	-	Non-porous
	Unit Weight (unsat.)	γ_{unsat}	kN/m^3	21.8
	Modulus of Elasticity	E_{ref}	kN/m^2	4,400,000
	Poisson's Ratio	ν	-	0.17

5.4.4. Modeling of Interfaces

Interfaces are the elements that supply appropriate modeling of soil-structure interaction. Interfaces can be added around geogrids or next to plates or they can be created between two soil clusters. They show up as the line at the side of the geometry line, and the plus and minus signs have no effect on the behavior, they are just distinguishing signs.

In this study, the virtual thickness factor is selected as 0.1 which is the default value. With the virtual thickness factor, it is possible to obtain virtual interface thickness, which is an imaginary dimension to define the material properties of the interface, by multiplying the global element size. By adjusting the global coarseness setting, the global element size can be determined during the mesh generation.

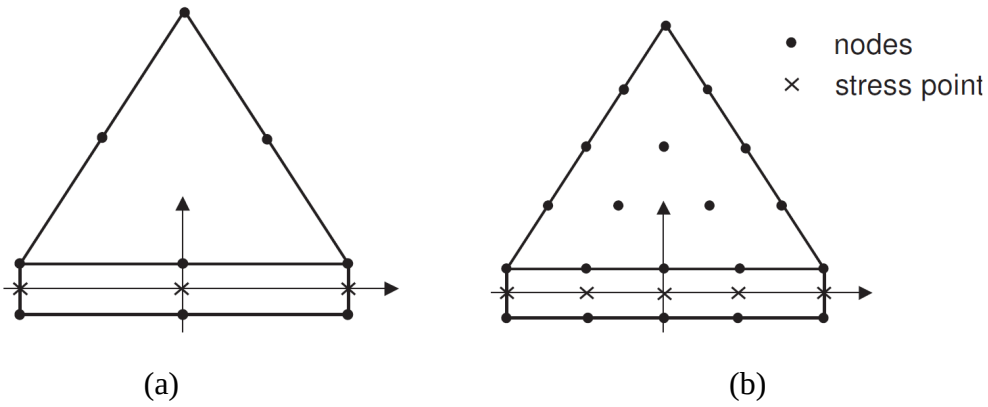


Figure 5.7. Distribution of nodes and stress points in interface elements and their connection to: (a) 6- node (b) 15- node soil elements (Brinkgreve, 2019b).

The parameter R_{inter} defines the interface strength, which can be opted for each soil. When R_{inter} is assigned as 1.0, the interface behaves rigid, which means it shows the same properties on the interface as soil properties except for Poisson's ratio.

An elastic-plastic model helps to understand the behavior of interfaces. To understand the elastic behavior Coulomb criterion is used for the small displacements and plastic interface behavior is used for the permanent slip occurrence (Brinkgreve, 2019b).

For the interfaces, there are 2 equations (Equation 5.9 and Equation 5.10) for the shear stress τ for the elastic and plastic conditions which are defined as (Brinkgreve, 2019b):

$$|\tau| = R_{inter} . tan\emptyset_{soil} \leq tan\emptyset_{soil} \quad (5.9)$$

$$|\tau| = \sigma_n . \tan \emptyset_i + c_i \quad (5.10)$$

In these equations, σ_n is the normal stress, τ is the shear stress, $\emptyset_i$ is the friction angle, c_i is the cohesion of the interface. These values are associated with R_{inter} for each soil and they can be calculated with the equations (Equation 5.11, Equation 5.12 and Equation 5.13) below (Brinkgreve, 2019b):

$$c_i = R_{inter} . c_{soil} \quad (5.11)$$

$$tan\emptyset_{inter} = R_{inter} . tan\emptyset_{soil} \leq tan\emptyset_{soil} \quad (5.12)$$

$$\psi_i = 0° \; for \; Rinter < 1, otherwise \; \psi_i = \psi_{soil} \quad (5.13)$$

In this study, interfaces are defined between the modular blocks, between the modular blocks and the soils and in between the soils, and between the geogrid and soils. In Table 5.6 strength reduction factors that are used in the analyses are provided.

Table 5.6. Strength reduction factors.

Material Properties	Symbol	Unit	Value
Backfill Soil	R_{inter}	-	1
Natural Soil	R_{inter}	-	1
Facing	R_{inter}	-	0.7

5.5. Boundary Modeling

By defining horizontal and vertical fixities, the displacement can be prevented on the related axis. When the horizontal fixity is applied, the horizontal displacement ($u_x = 0$) is disabled and when the vertical fixity is applied, vertical displacement ($u_y = 0$) is disabled. They can also be used together which means both vertical and horizontal fixities ($u_x = 0$ and $u_y = 0$) can be disabled. In this study, horizontal fixity is used for the left and the right boundary and the bottom boundary has total fixity in which both horizontal and vertical fixities are used. It is also possible to define this fixity properties by applying "standard fixities" option.

For dynamic calculations, absorbent boundaries are needed for the absorption of stress rises at boundaries by preventing the reflection inside the soil body. In order to prevent these artificial effects, "standard earthquake boundaries" are used in this study (see Table 5.7). When standard earthquake boundaries are used, PLAXIS automatically generates absorbent boundaries at the left and right side of the model and prescribed displacements at the bottom side with $u_x = 0.01$ m and $u_y = 0.00$ m. Furthermore, it is possible to define the boundaries by selecting "standard absorbent boundaries (dynamics)". When this option is selected, prescribed displacements (dynamic) should be drawn at the location that the earthquake is intended to be applied. With this option it is significant to define X and Y values of the prescribed displacement as $u_x = 0.01$ m and $u_y = 0.00$ m (Brinkgreve).

Table 5.7. Fixities and boundaries.

Boundary	Fixity/ Boundary
Left and Right Boundary	Horizontal Fixity
Bottom Boundary	Total Fixity
Absorbent Boundary	Standard earthquake boundaries

5.6. Mesh Generation

Since the model is defined completely and materials are assigned, the finite element mesh can be created to run finite element calculations. These meshes comprise triangular elements, nodes, and stress points. They are required to perform finite element analysis, and the mesh generation can be accomplished automatically. In PLAXIS, it is possible to change the refinement of the mesh, and it is even possible to refine some specific parts rather than other parts by refining clusters, lines, and points.

In a master thesis, displacements are compared with each mesh type and the results show that displacements converge after the “fine” mesh type (Raikar, 2016). Considering previous studies on similar studies, global coarseness is selected as “fine” in this study. Generated mesh for 8 m high wall for L/ H = 0.7 is provided in Figure 5.8, and the zoomed section of the reinforced area is given in Figure 5.9. Furthermore, the reinforced soil and 1 meter back of the reinforced soil are refined together by refining the cluster one time entirely. For 8 m high MSE Wall, the number of elements, nodes and stress points are provided in Table 5.8.

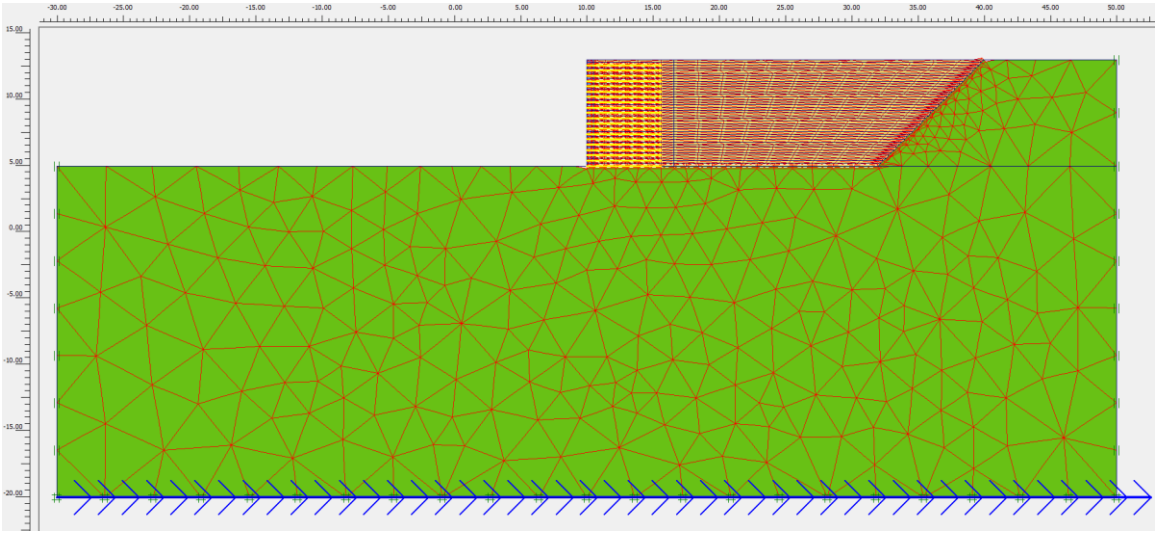


Figure 5.8. Connectivity plot of 8m high wall: L/ H ratio= 0.7 (Scale: 1.0).

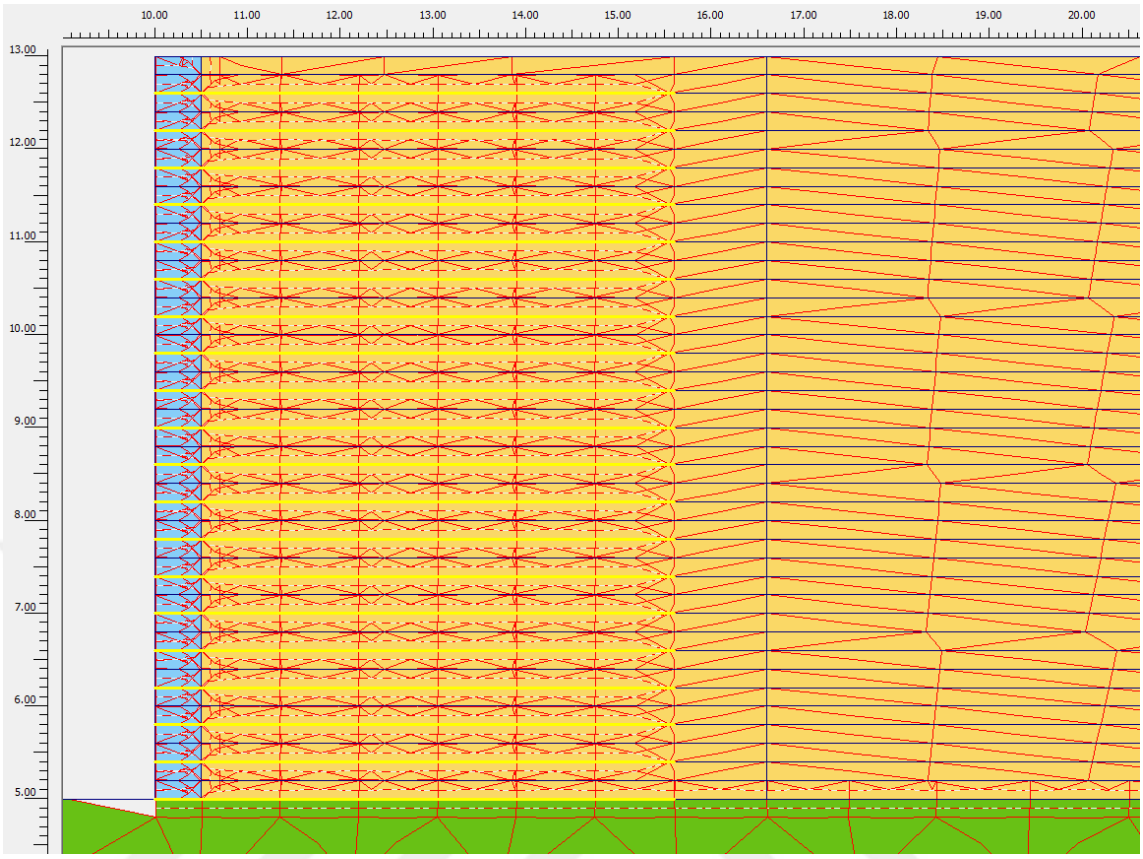


Figure 5.9. Reinforced fill area- connectivity plot of 8m high wall: L/ H ratio= 0.7 (Scale: 1.0).

Table 5.8. Number of elements, nodes, and stress points.

	H= 8 m, S_v= 0.4			**H= 8 m, S_v= 0.6**		
L/ H	**0.5**	**0.7**	**1**	**0.5**	**0.7**	**1**
Number of Elements	2008	2044	2105	1996	2020	2081
Number of Nodes	5087	5315	5590	4973	5129	5356
Number of Stress Points	6024	6132	6315	5988	6060	6243

5.7. Determining the Initial Conditions

The initial conditions must be defined after the mesh generation. During the initial conditions stage, the ground water level is defined, and the water pressures and the initial effective stress state are generated.

In this study, the ground water table was considered below the model and the initial stress of the soil occurs by the self- weight (see Figure 5.10). Naturally, the history of soil formation also affects the stresses. PLAXIS performs the initial stress analysis with the K_0-procedure, and then it is possible to continue with the calculations stage. The coefficient of lateral earth pressure at rest (K_0) values are calculated automatically with Jaky's formula given in Equation 4.14, and initial horizontal stresses are related to K_0 values provided in Equation 5.14 (Brinkgreve).

$$\sigma'_{h,0} = K_0 \,.\, \sigma'_{v,0} \qquad (5.14)$$

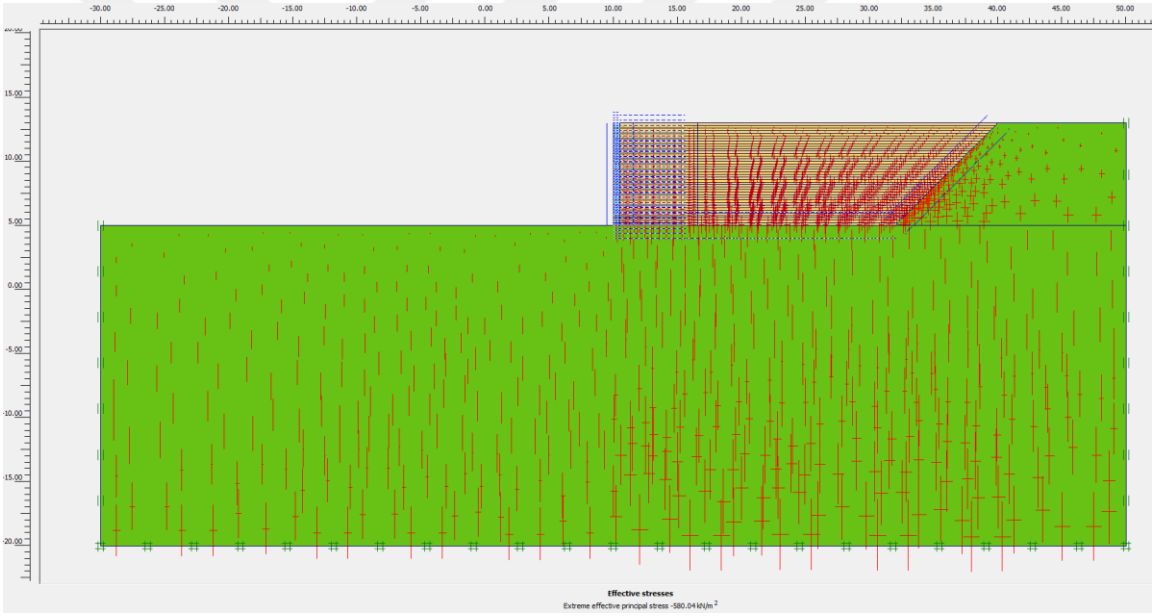


Figure 5.10. Initial effective stress state of the 8m high wall: L/ H= 0.7 (Scale: 0.005).

5.8. Staged Construction

To execute the elastic-plastic deformation analysis, the construction of the models was performed with the plastic calculation option. Time effects are not considered in the plastic calculation (Enunlu, 2007).

The staged construction was performed in 43 stages for the 8 m high wall. The reinforced area is filled at intervals of 0.2 meters layers, and reinforcements are placed following the defined reinforcement spacing. Each layer is compacted with 15 kN/m^2 distributed load extended to 5.1 m from back of the facing. After the layers are placed and compacted, a static distributed load of 12 kN/m^2 is applied along 19.5 m from the back of the facing.

5.9. Dynamic Analysis

Dynamic analysis is executed as the last stage of the stage construction. After the plastic analysis, a stage is defined to reset the displacements just before the dynamic analysis and to set existing displacements zero to study net seismic displacements before and after the dynamic load application.

5.9.1. Natural Frequency of the Wall

Estimating the natural (fundamental) frequency of MSE Wall is significant for deciding the suitable frequencies to perform the numeric analysis. With this goal, various equations are proposed. Wu (1994) proposed the fundamental frequency formula (see Equation 5.15) for a body which has rigid boundaries, two vertical boundaries and one base boundary which is exposed to horizontal shaking in a two-dimensional, linear elastic medium. In the equation, f_{11} is the estimated natural frequency, G is shear modulus, B is model width and υ is Poisson ratio (Bathurst & Hatami, 1998; Wu, 1994).

$$f_{11} = \frac{1}{4H}\sqrt{\frac{G}{\rho}}\sqrt{1+\left(\frac{2}{1-\nu}\right)\left(\frac{H}{B}\right)^2} \qquad (5.15)$$

The soil shows the purely elastic behavior only at very small strains in the order of 1*10^{-6}. After the very small strains are exceeded, soil stiffness reduces by the strain increase in compliance with the characteristic S-curve in logarithmic scale. For this reason, soil stiffness is mostly related to its non- linear behavior (Laera & Brinkgreve, 2015). Based on

the range of values presented in the literature (see Table 5.9) and using various correlations, all strain shear modulus (G_0) value was estimated as 155,000 kPa in this study. G/ G_0 ratio can be roughly estimated with the graph presented in Figure 5.11 (AASHTO, 1998). Using the experimental results from the literature and Figure 5.11, the G/ G_0 ratio is determined as 0.2 and the corresponding shear modulus (G) was calculated.

Table 5.9. Typical shear modulus values (AASHTO, 1998).

Soil Type	**Shear Modulus, G_0 (kPa)**
Dense Sands & Gravels	69,000- 345,000
Silty Sand	27,600- 138,000
Medium Stiff Clay	6,900- 34,500
Soft Clays	2,750- 13,750

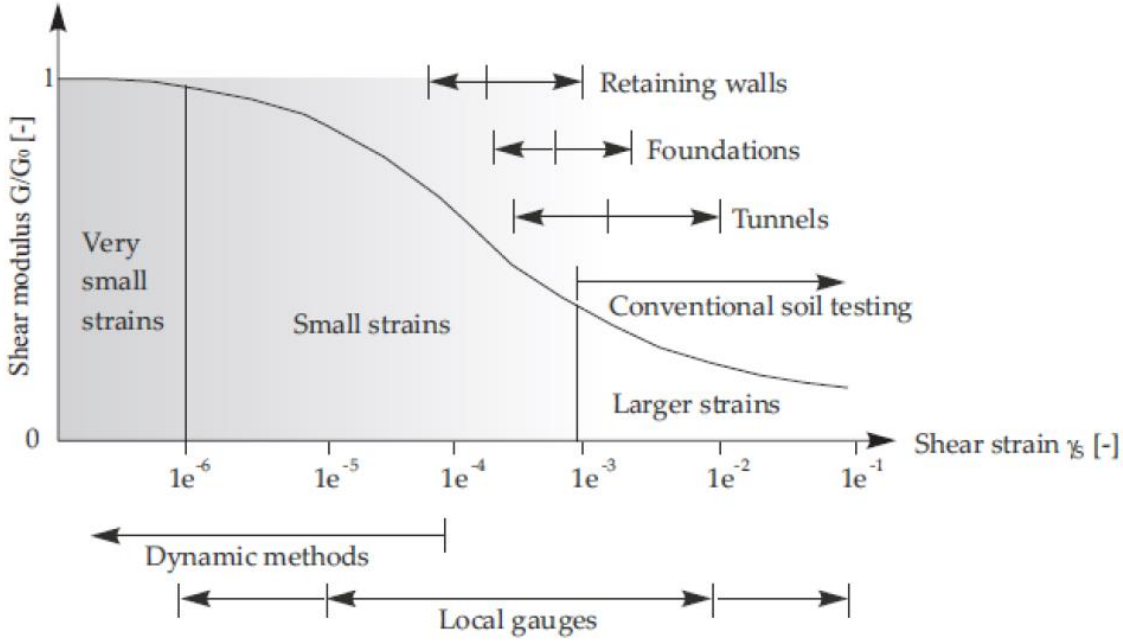


Figure 5.11. Stiffness strain behavior (Laera & Brinkgreve, 2015).

Besides Wu, there are also other methodologies asserted by Matsuo& Ohara (1960), Scott (1973), Richardson (1978), Chopra (2000). Matsuo & Ohara (1960) claimed that the natural frequency of the wall is located between two cases for the soil- rigid wall system. They asserted equations for both cases. The first case's calculation steps are provided in

Equation 5.16, 5.17, 5.18 and the second case's in Equation 5.19, and 5.20. The formulation given in Equation 5.17 for f_1 is to calculate the frequency of an infinitely long, uniform soil layer, and it is also used for the second case and it is also going to be used by Scott (1973). In the formulation, GF is defined as a geometric factor. (Hatami & Bathurst, 2000; Matsuo & Ohara, 1960).

Case 1:

$$f_{11}^{v=0} = f_1 * GF_{v=0} \quad (5.16)$$

$$f_1 = \frac{1}{4H}\sqrt{\frac{G}{\rho}} \quad (5.17)$$

$$GF_{v=0} = \sqrt{1 + \frac{8(1-v)}{1-2v}\left(\frac{H}{B}\right)^2} \quad (5.18)$$

Case 2:

$$f_{11}^{\sigma v=0} f_1 . GF_{\sigma v=0} \quad (5.19)$$

$$GF_{\sigma v=0} = \sqrt{1 + \frac{2-v}{1-v}\left(\frac{H}{B}\right)^2} \quad (5.20)$$

In which f_1 is the frequency of infinite long uniform soil, (GF_s) is the geometric factor and (f_{11}^s) is the natural frequency of the MSE Wall, as explained previously. Scott (1973) proposed the equation given in Equation 5.21 which is for two-dimensional soil wall-systems with uniform depth by assuming the backfill as a one-dimensional shear beam which is

attached to the wall with elastic springs. Scott also used f_1 and GF_s to calculate f_{11}^S (see Equation 5.22) (Hatami & Bathurst, 2000; Scott, 1973).

$$f_{11}^S = f_1 . GF_S \quad (5.21)$$

$$GF_s = \sqrt{1 + \frac{64}{\pi^2}\left(\frac{1-v}{1-2v}\right)\left(\frac{H}{B}\right)^2} \quad (5.22)$$

Richardson (1978) proposed an empirical formula (see Equation 5.23) for fundamental frequency in which he made the formulation directly dependent on the wall height (H) (Hatami & Bathurst, 2000; Richardson, 1978).

$$f_{11}^R = \frac{38.1}{H} \quad (5.23)$$

Chopra (2000) published a formulation for the first natural period (T) of the walls whose center of gravity are at their mid-height by assuming a plane strain cantilever shear deformation mode (see Equation 5.24) (Chopra, 2001; Walthall, Wang, Kiousis, & Khan, 2012).

$$T = 2\pi H \sqrt{\frac{\rho}{2G}} \quad (5.24)$$

All the values obtained from the introduced methods are summarized in Table 5.10. A mean value of 4.624 Hz is calculated from this study and the range of frequencies used in the FEM analysis were based on this value.

Table 5.10. Natural frequency calculation of the MSE Wall.

Method		Frequency (in Hz)
Wu (1994)- Bathurst & Hatami (1998)		4.407
Matsuo and Ohara (1960)	**Case 1**	5.386
	Case 2	4.374
Scott (1973)		5.161
Richardson (1978)		4.763
Chopra (2000)		3.656
Average		4.624

5.9.2. Damping

For dynamic analysis, damping is a significant factor. In PLAXIS, Rayleigh damping is commonly used for the material damping for plane strain condition. In PLAXIS, soil models do not possess viscous damping, Rayleigh damping is introduced for damping. The damping correlation (C) is a numerical feature, in which a damping matrix is mainly constituted of mass (M) and stiffness (K), as defined in Equation 5.25. α and β are known as Rayleigh coefficients (Brinkgreve):

$$C = \alpha M + \beta K \qquad (5.25)$$

The response of soil- structures are considerably influenced by damping. For highly non-linear materials such as soils, obtaining damping is difficult. The damping ratio is a geotechnical parameter that shows how fast the oscillations decay during dynamic or cyclic loading, and it is symbolized with ξ and typically expressed in percentages. For ξ in which C_c is defined as the critical damping coefficient is provided in Equation 5.26 (Kramer, 1996).

α and β values used in Equation 5.27 are related to ξ and angular frequency (ω). The Equation 5.27 for the relation is provided below (Ling *et al.*, 2010):

$$\xi = \frac{c}{c_c} \qquad (5.26)$$

$$\xi = \frac{\alpha}{2\omega} + \frac{\beta\omega}{2} \qquad (5.27)$$

According to Equation 5.26 when the alpha (α) has higher values, the lower frequencies are damped, and when the beta (β) has, the higher frequencies (see Figure 5.12).

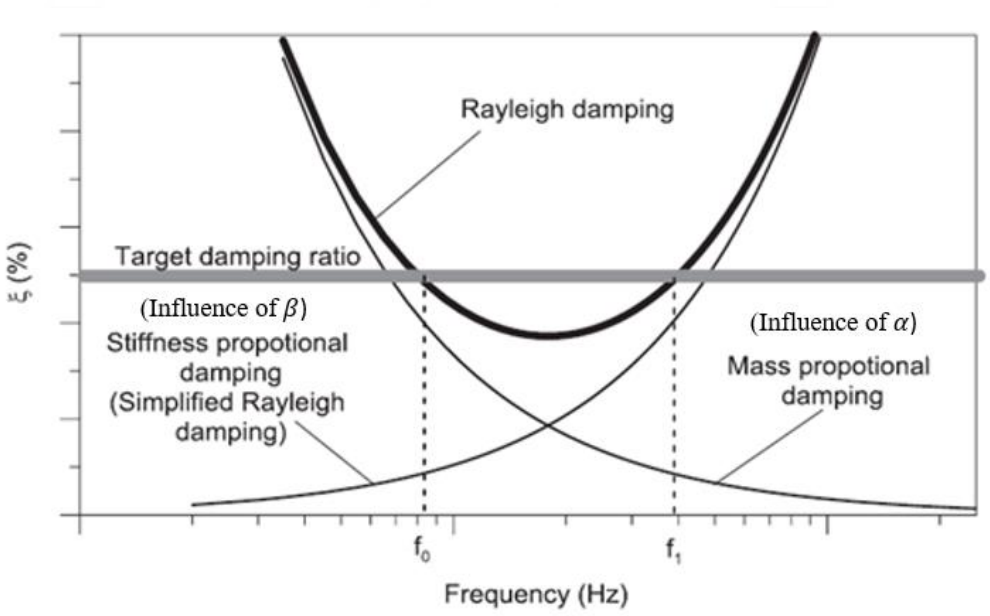


Figure 5.12. Variation of Rayleigh damping parameters (Brinkgreve, 2019b; Tsai, Park, & Chen, 2014).

Before selecting the range of frequencies for the analysis, determining the damping ratio has an importance on the soil's behavior. In the literature, there are many studies and proposals on the selection of the damping ratio. However, different modal viscous damping ratios are typically in the range of 6.6-15.9%. Elgamal *et al.* (1996) suggested that assuming 5% damping is conservative for typical reinforced concrete cantilever walls with heights less than 10m (Elgamal, Alampalli, & Laak, 1996). Woodward & Griffiths (1996) applied 5 and 10% damping ratios to gravity retaining walls (Woodward & Griffiths, 1996). Bathurst & Hatami (1998) inspected the effect of increasing the damping ratio from 5% to 10 and 20%.

They reported from the test results that the frequency is the most significant factor for the determination of the viscous damping ratio (Bathurst & Hatami, 1998). According to studies which are reported by Burke *et al.* (2005), different optimum damping ratios were found when shake table tests were performed with various accelerations. For example, these studies indicate that for an acceleration of 0.4g, 15% damping is sufficient, and for the maximum acceleration of 0.8g, 5% is found convincing. These results indicate that for lower strain levels, larger damping values more realistic for the models; however, the situation is inverse when there are large strains and lower applying a lower level of damping can be sufficient (Burke, Ling, & Liu, 2004; Ling *et al.*, 2010). In a study performed by Moradi (2014), the damping ratio is taken 10% for MSE Walls (Moradi, 2014). Brinkgreve *et al.* (2007) presented the relation for damping ratio as a function of the cyclic shear strain (γ_c) for various values of shear strain at $0.7G_0$ ($\gamma_{0.7}$) and small- strain shear modulus/ unload-reload shear modulus ratios (G_0/ G_{ur}) as shown in Figure 5.13. As a result of the study, higher damping values are obtained at smaller shear strain values (Brinkgreve, Kappert, & Bonnier, 2007). According to the study by Amorosi *et al.* (2010), a curve of the damping ratio and the shear modulus as a function of the shear strain (γ) is proposed and adopted in the computer program EERA (see Figure 5.14) (Amorosi, Boldini, & Elia, 2010).

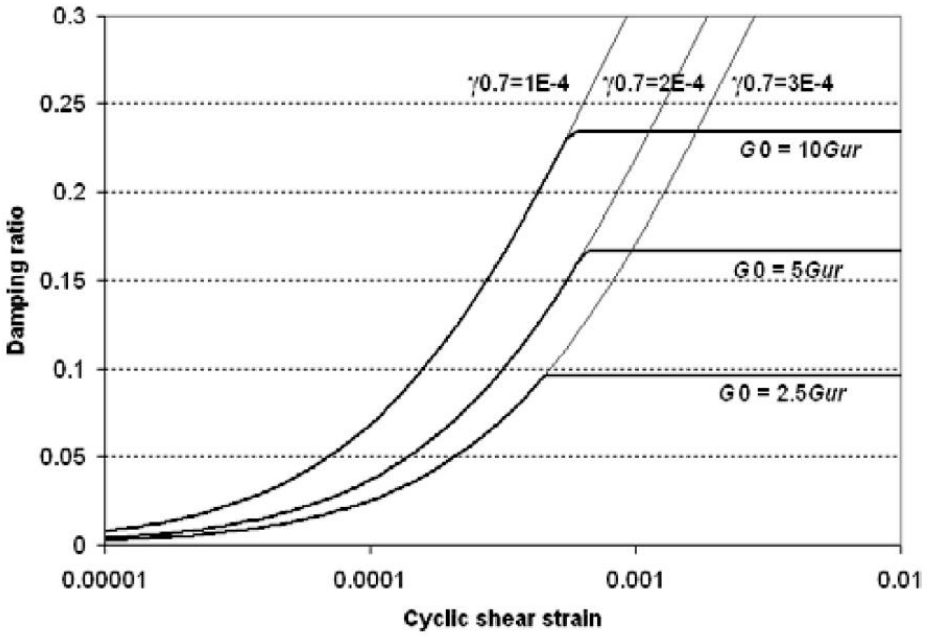


Figure 5.13. Damping ratio (ξ) as a function of cyclic shear strain (γ_c) (Brinkgreve *et al.*, 2007).

Ling (2010) indicated that the determination of Rayleigh damping coefficients is rather empirical and based on previous experience, Rayleigh alpha and beta values are set according to a system viscous damping ratio (Rayleigh damping) of 10% (Ling *et al.*, 2010).

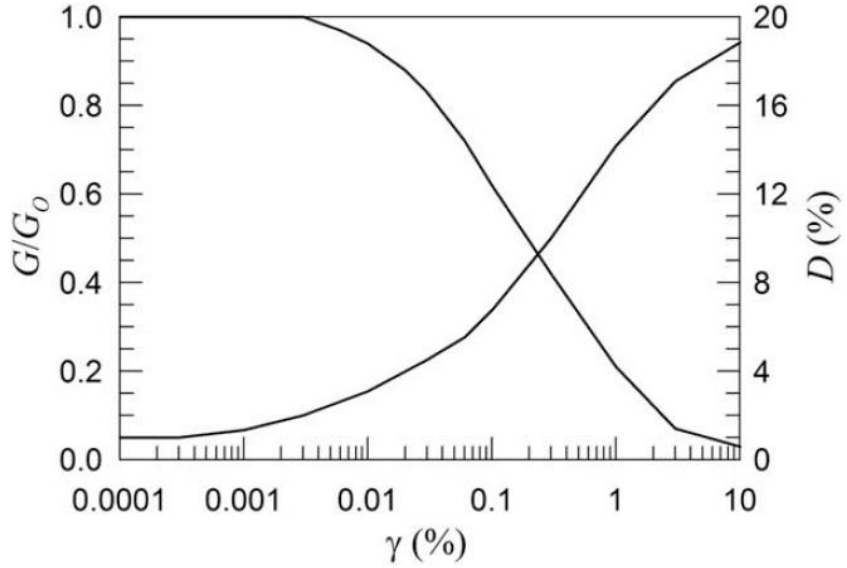


Figure 5.14. Modulus reduction curve (G/ G_0) and variation of damping ratio (D%) with the shear strain ($\gamma(\%)$) (Amorosi *et al.*, 2010).

To apply the Rayleigh damping, one or two frequencies are required to define damping features. Tsai *et al.* (2014) conducted a study on optimal frequencies for Rayleigh damping to minimize the effect of damping's frequency dependence. The results indicate that damping at frequencies between two frequencies, namely f_0 and f_1 are underestimated and beyond the bracket of these frequencies damping is overestimated. This study shows that these two frequencies have a significant effect on the propagated ground motion (see Figure 5.12) (Tsai *et al.*, 2014). Various studies were performed to find the optimal frequency bracket values (f_0 and f_1) for the soil damping formulation. Hudson *et al.* (1994) suggested using one of the frequency as the fundamental frequency of the soil, and the second as the closest odd number obtained from the division of fundamental frequency of the bedrock to the fundamental frequency of soil (Hudson, Idriss, & Beirkae, 1994; Jia, 2018). Kwok *et al.* (2007) suggested using the natural frequency and five times of the natural frequency as two selected frequencies (Kwok *et al.*, 2007).

For PLAXIS input, the unknown values of α and β can be determined using a minimum of 2 equations (see Equation 5.28). In these equations, damping ratios can be selected according to corresponding frequencies of vibration ω_i (see Equation 5.29) (Brinkgreve).

$$\alpha + \beta\, \omega_i^2 = 2\, \omega_i\, \xi_i \qquad (5.28)$$

$$\omega = 2\, \pi\, f \qquad (5.29)$$

With determined frequencies f_1 and f_2 for the selected damping ratio, the required Rayleigh α and β values were calculated from Equation 5.30 and Equation 5.31 respectively which are derived from the Equation 5.29.

$$\alpha = 2\, \omega_1 \omega_2 \frac{\omega_1 \xi_2 - \omega_2 \xi_1}{\omega_1^2 - \omega_2^2} \qquad (5.30)$$

$$\beta = 2 \frac{\omega_1 \xi_1 - \omega_2 \xi_2}{\omega_1^2 - \omega_2^2} \qquad (5.31)$$

In this study, based on the detailed literature review performed, and also considering both the model's fundamental frequency and the input ground motion frequencies considered. target bracket frequencies f_0 and f_1 for the Rayleigh parameter calculation were selected as 2 and 8 Hz. Angular velocities were calculated using Equation 5.29 for a damping ratio of 10%.

In this study, Rayleigh α and β values are defined to all clusters of the modular facing, backfill and foundation soil for all models. No specific damping ratio is assigned to the geogrid. The calculated Rayleigh alpha and beta values are provided in Table 5.11.

Table 5.11. Rayleigh α and β coefficients.

Title	Material Properties	Symbol	Unit	Value
Damping	Rayleigh alpha	α	-	2.011
	Rayleigh beta	β	-	0.00318

5.9.3. Seismic Loading

The seismic loading, which is shown as horizontal right arrows on the base of the wall, is applied to the models using prescribed displacements. The absorbent boundary is used on boundaries to absorb the increments of stresses which is caused by the dynamic loading. Since absorbent boundaries are applied, the reflection is prevented inside the soil. C_1 and C_2 are identified as relaxation coefficients which improve the wave absorption on the boundaries. C_1 functions on the axis normal to the boundary, and C_2 on the same in the tangential direction (Dey *et al.*, 2011). For seismic loading, the standard setting for the absorbent boundary is considered and hence, C_1= 1, and C_2= 0.25. This is proposed by Lysmer & Kuhlemeyer's (1969) method in which the normal and shear stresses which are related to the normal ($\dot{w}$) and tangential ($\dot{u}$) velocities are expressed in Equation 5.32 and Equation 5.33, respectively. In the expressions, ρ stands for density, V_{p} for longitudinal wave velocity, and V_s for shear wave velocity (Kouroussis, Verlinden, & Conti, 2011). However, as there is not a clear criterion to find C_1 and C_2 coefficients with certainty, Morales-Esteban *et al.* (2010) suggested that boundaries should be moved far away from the region of interest (Falcon, 2014). In this study, boundaries were placed at a distance as explained in the Chapter 5.3.

$$\sigma = a\,\rho\,V_{\mathrm{p}}\,\dot{w} \qquad (5.32)$$

$$\tau = b\,\rho\,V_s\,\dot{u} \qquad (5.33)$$

In the dynamic analysis, time integration is performed using the Newmark method. The coefficients alpha (α) and beta (β) determine the numerical time integration, and they

should not be confused with Rayleigh alpha (α) and beta (β) coefficients. These coefficients are taken as standard damped Newmark scheme that Newmark α value is taken as 0.3025, and Newmark β value is taken as 0.6. There are two conditions given in Equation 5.36 that these parameters have to satisfy in order to obtain an unconditionally stable solution (Brinkgreve):

$$\beta \geq 0.5 \; and \; \alpha \geq 0.25 \; (0.5 + \beta \;)^2 \qquad (5.34)$$

5.9.4. Accelerogram

In PLAXIS, after selecting "dynamic analysis" as calculation type, it is possible to excite the model by either inputting an earthquake record data file or inputting a harmonic ground motion data file. In this study, the harmonic loading is applied at the prescribed displacements, at the bottom boundary of the model. PLAXIS obtains the displacements from the integration of the accelerograms which is executed by Newmark's integration method. By this way, the seismic input is applied through dynamic multipliers (see Equation 5.35) and loaded from data file as "accelerations" in this study.

$$Prescribed\ displacement(t) = Input\ motion\ (t) x\ Dynamic\ multiplier \qquad (5.35)$$

The desired time interval has to be selected in PLAXIS loading input tab. In this study, to reduce the calculation time, input duration was set as 5 seconds and the calculation for each analysis case took around 6 to 8 hours using a standard personal computer (PC). In order to determine the input accelerogram, Equation 5.36, published by Bathurst & Hatami (1998) was utilized (Bathurst & Hatami, 1998). The peak ground acceleration (PGA) was selected as 0.2g (g= gravitational acceleration) which provides PGA of 2 m/s^2 and equals to 200 Gal. The accelerogram was generated/calculated with time intervals of 0.005 seconds using Excel.

$$\ddot{u}(t) = \sqrt{\beta\, e^{-\alpha t} t^{\xi}}\, \sin(2\pi f t) \qquad (5.36)$$

Considering the estimated natural frequency of the wall, various frequencies in the range of 1 Hz to 8 Hz (i.e., 1, 1.5, 2, 3, 4, 6, 8 Hz) were used in Equation 5.36, corresponding to seven (7) different input ground motion record accelerogram. Each accelerogram was applied to all cases of models with various reinforcement parameters. The accelerogram recommended by Bathurst & Hatami (1998), generated using f= 3 Hz is provided in Figure 5.15. The accelerograms that are created with the lowest (f= 1 Hz) and the highest (f= 8 Hz) frequencies are also provided in Figure 5.16.

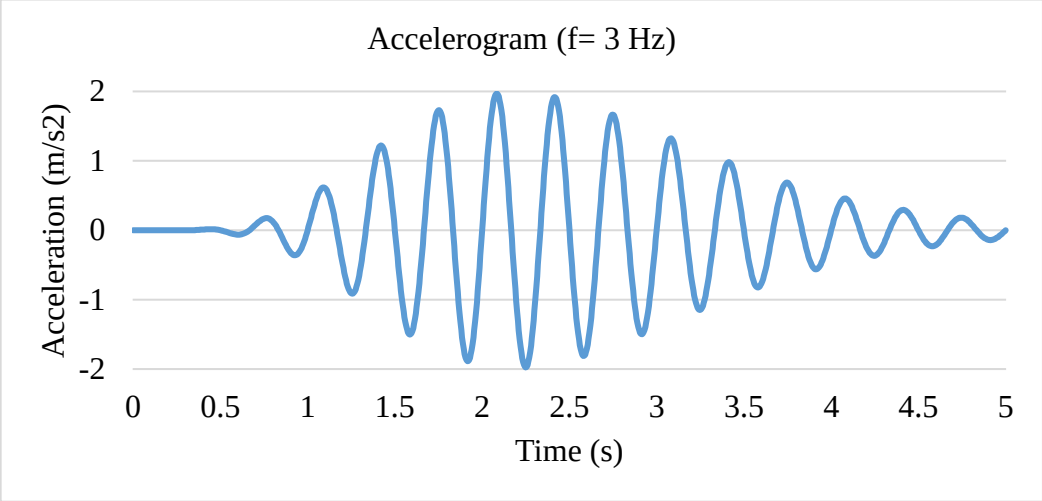
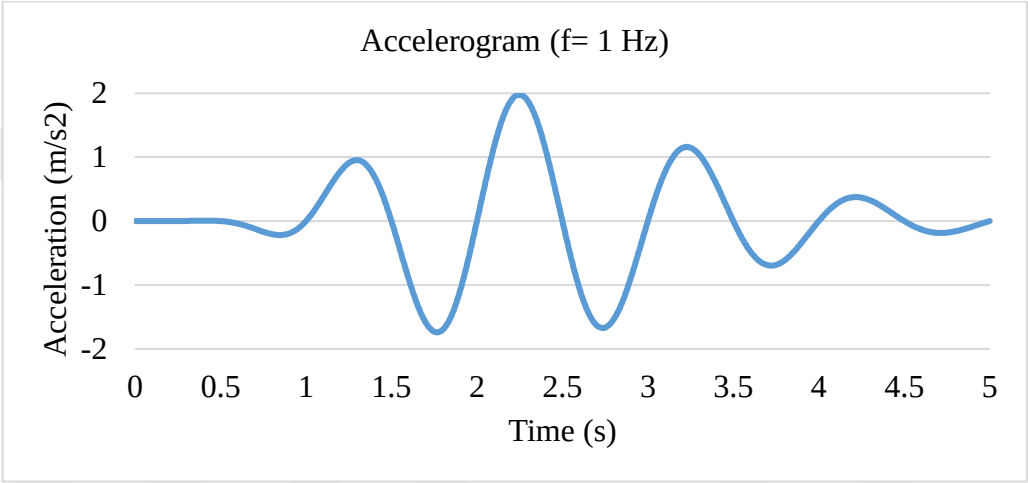


Figure 5.15. Accelerogram using Bathurst & Hatami (1998): f= 3 Hz.

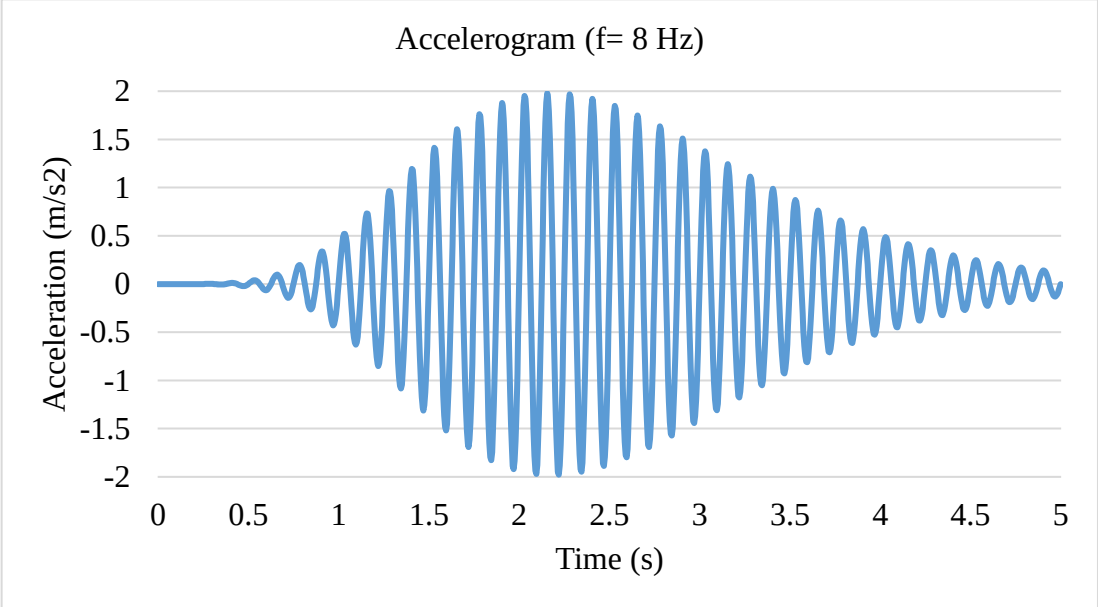
Arias Intensity (I_a) is defined as a ground motion parameter which is depended on the spectrum of the total energy per unit weight. The equation for Arias Intensity for ground motion is provided in Equation 5.37. In this equation, t_d is the total time of excitation, and $a(t)$ is the corresponding acceleration time history (Arias, 1970). In this study, acceleration is applied with 0.005 s time intervals for 5 seconds in all of the seven (7) input ground motion cases. When Arias Intensity is estimated for all of the input ground motion cases, the value is found around 0.5003 for 5 seconds excitation. Thus, this means that the Arias intensity and hence, the total amount of energy applied for each ground motion corresponding to each

frequency in the 1 Hz to 8 Hz bracket is the same. This simply means Bathurst & Hatami (1998) generates input ground motions with different frequency inputs but the same energy.

$$I_a = \frac{\pi}{2g}\int_0^{t_d} a(t)^2 dt \qquad (5.37)$$



(a)



(b)

Figure 5.16. Accelerogram using Bathurst & Hatami (1998): (a) f= 1 Hz (b) f= 8Hz.

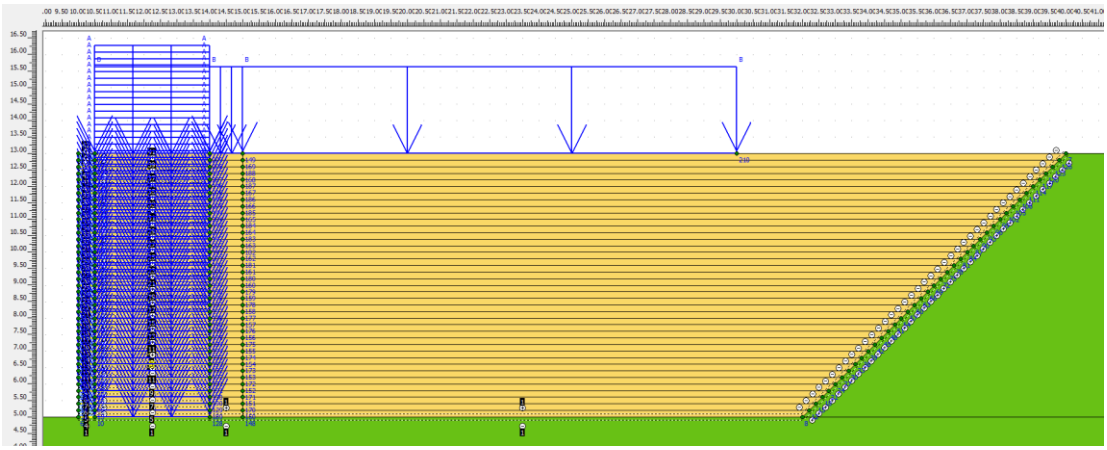
5.10. Configurations & FEM Analysis Cases

According to the defined material properties, two S_v 0.4 m and 0.6 m are decided. Each S_v is modeled with three different reinforcement lengths and each length is compared with two axial stiffnesses. In this way, 12 configurations are occurred, and each configuration is analyzed with 7 different frequencies which are 1, 1.5, 2, 3, 4, 6, and 8 Hz. Thus 84 cases are prepared in total, and their case numbers are given in Table 5.12.

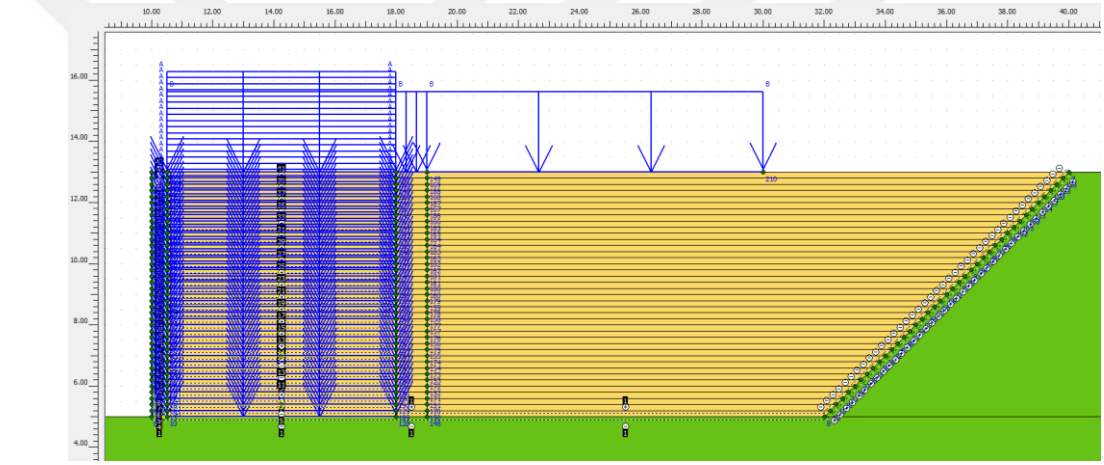
Table 5.12. MSE Wall configurations for reinforcement design parameters.

Nr.	Configurations
1	S_v= 0.4m, EA= 600kN/m, L/H= 0.7
2	S_v= 0.4m, EA= 1200kN/m, L/H= 0.7
3	S_v= 0.4m, EA= 600kN/m, L/H= 1
4	S_v= 0.4m, EA=1200kN/m, L/H= 1
5	S_v= 0.4m, EA= 600kN/m, L/H= 0.5
6	S_v= 0.4m, EA= 1200kN/m, L/H= 0.5
7	S_v= 0.6m, EA= 600kN/m, L/H= 0.7
8	S_v= 0.6m, EA= 1200kN/m, L/H= 0.7
9	S_v= 0.6m, EA= 600kN/m, L/H= 1
10	S_v= 0.6m, EA= 1200kN/m, L/H= 1
11	S_v= 0.6m, EA= 600kN/m, L/H= 0.5
12	S_v= 0.6m, EA= 1200kN/m, L/H= 0.5

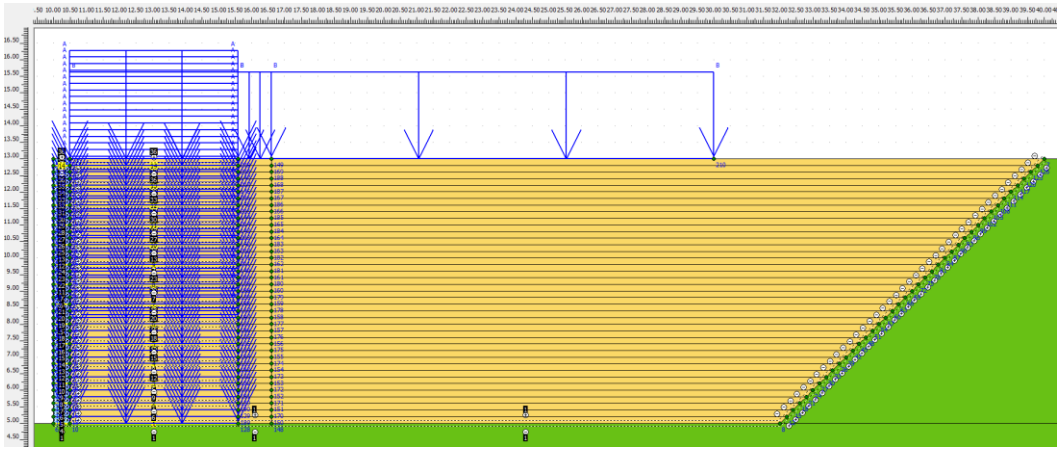
In Figure 5.17a, Figure 5.17b and Figure 5.17c screenshots from PLAXIS input window, for L/ H= 0.5 and S_v= 0.4 m, L/ H= 0.5 and S_v= 0.6 m and for L/ H= 0.7 and S_v= 0.6 m are provided respectively.



(a)



(b)



(c)

Figure 5.17. Models' input screen (a) Sv=0.4 m, L/ H=0.5 (b) Sv=0.4 m, L/ H=1 (c) Sv=0.6 m, L/ H=0.7.

6. RESULTS AND DISCUSSIONS

6.1. Results of FEM Analysis

Results of the FEM analysis performed on the 8 m high MSE Wall model are presented in this chapter. Both static (end-of construction) and seismic analysis results, collected from all cases analyzed are discussed. In the parametric study, in order to determine the effect of each desired parameter, all other design parameters are kept constant in each model corresponding to each case. Reinforcement axial forces, displacements, and acceleration values are presented for both static and seismic loading conditions for each case.

The connectivity loads between the facing and the reinforcements are mostly defined as T_0 values. In this study, peak axial envelope forces generally occurred at facing connections at the reinforcements. For this reason, besides defining these loads as connectivity loads, they are defined as extreme loads (T_{max}) for each reinforcement. Positive sign convention is used for tensile loads, and hence, the axial forces on the reinforcements are positive. Additionally, with the horizontal displacement values obtained for the reinforcements are presented as absolute values for ease in comparison. In tables and figures of this Chapter, following abbreviations are used: " env." for envelope, "abs." for absolute, "ext." for extreme, "acc." for acceleration, "disp.", "hor." for horizontal, "reinf." for reinforcement, "diff." for difference, "max." for maximum, sec. for second, "conf." for configuration, and "SL" for seismic loading. As an example, SL=1.5Hz correspond to the harmonic input ground motion generated using Bathurst & Hatami (1998) formula, and a frequency of 1.5 Hz and a PGA of 0.2g.

The general geometry of the reinforced area pertaining to the Configurations 1 & 2 is provided as an example in Figure 6.1. The wall is 8 meters high and reinforcements are 5.6 meters long. Reinforcements are placed with 0.4 meters spacing. Two separate reinforcement stiffness values: EA=600, and 1200 kN/m are used for Configuration 1 and Configuration 2, respectively. Additionally, in Figure 6.1, selected nodes for load-displacements curves are also presented. 10 stress points are selected in order to investigate the force and deformation results at each point. The node A is not visible in Figure 6.1,

because it is located at the base of the foundation soil. The points selected have fixed coordinates for all of the models, except E, and H points as they are behind the reinforced area, their coordinates change with the change in L/ H ratio of the models. However, they are always located 0.5 m behind the reinforced area in all models. In this chapter, the results obtained from the selected Point J are provided as it is the topmost point in the reinforced fill. Its location is presented in Figure 6.1. The acceleration outcomes provided for Point J in charts are maximum absolute horizontal acceleration values in terms of g.

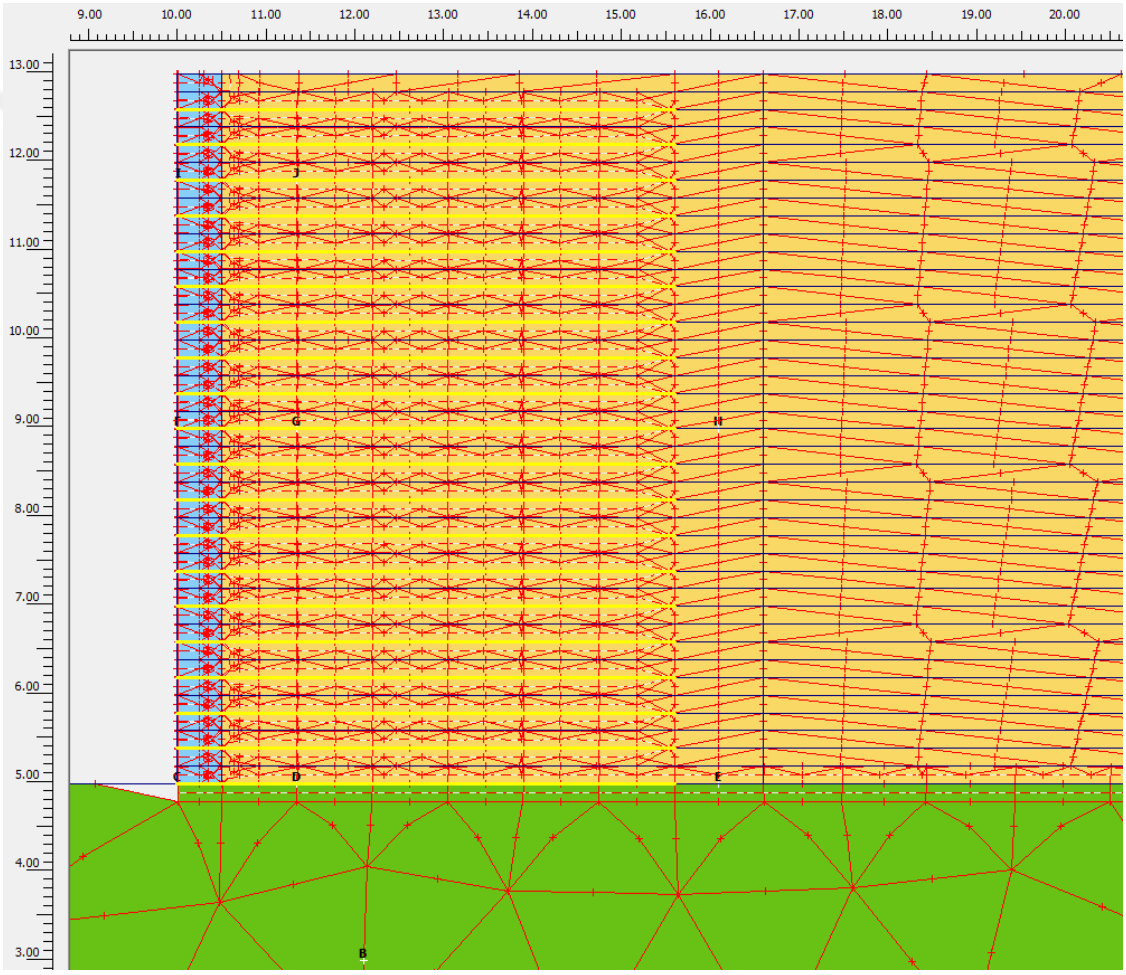


Figure 6.1. Selected nodes for load/displacement curves on the connectivity plot.

6.2. Results of FEM Analysis for Static (End of Construction) Case

When the static results of the models are evaluated, it can be seen that the displacements and axial forces are higher at the mid-section of the wall than it is at the top and the bottom. In order to better understand the behavior, the effect of EA, L/ H, and S_v on the displacements and axial forces are investigated.

Figure 6.2 shows the horizontal displacement distribution on the reinforcements. As seen in Figure 6.2, the displacement distribution gathers from the center to the rear end at top reinforcements and on the front at bottom reinforcements. This observation can be explained by the bulging (swelling) behavior observed in the deformed shape of the model at the end of the construction phase as seen in Figure 6.4. As bulging occurs, the top reinforcements' center portion moves down, following the shape of bulging. This ends up creating higher displacements closer to their rear end of the reinforcements. Moving towards the bottom of the wall, higher displacements starts shifting towards the front of the reinforcements. It is possible to see this shift in Figure 6.5 as the total displacements are shown with shadings. The bulging effect is reduced at the bottom, and following the displacement of the toe, the maximum displacement is observed at the front end of the bottommost reinforcement.

In Figure 6.3, the axial force (envelope) distribution on selected five reinforcements at various depths are provided. It is possible to deduce from these plots that the maximum tensile stresses occur at connection points between reisnforcements and modular blocks. Besides this, the axial loads increase at the mid-section of the wall as the bulging is most dominant at that point and the reinforcements resist against the pulling forces due to this bulging.

In Figure 6.6 and 6.7, the effect of EA, in Figure 6.8 and 6.9, the effect of L/ H, in Figure 6.10 and 6.11, the effect of S_v on horizontal displacements and axial stresses for the static case are provided.

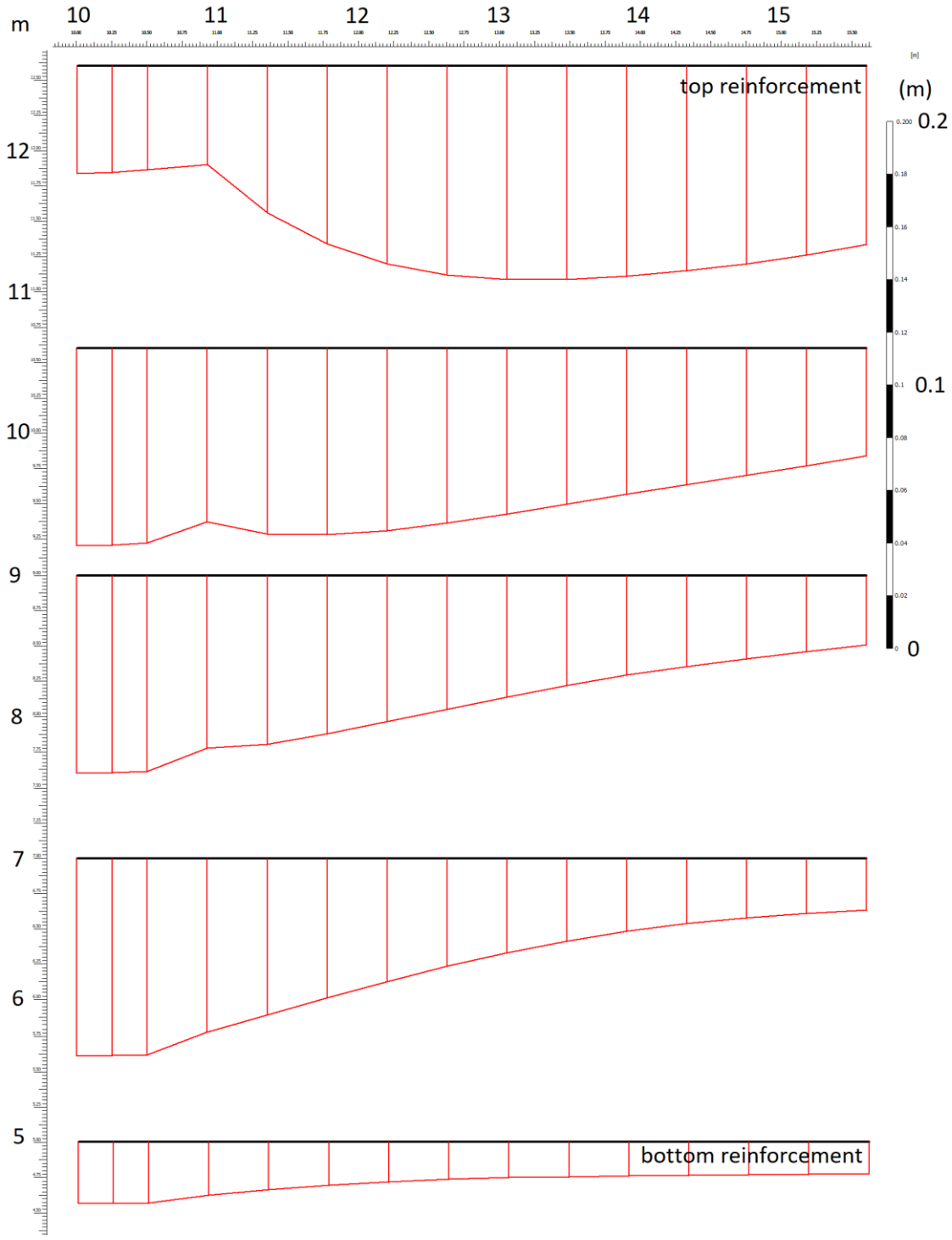


Figure 6.2. Horizontal displacement distribution along reinforcements at various depths: Configuration 1, Static case (Scaled to 20.0).

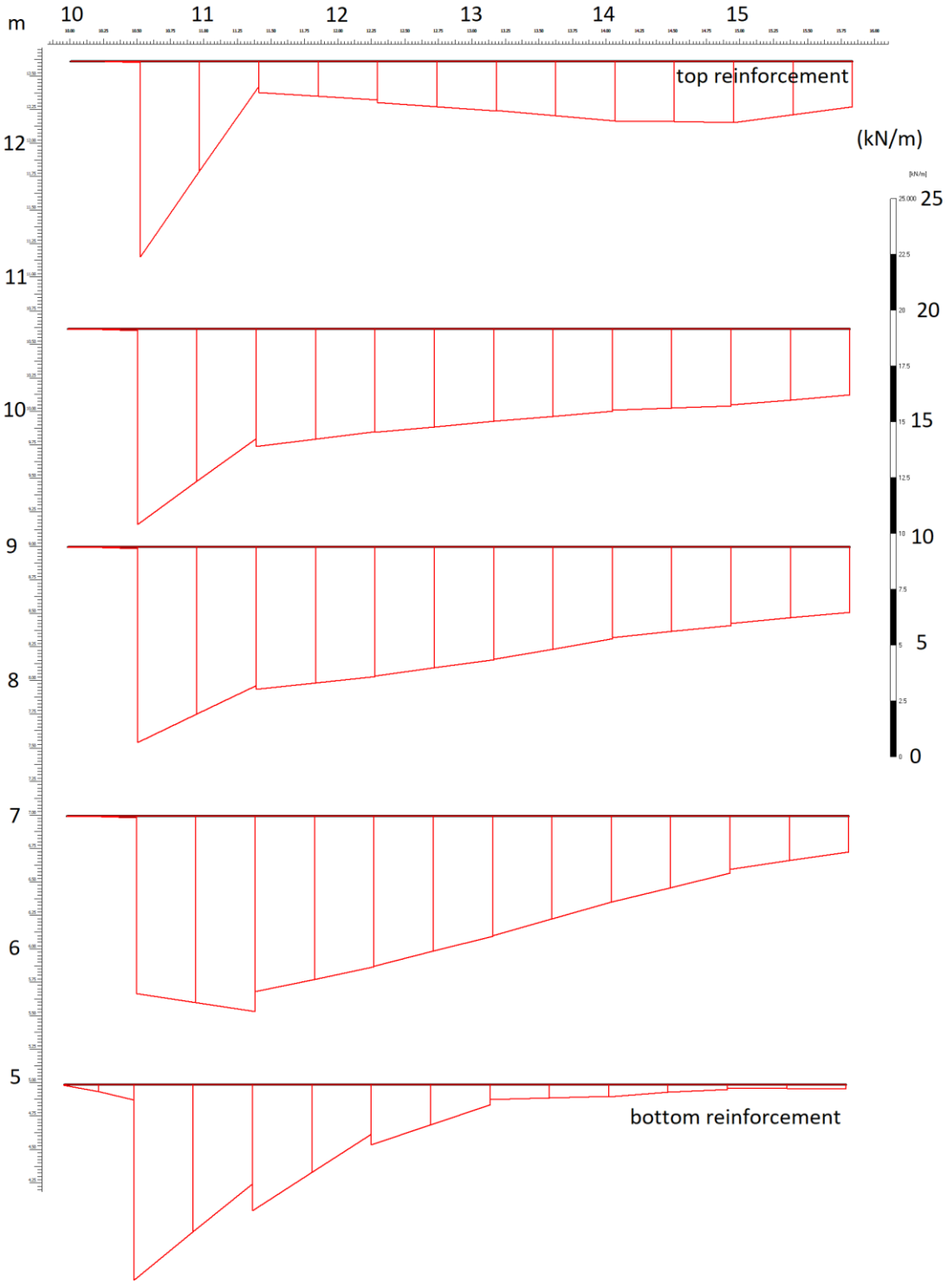


Figure 6.3. Axial force (envelope) distribution along reinforcements at various depths: Configuration 1, Static case (Scaled to 1.0).

At the end-of-construction stage, as axial normal stresses increase towards the bottom of the wall, following from the bulging phenomenon, axial forces are observed more at the mid-height of the wall. Higher horizontal displacements are observed also at mid-height that are also related to bulging behavior.

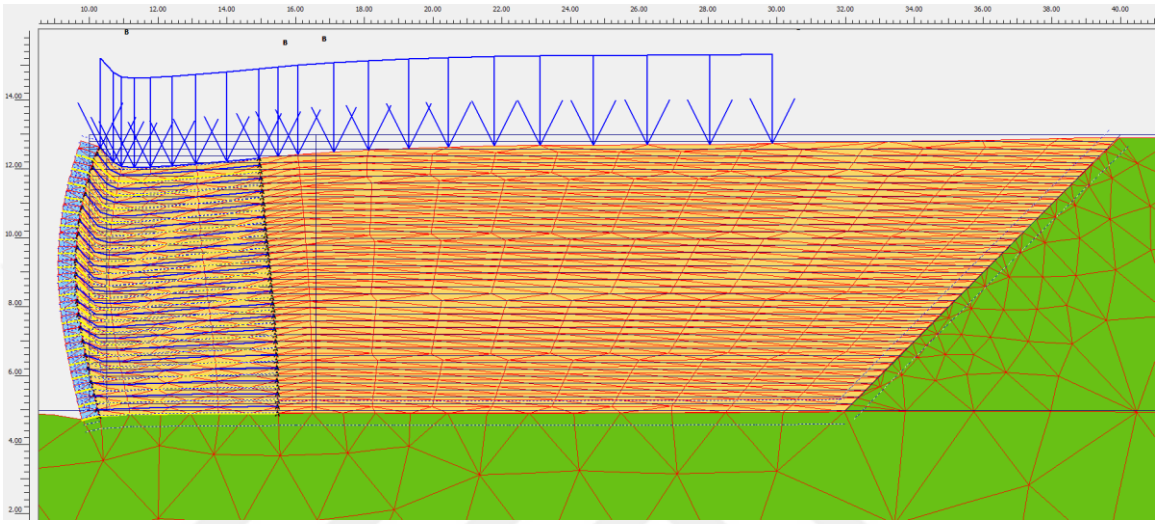


Figure 6.4. Deformed mesh: Configuration 1, Static case (Scaled to 10.0) (Zoom-in view).

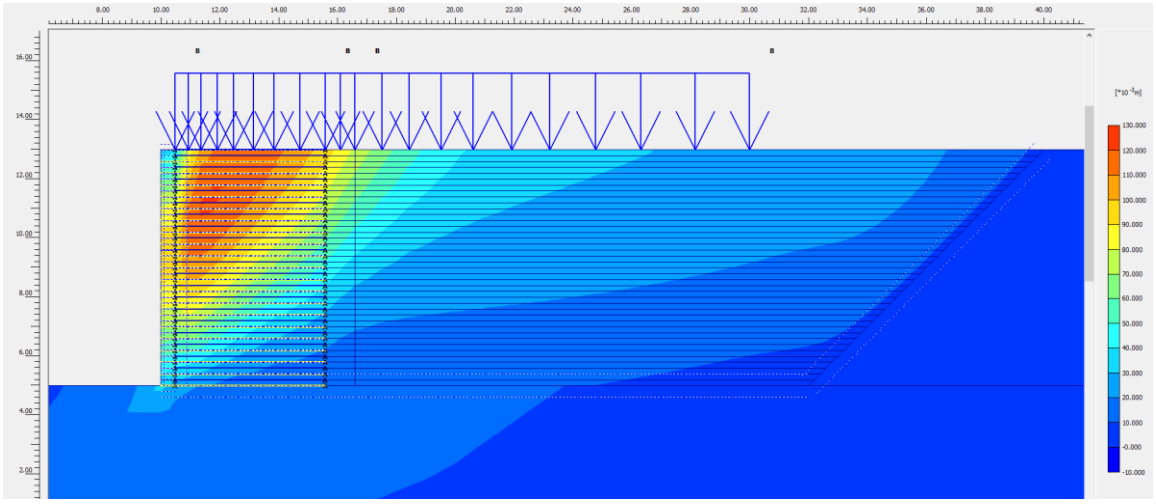


Figure 6.5. Total displacements distribution for Configuration 1, Static case (with shadings).

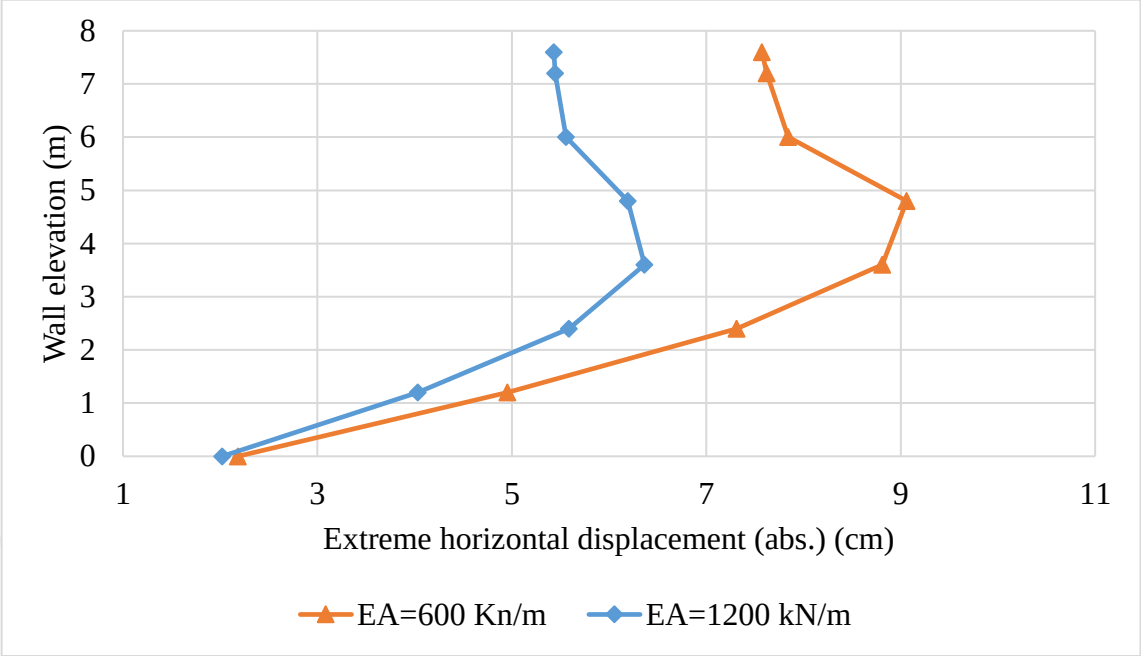


Figure 6.6. Extreme horizontal displacement (abs.) versus wall elevation: Static case, Configuration 1-2 (S_v= 0.4m, L/H= 0.7).

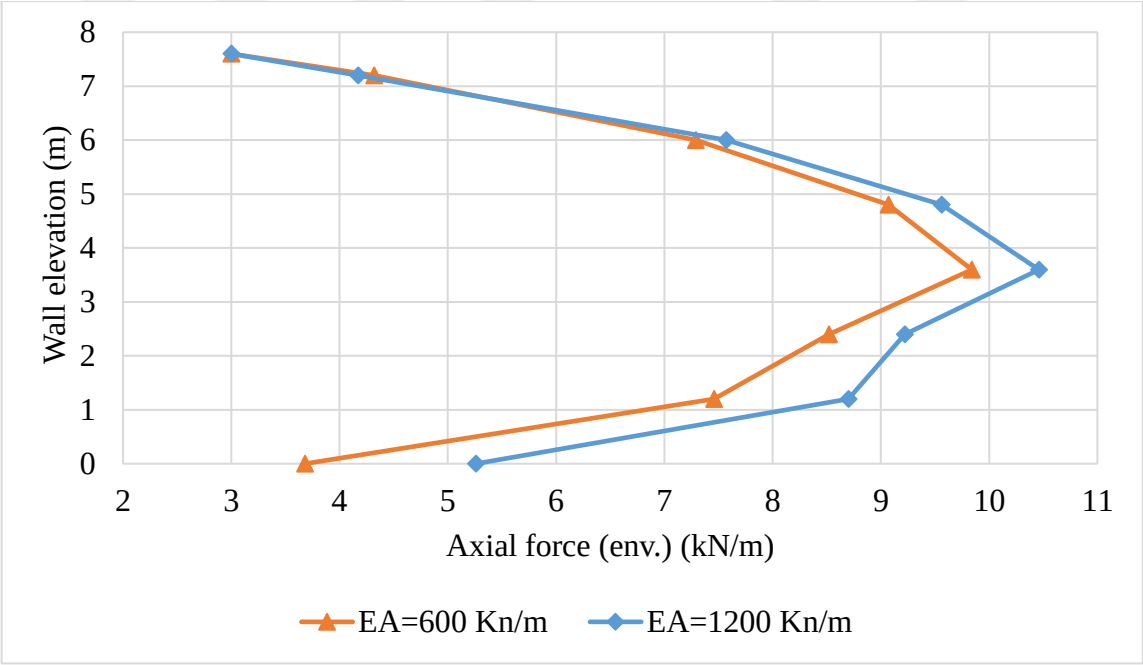


Figure 6.7. Axial force (env.) versus wall elevation: Configurations 1-2, Static case (S_v= 0.4m, L/H= 0.7).

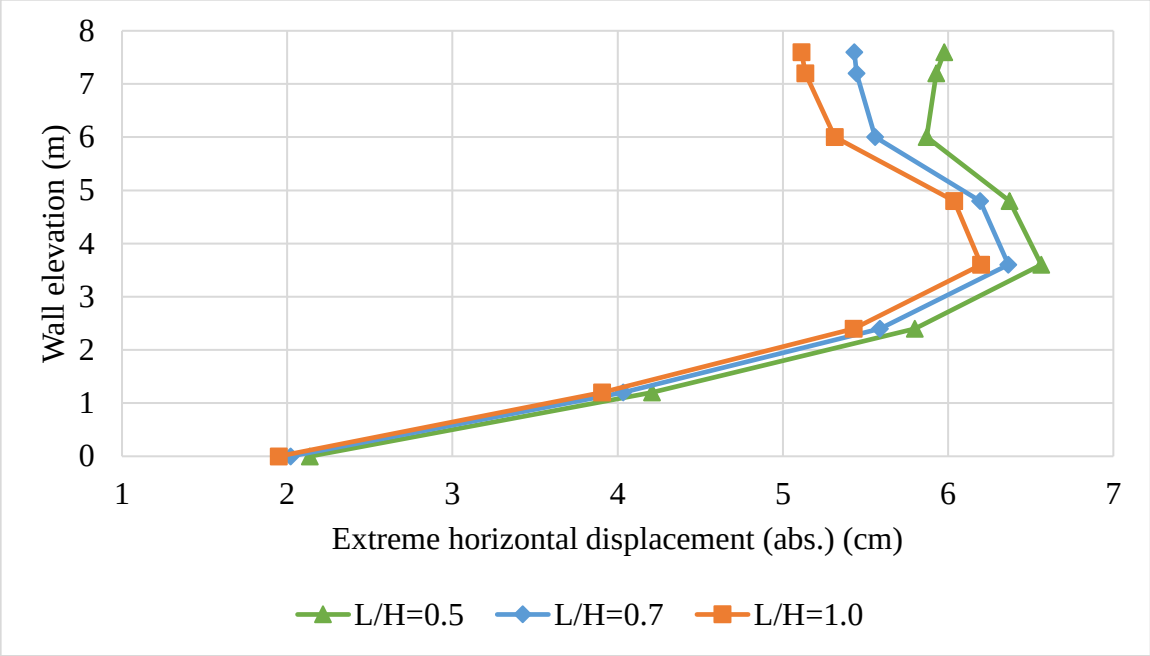


Figure 6.8. Extreme horizontal displacements (abs.) versus wall elevation: Configuration 2- 4- 6, Static case (S_v= 0.4m, EA= 1200kN/m).

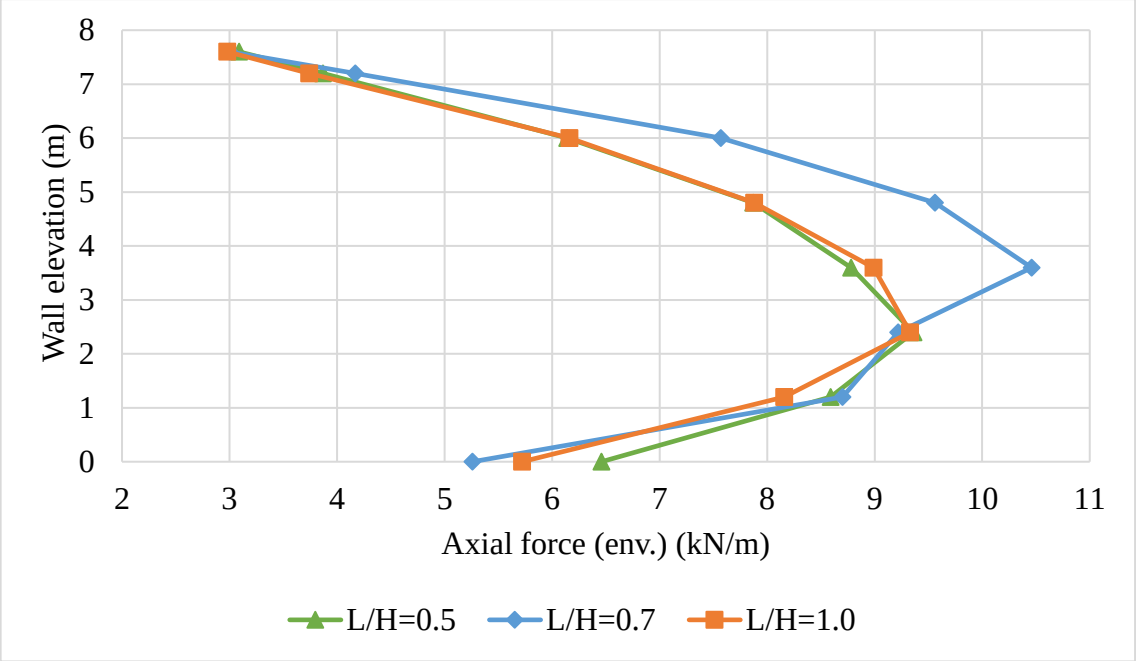


Figure 6.9. Axial force (env.) versus wall elevation: Configuration 2- 4- 6, Static case (S_v= 0.4m, EA= 1200kN/m).

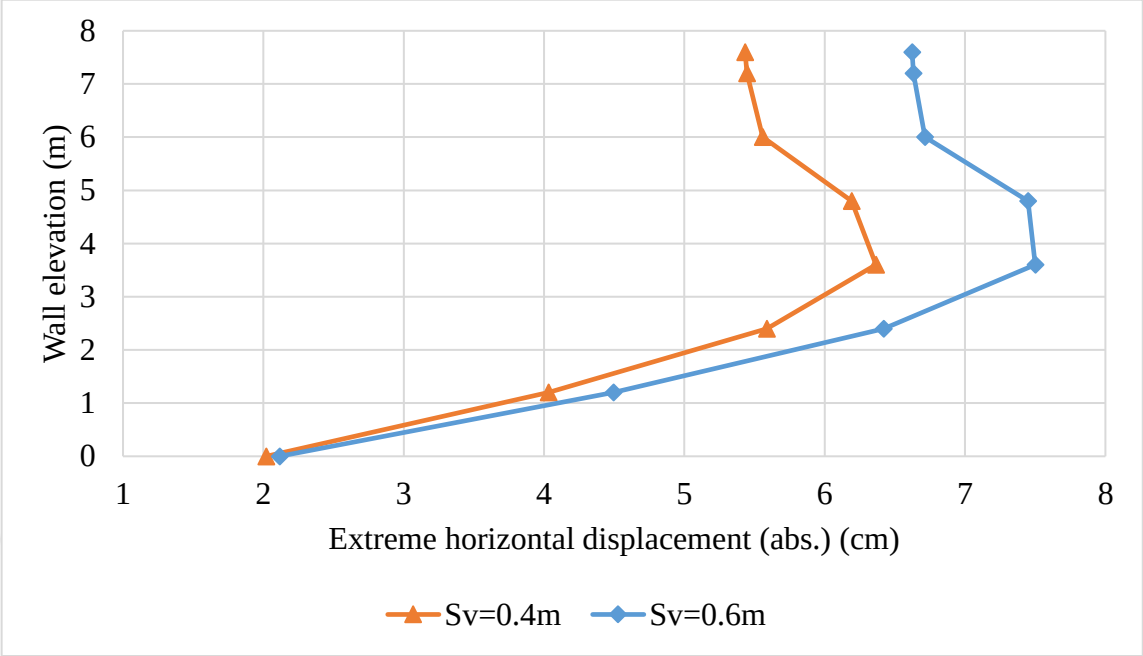


Figure 6.10. Extreme horziontal displacements (abs.) versus wall elevation: Configuration 2-8, Static case (EA= 1200kN/m, L/H= 0.7).

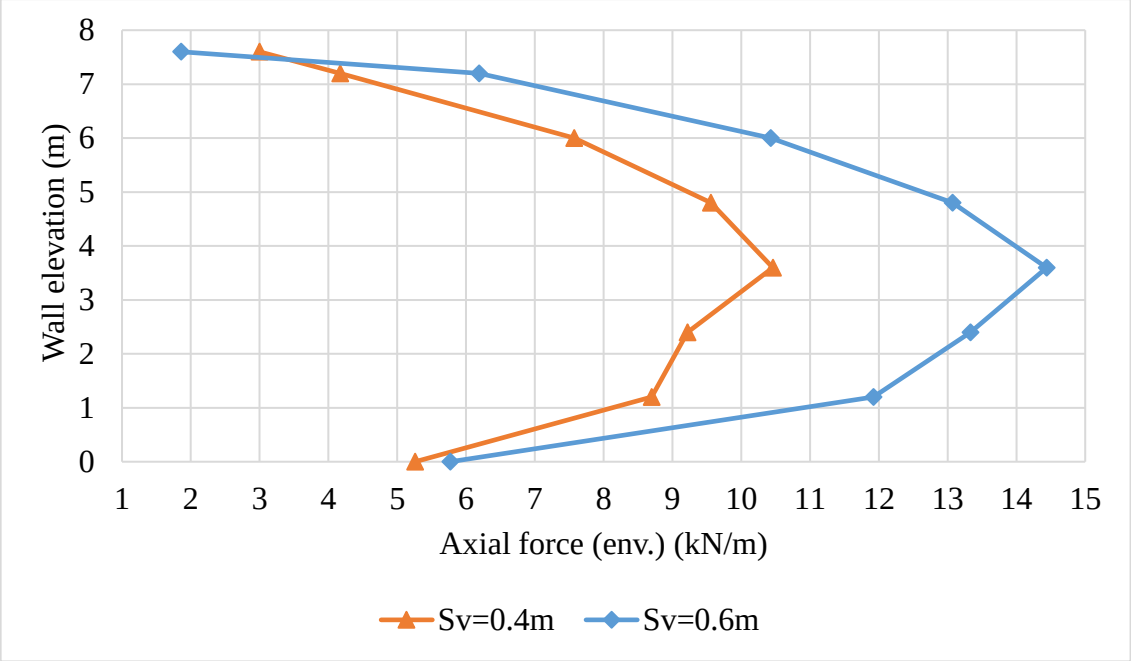


Figure 6.11. Axial force (env.) versus wall elevation: Configuration 2-8, Static case (EA= 1200kN/m, L/H= 0.7).

6.3. Results of FEM Analysis for Seismic Case

Figure 6.12 shows the deformed mesh for the seismic case for Configuration 1 for SL= 1.5 Hz. Comparing Figure 6.12 with Figure 6.4, it is possible to distinguish that the seismic behavior of the model is different from the static one. The outward movement of the wall, due to the seismic excitation is visible from the deformed shape. Additionally, it is possible to observe the reinforcements' deformed shape due to bending experienced at the joints. Based on the results, model's outward behavior under seismic loading is similar to that of cantilever retaining wall.

In Figure 6.14, the horizontal displacement directions inside and backside of the reinforced zone are shown with arrows. The direction of arrows is reversed just behind the reinforced area. While the reinforced area moves to the left, the retained fill tends to move to the right direction, which indicates the sort of detachment of the two. This affects the shear strains which can be seen in Figure 6.13 for seismic loading SL= 1.5 Hz and in Figure 6.15 for SL= 4 Hz. Especially for the case of SL=1.5 Hz, it is possible to see the stripping of top reinforcements from the retained fill. This can be related to the overturning tendency and the corresponding direction of horizontal displacements provided in Figure 6.14.

Figure 6.16 shows the horizontal displacements along reinforcements at various depths and in Figure 6.17 axial force (envelope) distribution along the reinforcement is provided for SL=1.5 Hz with Configuration 1. It is possible to identify the increase in the axial load at the rear of upper reinforcements as the shear strain increases at these portions. In addition, mid and lower level reinforcements (that are closer to the bottom of the wall) experience higher axial forces than the upper ones and this is visible in Figure 6.17. This can be related to the normal stress, pullout and friction mechanisms. The figures provided correspond to models with L/H=0.7. As it can be seen in L/H=0.7 models, the displacement distribution is uniform along the reinforcement.

Figure 6.18 shows the mean effective stresses for SL=1.5 Hz with Configuration 1. From the shading, it is also possible to observe the model's tendency to overturning.

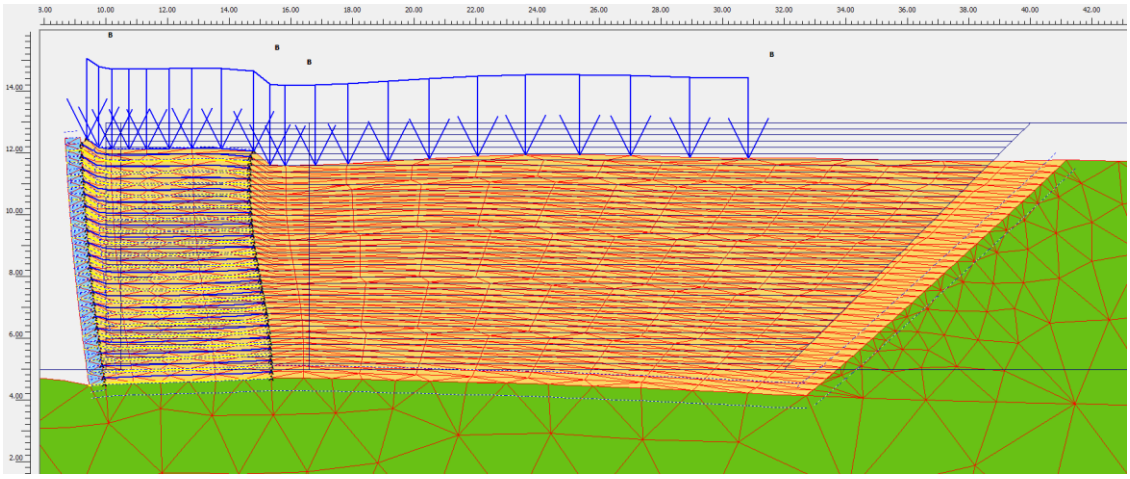


Figure 6.12. Deformed mesh: Configuration 1, SL=1.5 Hz (Scaled to 10.0).

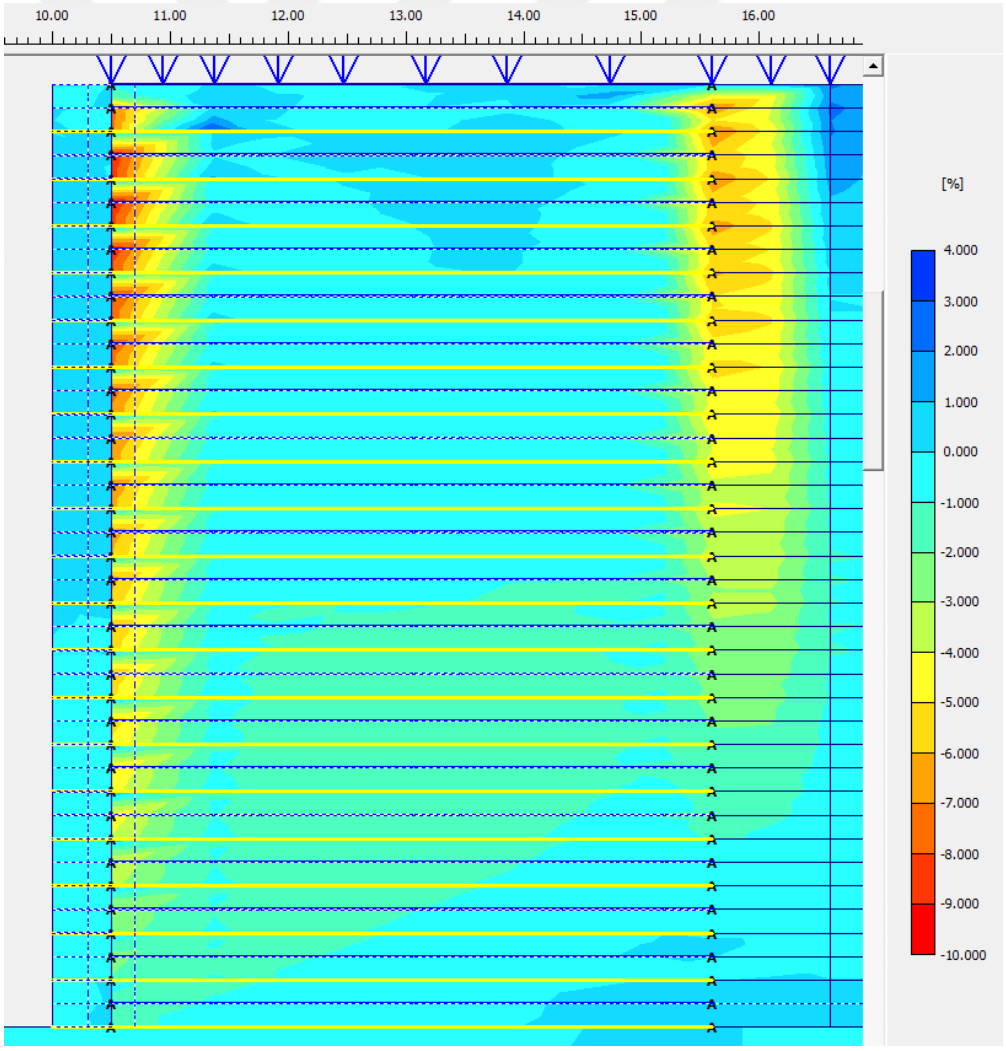


Figure 6.13. Configuration 1 for SL=1.5 Hz: shear strain distribution.

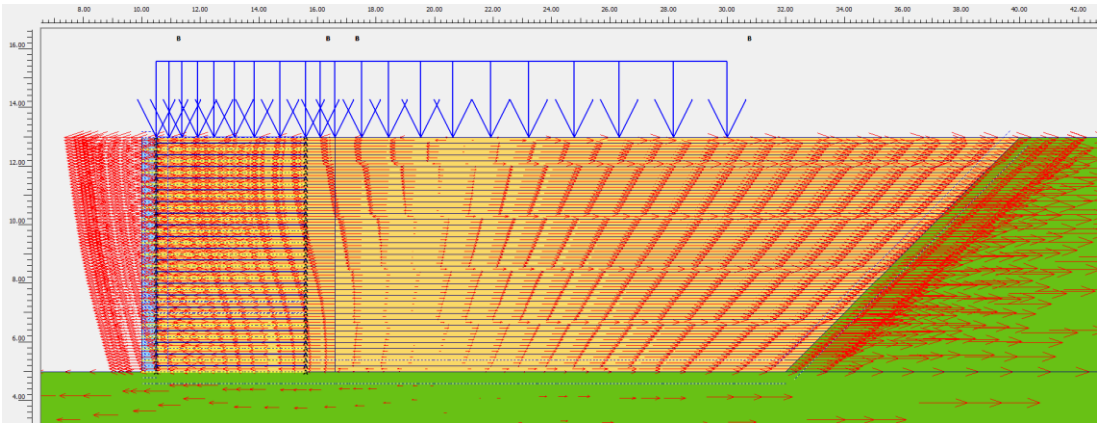


Figure 6.14. Distribution of horizontal displacements: Configuration 1, L/H=0.7, for SL=1.5 Hz (Scaled to 20.0) (zoom-in view) (with arrows).

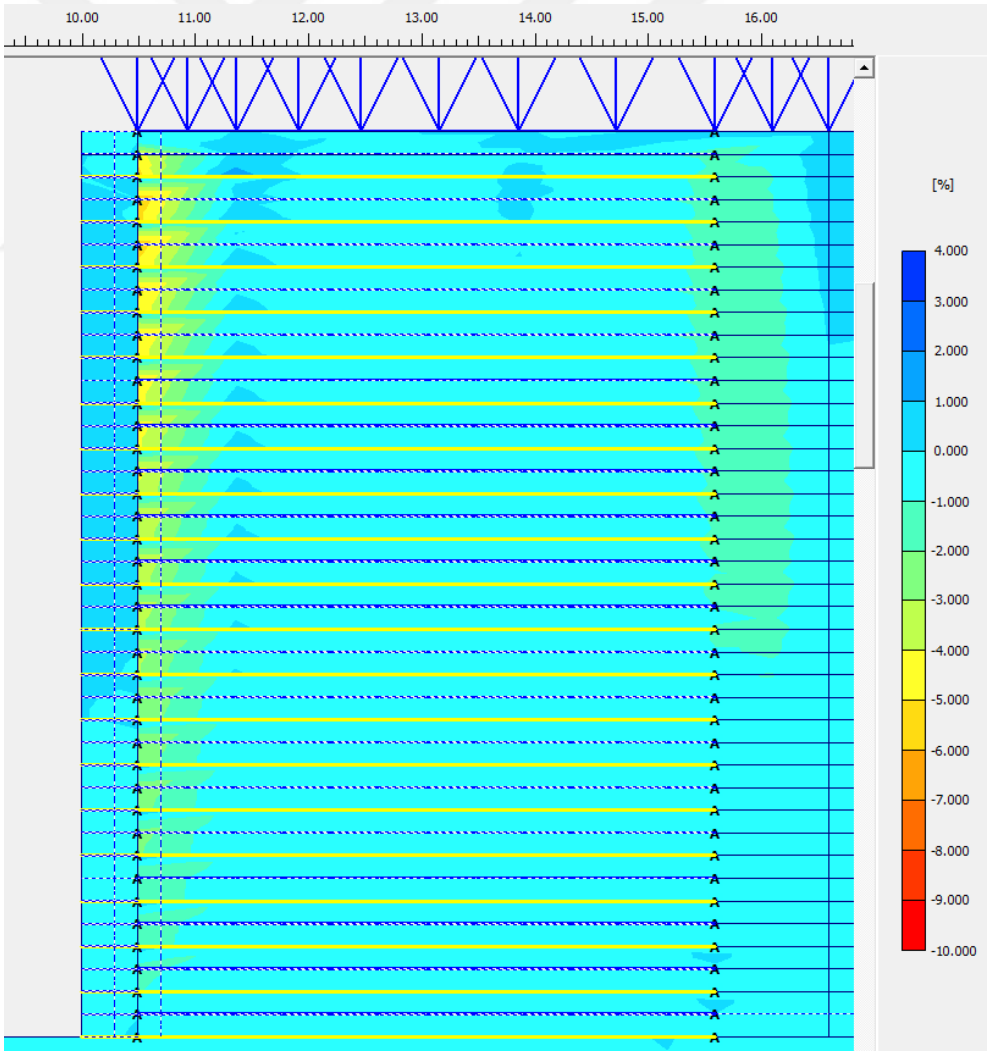


Figure 6.15. Configuration 1 for SL=4 Hz: shear strain distribution.

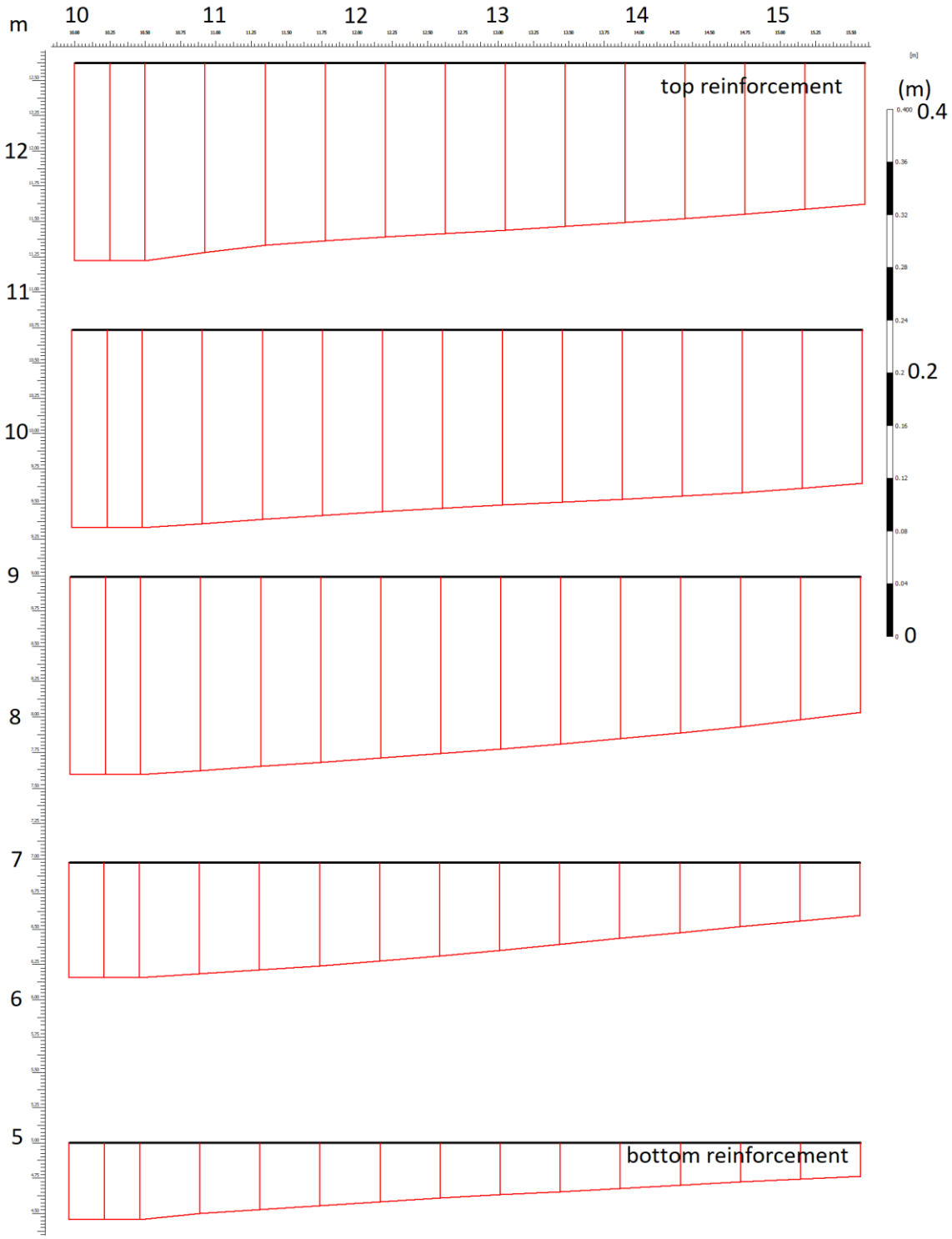


Figure 6.16. Horizontal displacement distribution along reinforcements at various depths: Configuration 1 for SL=1.5 (Scaled to 10.0).

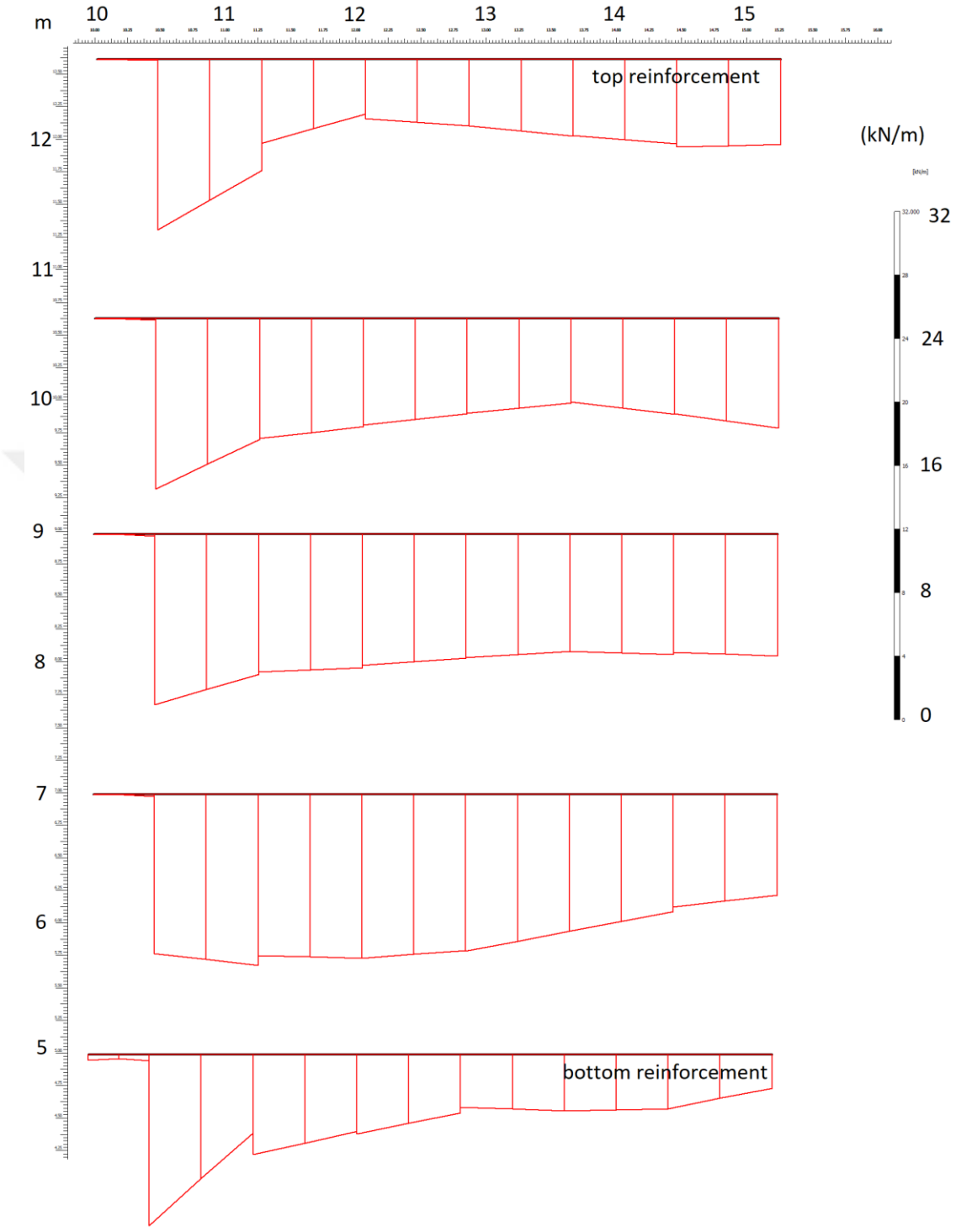


Figure 6.17. Axial force (envelope) distribution along reinforcements at various depths: Configuration 1 for SL=1.5 (Scaled to 1.0).

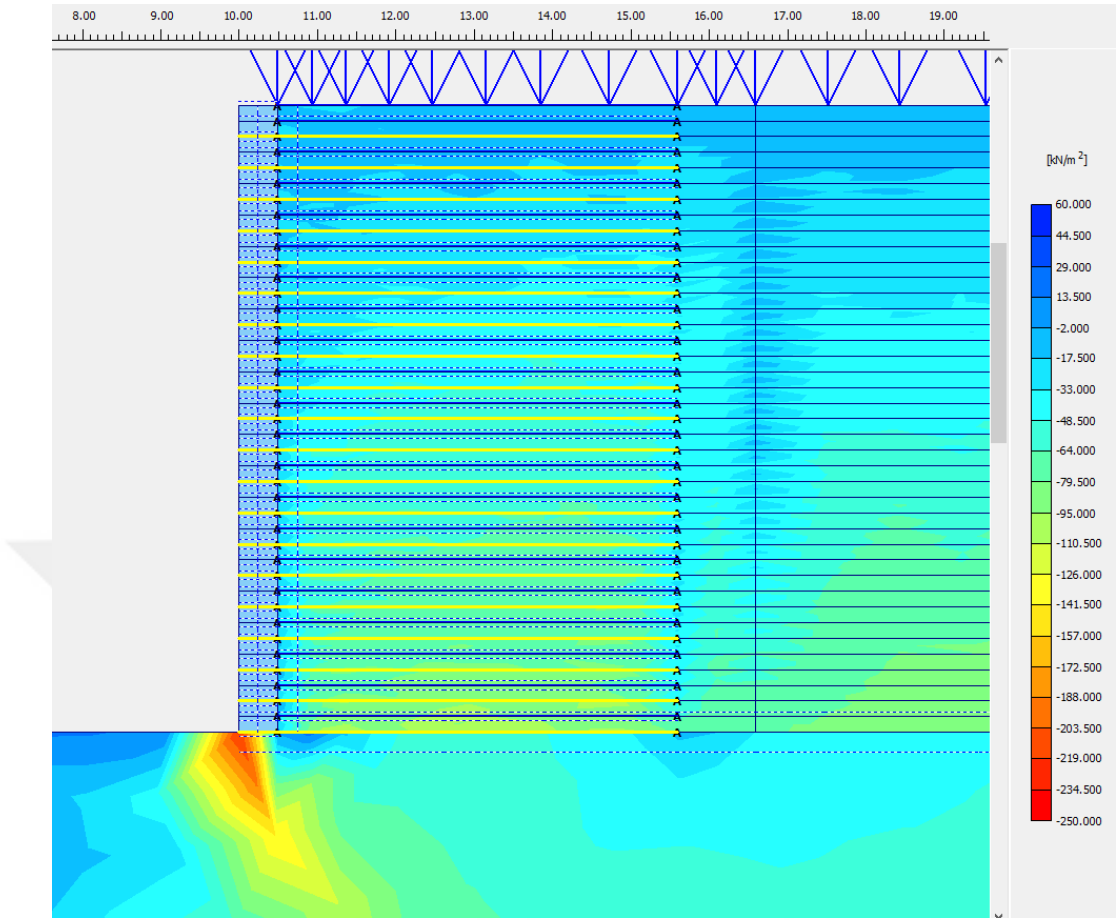


Figure 6.18. Effective mean stress for Configuration 1 SL= 1.5 Hz (with shading).

6.4. Effect of Loading Frequency on Acceleration, Displacements and Axial Stresses

Seismic response of short-period structures' is dominated by their natural frequency as it is illustrated (Hatami & Bathurst, 2000). Therefore, each of the previously presented 12 MSE Wall configurations was excited with seven harmonic ground motion input data (corresponding to seven frequencies of SL= 1, 1.5, 2, 3, 4, 6, 8 Hz) around the natural frequency of the wall.

6.4.1. Effect of Frequency on Amplification

In Figure 6.19, acceleration amplification factor versus height comparison plot is provided for each frequency case. In the horizontal axis, the amplification factor which is the ratio of the maximum acceleration at the given level to 0.2g (base excitation) is presented.

Acceleration of seismic excitation amplifies at the frequencies below 2 Hz, and de-amplifies above 2 Hz in the foundation soil. The maximum amplification in the wall occurs for SL=4 Hz which is equal to the estimated natural frequency of the 8m MSE Wall model. Despite that, when the foundation and MSE Wall are considered together as an overall system, the amplification is highest for SL= 1.5 Hz. At the top of the wall, the maximum amplification factor is calculated as 1.75 for SL= 1.5Hz. As the amplification for SL=1.5 Hz is greater than the amplification for SL= 4 Hz in the foundation, this results with a higher acceleration at the top of the wall for SL=1.5 Hz case.

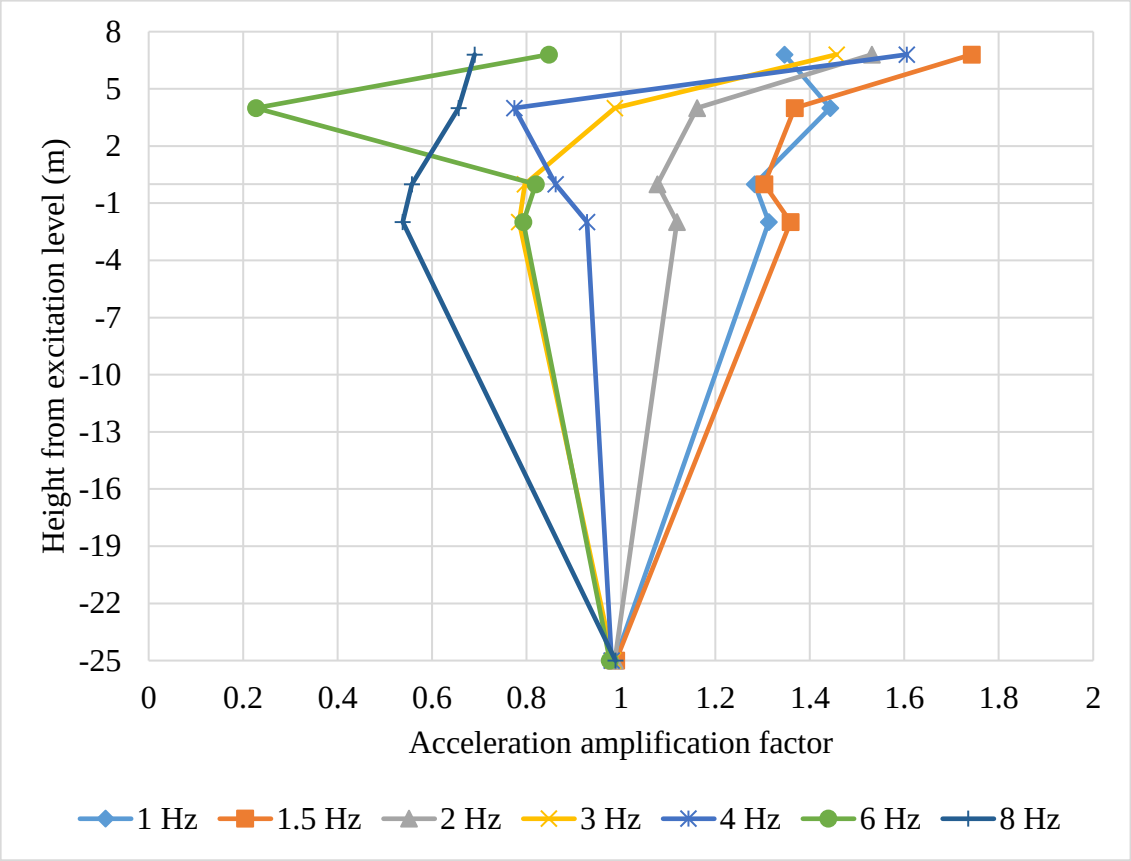


Figure 6.19. Acceleration amplification factor versus height from base excitation level: Configuration 1, SL= 1, 1.5, 2, 3, 4, 6, & 8 Hz.

In Figure 6.20, the acceleration variation is the plot in different zones of the MSE Wall: facing, reinforced and retained soils, utilizing the points selected prior to the calculation. The data is gathered from three points at the facing, three points at the reinforced soil, two points at the retained soils (see Figure 6.1). Two frequency (1.5 and 4 Hz) levels, the ones that have

the maximum range are selected for this plot. The amplification ratios are greater in the retained soil compared to that of reinforced soil at the mid-height of the wall.

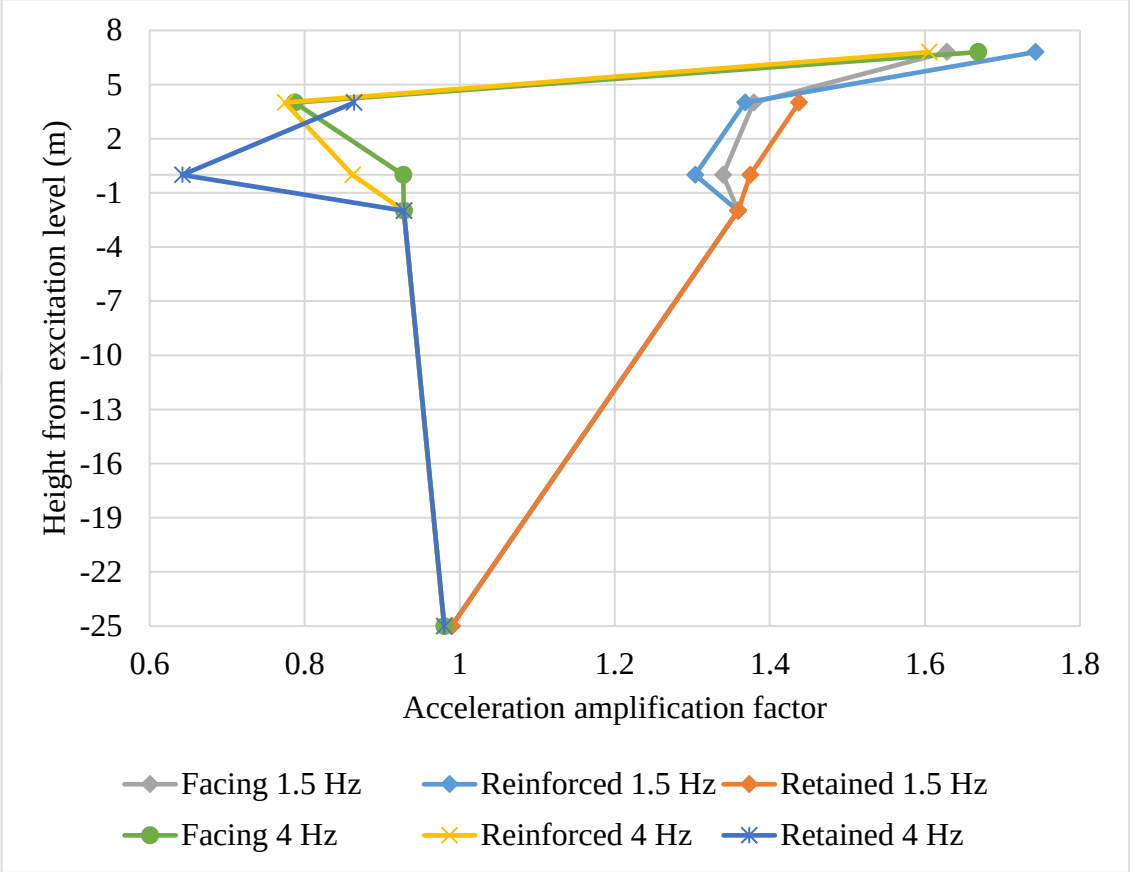


Figure 6.20. Configuration 1, Amplification factor versus height from the base level for SL= 1.5 & 4 Hz.

6.4.2. Effect of Frequency on Displacements

In Figure 6.21, horizontal displacement (absolute) change with wall elevation is provided with Configuration 1 for each frequency case. This plot illustrates that most displacement is captured for SL=1.5 Hz at all levels and it is followed by SL= 2 Hz and SL= 1 Hz cases, respectively.

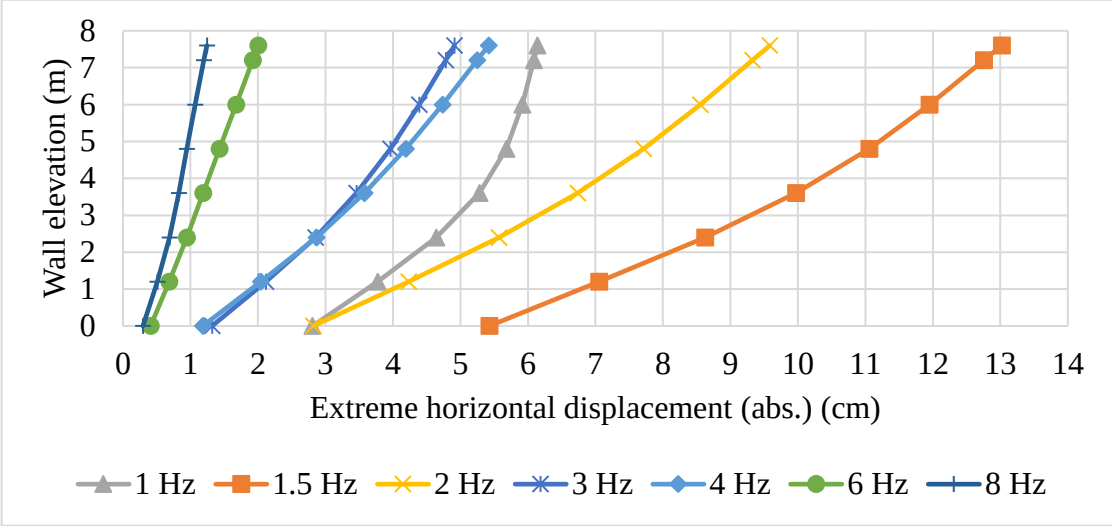


Figure 6.21. Extreme horizontal displacement (abs.) versus wall elevation: Configuration 1, SL= 1, 1.5, 2, 3, 4, 6, & 8 Hz.

6.4.3. Effect of Frequency on Axial Stresses

In Figure 6.22, axial force (envelope) versus wall elevation for each frequency case with Configuration 1 is shown.

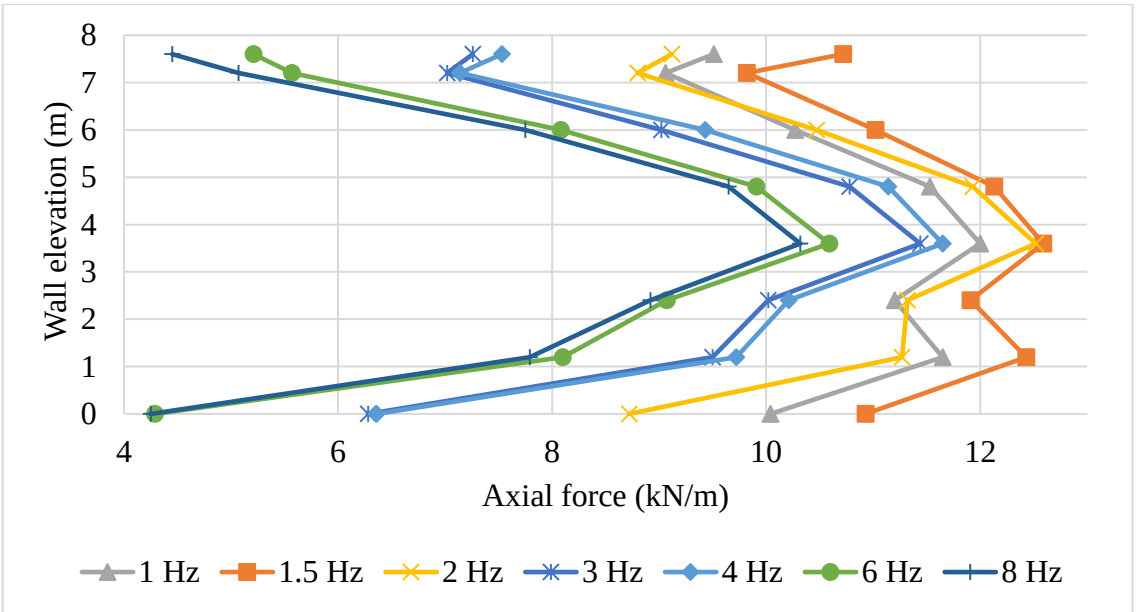


Figure 6.22. Axial force (envelope) versus wall elevation: Configuration 1 (S_v= 0.4m, EA= 600kN/m, L/H= 0.7), for SL= 1, 1.5, 2, 3, 4, 6, & 8 Hz.

The maximum axial force occurs for SL=1.5 Hz for each height level. Moreover, it can be inferred that axial forces reach a maximum value at a height of 3.6 m for each frequency case. The plot also indicates that mid and lower reinforcements carry more axial stresses than the ones located closer to the top of the MSE Wall.

6.5. Effect of Reinforcement Stiffness (EA) on Displacements and Axial Stresses

To evaluate the effect of reinforcement stiffness on the seismic behavior of MSE Wall, models were prepared with two reinforcement strengths of 600 and 1200 kN/m.

6.5.1. Effect of EA on Displacements

As indicated previously, displacements are outwards from the wall and therefore, all have a negative sign, for ease of display absolute (abs.) values of displacements are provided in all figures. In Figure 6.23, the effect of EA on extreme horizontal displacements at various wall levels are provided.

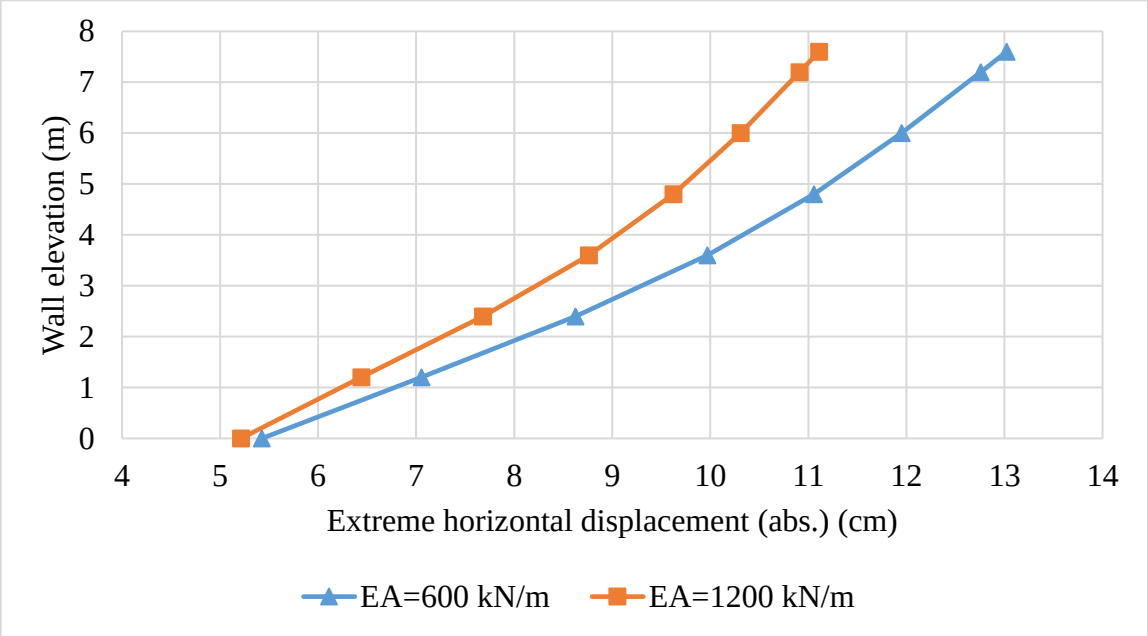


Figure 6.23. Ext. hor. (abs.) displacement versus wall elevation: Configuration 1-2 (Sv=0.4m, L/H=0.7), for SL=1.5 Hz.

Figure 6.24 is mainly provided to investigate the behavior of uppermost reinforcement under different loading frequencies. In Figure 6.25, the variation of extreme horizontal displacement at top reinforcement with EA is compared for all configurations for SL=1.5 Hz.

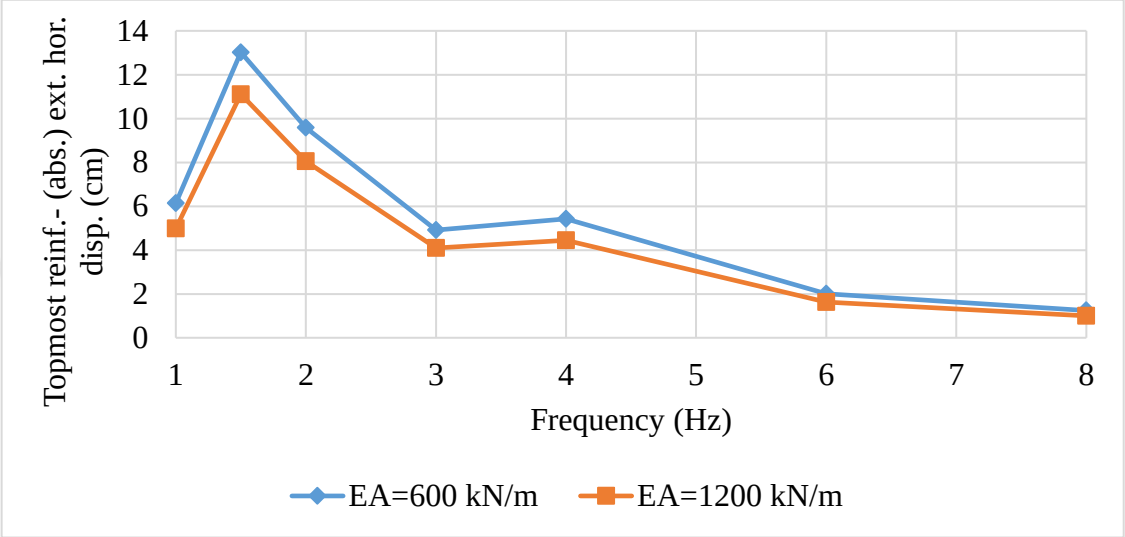


Figure 6.24. Frequency versus extreme (abs.) horizontal displacement at uppermost reinforcement: Configuration 1-2 (Sv=0.4m, L/H=0.7), SL= 1, 1.5, 2, 3, 4, 6, & 8 Hz.

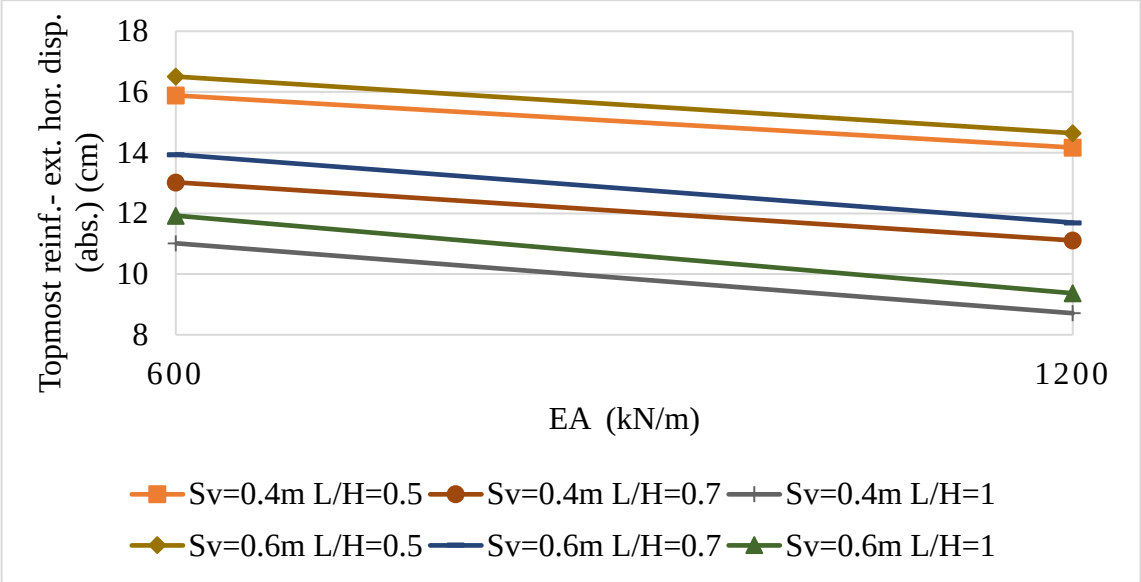


Figure 6.25. Reinforcement stiffness (EA) versus extreme horizontal displacement (abs.) of top most reinforcement, SL=1.5 Hz.

6.5.2. Effect of EA on Axial Stresses

EA has an effect on the uppermost reinforcements' horizontal displacement but there is no significant effect on its' axial force for any of the earthquake frequencies. To clarify this, a comparison of the axial forces in uppermost reinforcement between Configuration 1 and 2 are provided in Figure 6.26. The curves of other configurations also show similar characteristics. Normally, it is expected to have higher axial stresses when the strength of the reinforcement is high. Moreover, when the reinforcement strength is insufficient, reinforcement breaking can occur. This situation can continue with higher displacements with tensile failure and collapse of the wall by the occurrence of the slip at the soil reinforcement (Mahmood, 2009). However, in this study, in terms of axial force, significant differences do not occur at the uppermost reinforcement between the model with EA of 600 and 1200 kN/m (see Figure 6.27). This may be explained with the fact that tensile failure and slip at the reinforcements do not occur, accordingly the MSE Wall does not experience a progressive failure due to reinforcement. However, in Figure 6.28 it is observed that the variation of axial forces occurs at lower reinforcements rather than upper reinforcements. This clearly shows that the effect of reinforcement stiffness (EA) becomes more noticeable towards the bottom of the MSE Wall. At the bottommost reinforcement, axial envelope force increases 44% when EA is doubled.

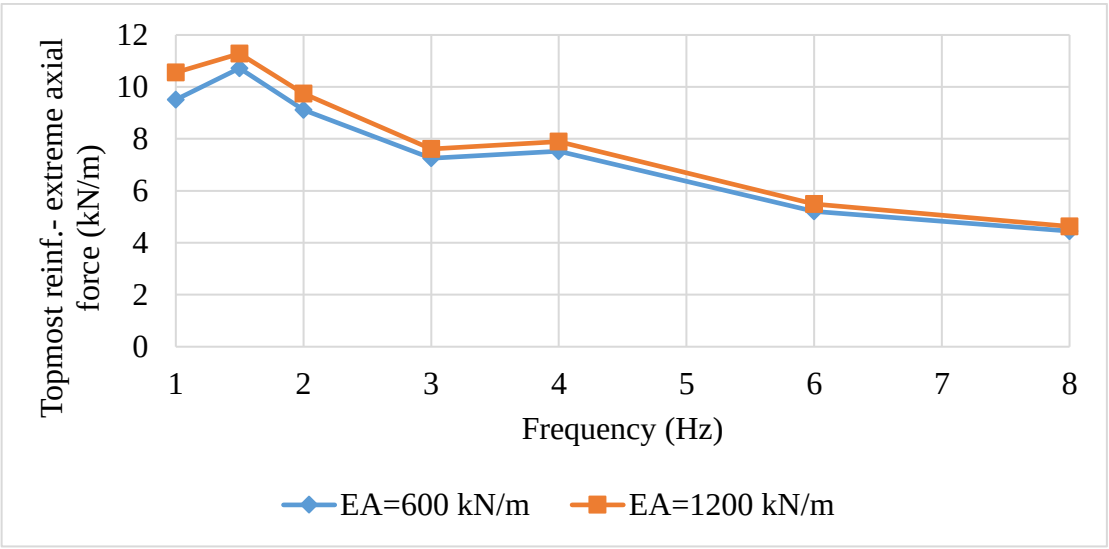


Figure 6.26. Extreme axial force (env.) for for the uppermost reinforcement: Configuration 1-2 (Sv=0.4m, L/H=0.7).

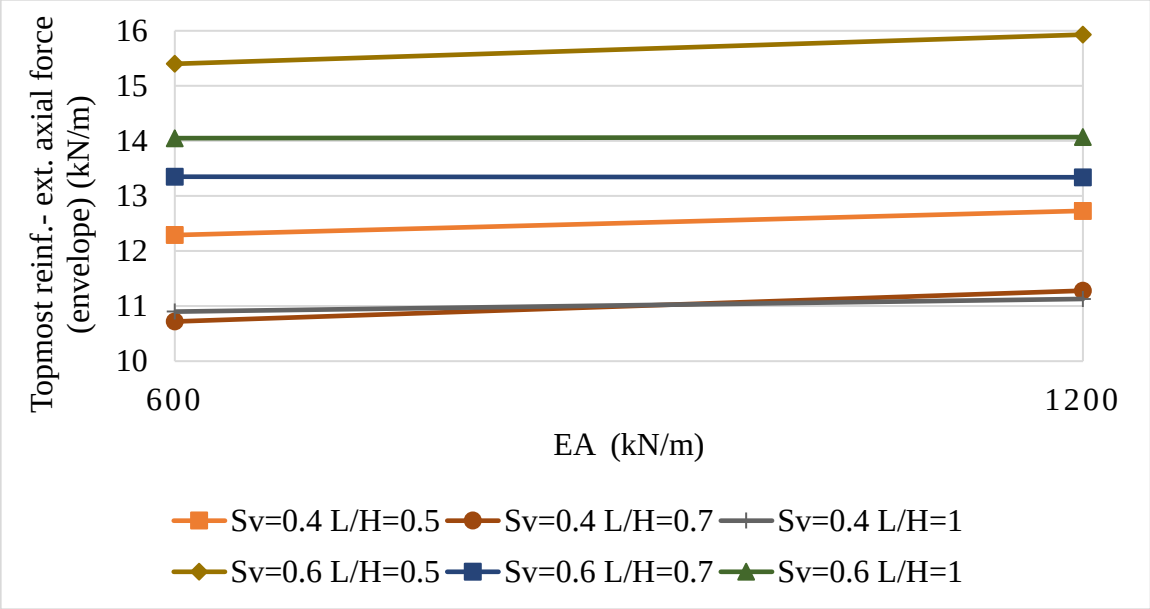


Figure 6.27. Axial force (env.) at the uppermost reinforcement versus reinforcement stiffness variation for SL=1.5 Hz.

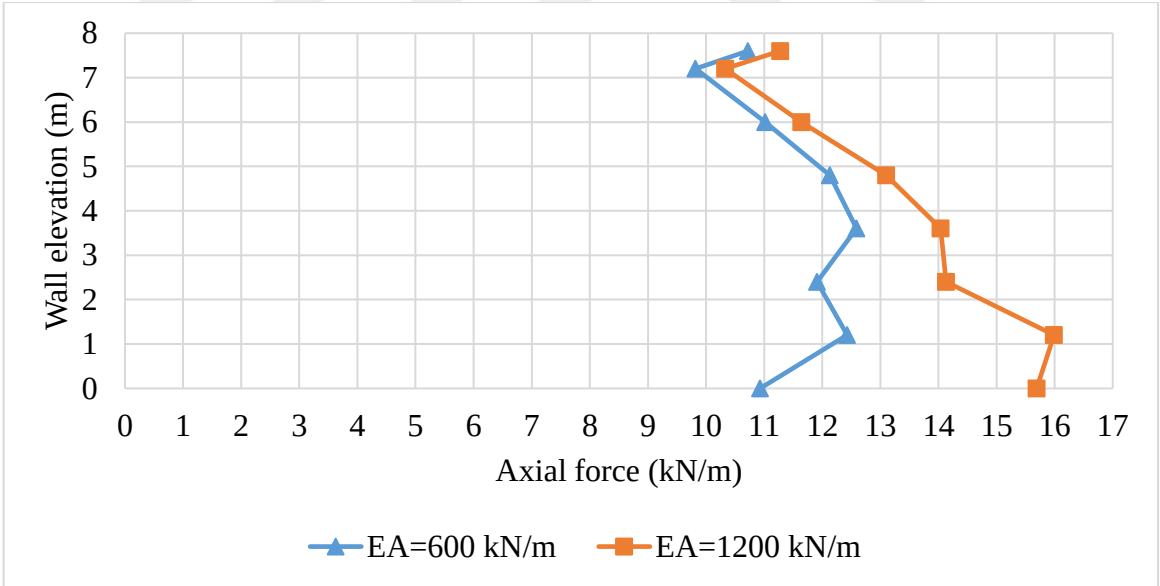


Figure 6.28. Axial force (env.) versus wall elevation: Configuration 1-2 (Sv=0.4m, L/H=0.7) for SL=1.5 Hz.

6.6. Effect of L/ H on Displacements and Axial Stresses

To evaluate the effect of L/H, three L/H ratios: 0.5, 0.7 and 1.0 were considered in this study.

6.6.1. Effect of L/ H on Displacements

In Figure 6.29, the change of extreme horizontal displacement at different wall height levels can be seen. It can be inferred from this plot that the difference of horizontal displacements between different reinforcement lengths increases from bottom to top of the MSE Wall. When the effect of L/H on uppermost reinforcement's displacements are investigated, it is seen that displacements increase from L/H= 1.0 to L/H= 0.5 at 1.5 Hz and the curves converge towards 8 Hz for all MSE Wall configurations (see Figure 6.30). The comparison graphs of extreme horizontal displacement versus wall elevation for L/H ratios 0.5 and 0.7, and 1.0 for each earthquake frequency are shown in Figure 6.31 and Figure 6.32 respectively. It can be indicated that when the stiffness of the wall is increased by increasing the reinforcement length, extreme horizontal displacements also increase at the topmost reinforcement.

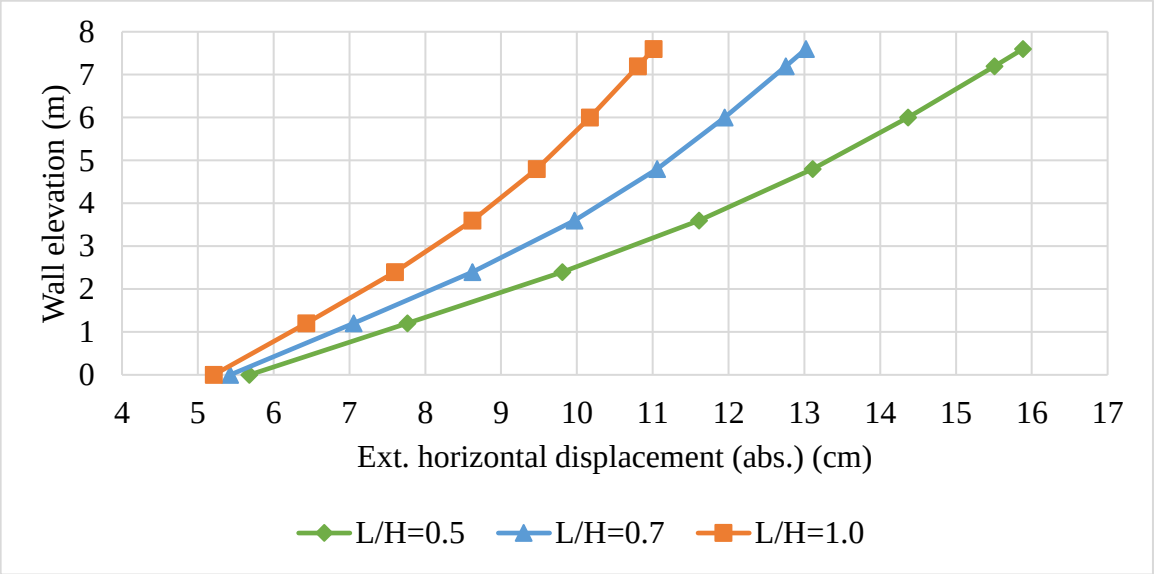


Figure 6.29. Ext. hor. displacement (abs.) versus wall elevation: Configuration 1-3-5 (S_v= 0.4m, EA= 600kN/m), SL=1.5.

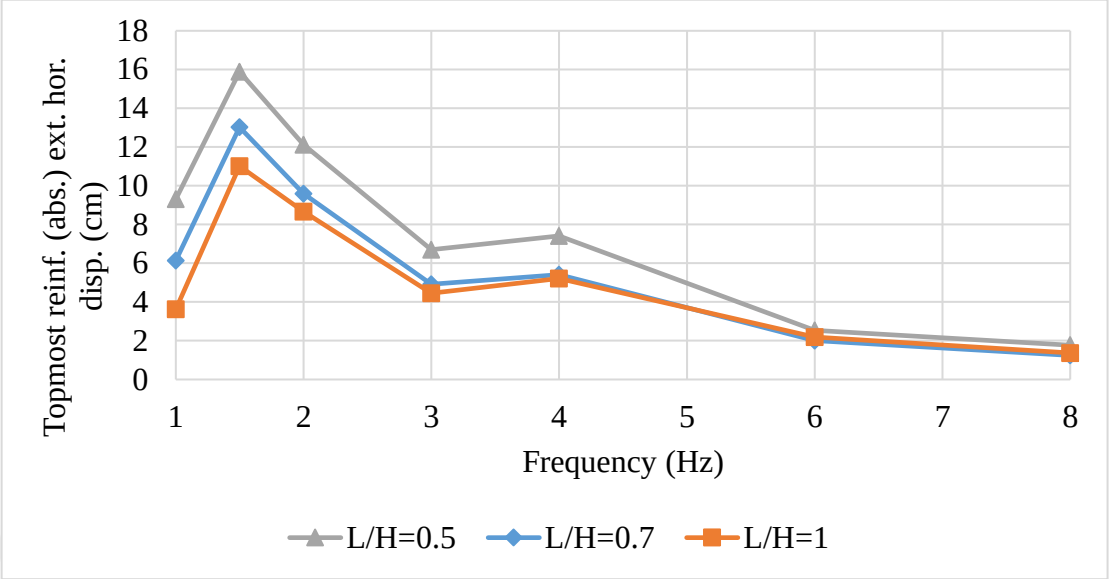


Figure 6.30. Frequency versus extreme horizontal displacement (abs.) at uppermost reinf.: Configuration 1-3-5 (S_v= 0.4m, EA= 600kN/m).

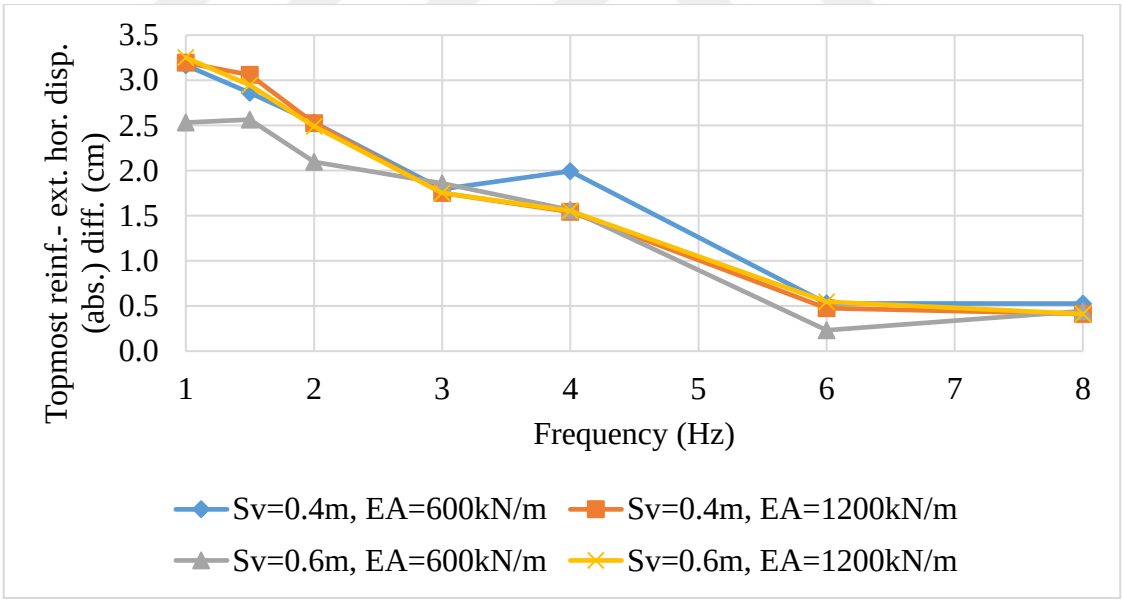


Figure 6.31. Frequency versus ext. hor. disp. (abs.) difference (from L/H=0.5 values, L/H=0.7 values subtracted) at the uppermost reinforcement.

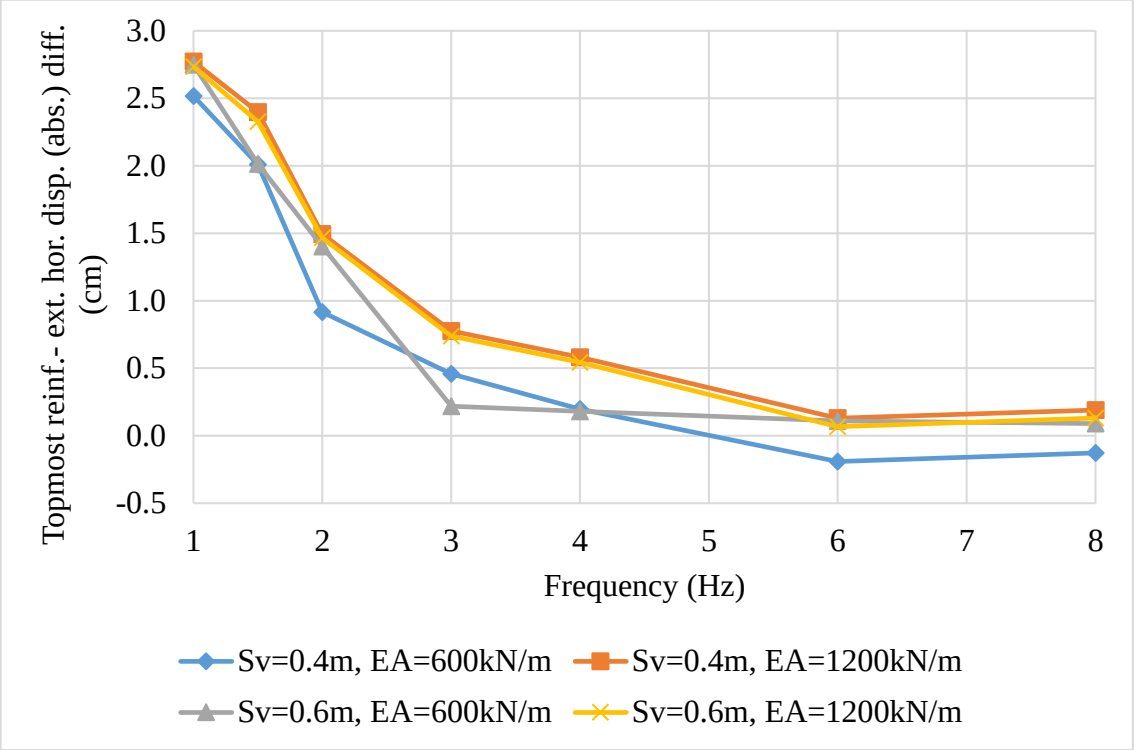


Figure 6.32. Frequency versus extreme hor. disp. (abs.) difference (from L/H=0.7 values, L/H=1.0 values subtracted) at the uppermost reinforcement.

L/H ratio versus extreme topmost reinforcement plots are presented for Configurations 1-3-5 in Figure 6.33. The change in the displacements towards L/H=1.0 is visible in the figure, especially for SL=1.5 Hz case. The effect of frequency can be clearly seen in this plot. The plots generated for other MSE Wall configurations were in agreement with this one, so their graphs are not shared herein.

Previous studies in the literature indicate the effect of reinforcement length on the location of the Rankine failure surface. Reinforcements should be able to develop enough frictional resistance along their surface to resist against the pullout force. When the reinforcement cuts across the Rankine failure plane and goes beyond the failure line, the horizontal displacements will reduce after that point (Kibria, Hossain, & Khan, 2013). In this study, displacements reduced around 3 cm, with the increase from L/H= 0.5 to L/H= 0.7 and reduced around 2.5 cm, with the increase from L/H= 0.7 to L/H= 1.0 for SL= 1.5 Hz. The observed differences in displacements were even less for the other earthquake frequencies.

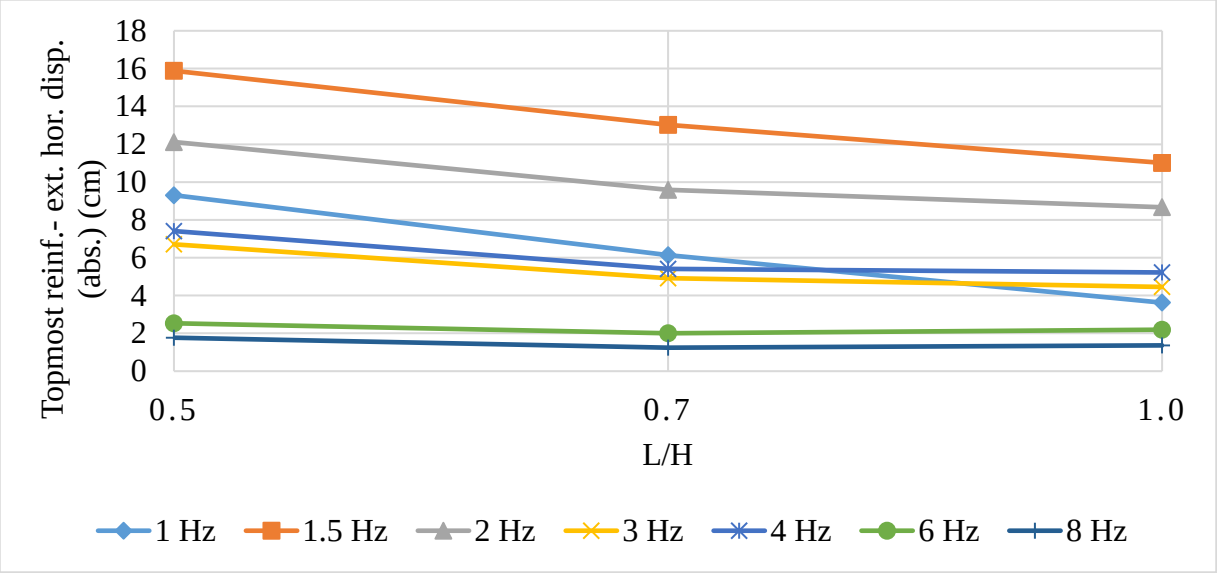


Figure 6.33. L/H versus extreme hor. disp. (abs.) at uppermost reinforcement for each frequency: Configuration 1-3-5 (Sv=0.4m, EA=600kN/m).

6.6.2. Effect of L/ H on Axial Stresses

When the effect of L/H on axial stress of the uppermost reinforcement is evaluated (see Figure 6.34), it is seen that it has an effect on axial stresses between L/H ratios of 0.5 and 0.7. With the increase from L/H =0.5 to L/H= 1.0, axial stresses decrease by about 1.5-2.5 kN/m (see Figure 6.35) for SL= 1.5 Hz. The lines converge towards 8 Hz, in essence, the difference is minimized with increasing earthquake frequency. However, when the plots corresponding to L/H =0.5 to L/H= 1.0 are compared with each other, it can be seen that these overlap with each other (see Figure 6.34), indicating that after the ratio reaches 0.7 its further increase has minimal effect on the axial stresses.

In order to observe the effect of reinforcement length, a comparative plot of frequency versus the axial force of the topmost reinforcement with Configurations 1-3-5 is provided in Figure 6.36. This plot is considered to be representative of other MSE Wall configurations as they show a similar tendency. Moreover, the chart indicates that changing the L/ H ratio from 0.7 to 1.0 has a visible effect on horizontal displacements (see Figure 6.33) but this change does not possess a significant effect on axial forces.

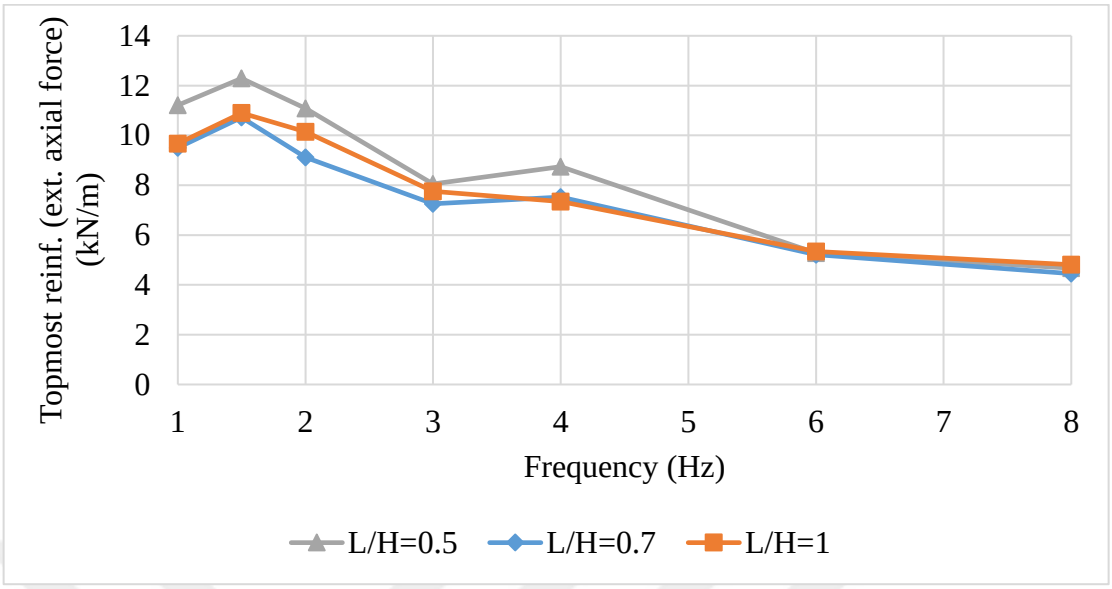


Figure 6.34. Frequency versus extreme axial force (env.) at the uppermost reinforcement: Configurations 1-3-5 (S_v= 0.4m, EA= 600kN/m).

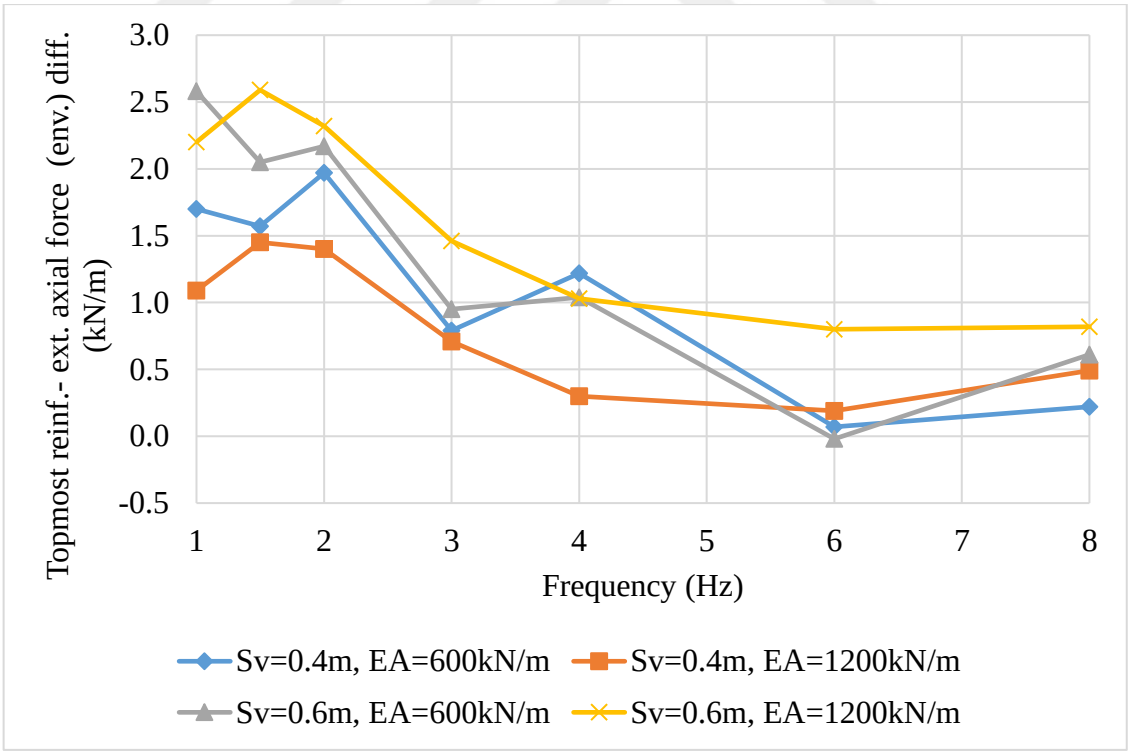


Figure 6.35. Frequency versus extreme axial force (envelope) difference (From L/H=0.5 values, L/H=0.7 subtracted) at the uppermost reinforcement.

In FHWA, minimum L/H ratio is recommended as 0.7 for static loading, and L/H ratio is recommended in the 0.8 to 1.1 range for seismic loading (Berg *et al.*, 2009). Figure 6.36 implies that when an L/H ratio of 0.5 is used, the reinforcements carry 2 kN/m less axial force at the uppermost reinforcement level for SL= 1.5 Hz.

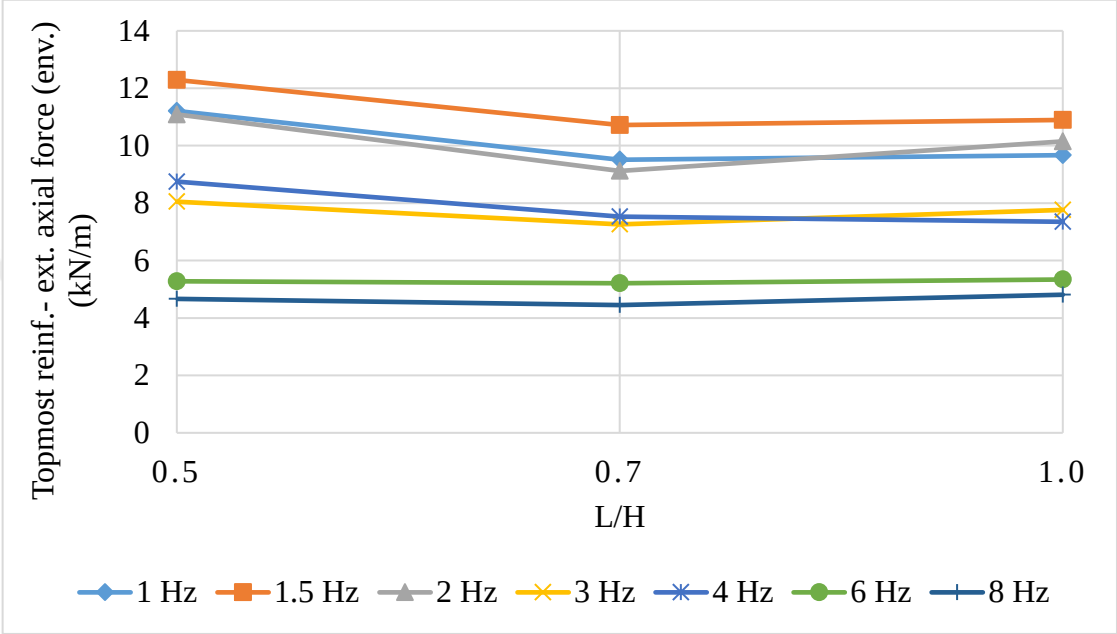


Figure 6.36. L/H: Configurations 1-3-5 (S_v=0.4m, EA=600kN/m) versus extreme axial forces (env.) at uppermost reinforcement.

6.7. Effect of S_v on Displacements and Axial Stresses

In MSE Walls, S_v (reinforcement vertical spacing) range between 0.2- 0.8m which is recommended by AASHTO (Bilgin, 2009). In this section, Configurations from 1 to 6 (S_v = 0.4 m) are compared with Configurations 7 to 12 (S_v = 0.4 m) respectively to evaluate the effect of reinforcement spacing (S_v) on the MSE Wall seismic behavior.

6.7.1. Effect of S_v on Displacements

In Figure 6.37, the uppermost reinforcement axial force variation with frequency are provided for S_v= 0.4 and Sv= 0.6m with Configurations 1 and 7. The difference in the plots can be observed for SL= 1.5 Hz and the lines converge towards 8 Hz.

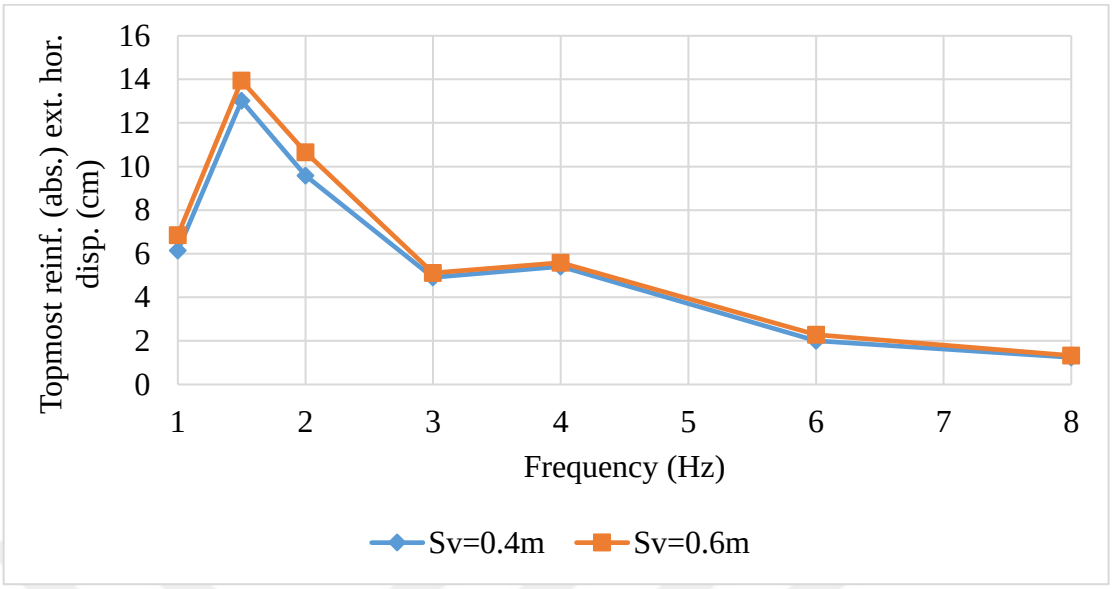


Figure 6.37. Frequency versus extreme horizontal displacements (abs.) at the uppermost reinforcement: Configurations 1-7 (EA=600kN/m, L/H= 0.7).

For SL=1.5 Hz, the effects of the vertical spacing on the extreme horizontal displacements along the wall height are investigated in Figure 6.38.

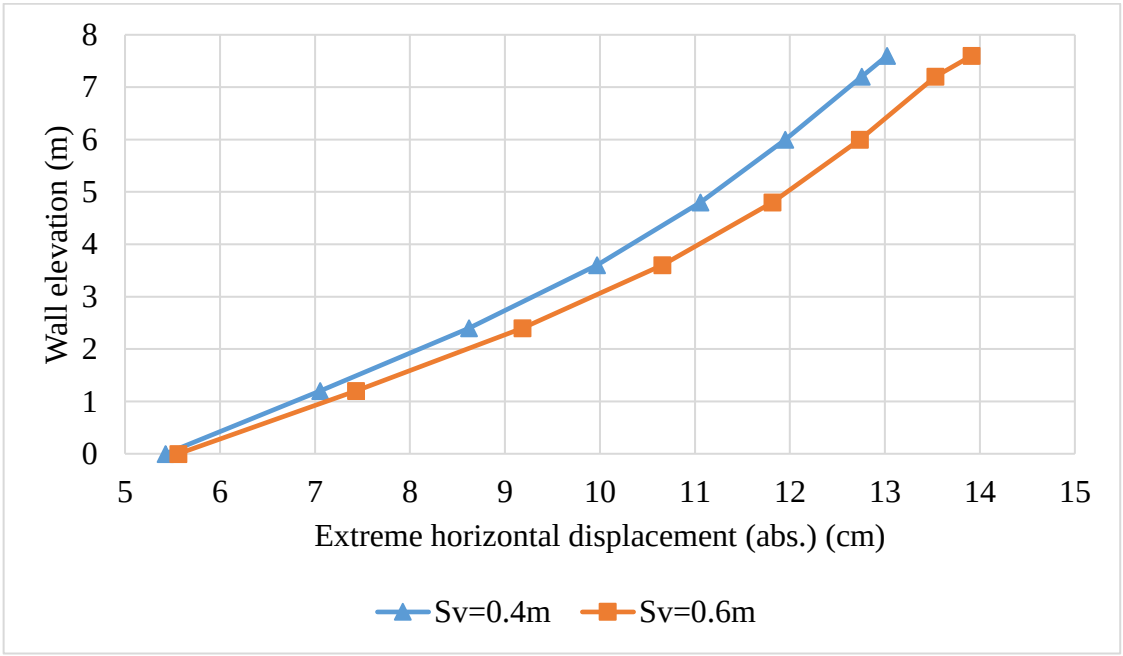


Figure 6.38. Extreme horizontal displacement (abs.) versus wall elevation: reinforcement spacing comparison, Configuration 1-7 (Sv=0.4m, L/H=0.7), for SL=1.5 Hz.

The variation of the horizontal displacement of the uppermost reinforcement with the change in reinforcement spacing is shown in Figure 6.39, for SL=1.5 Hz. A maximum horizontal displacement difference of 0.9 m is observed with vertical spacing change at the uppermost reinforcement for SL= 1.5 Hz. This difference is much less at lower layers of reinforcement.

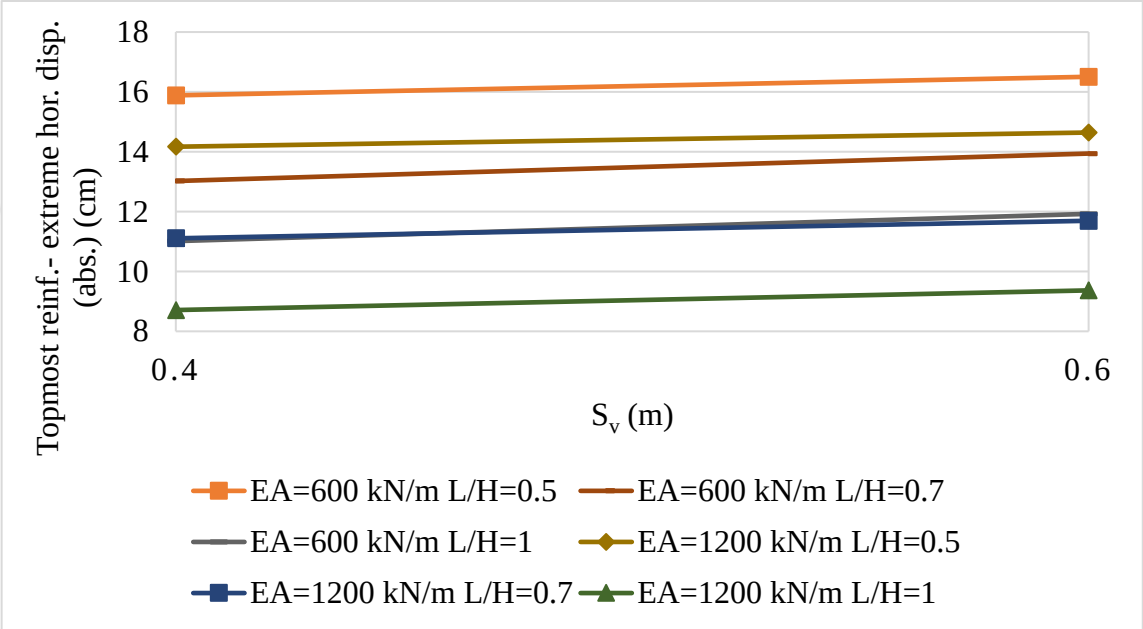


Figure 6.39. S_v versus extreme horizontal displacement (abs.) at uppermost reinforcement versus variation for SL=1.5.

6.7.2. Effect of S_v on Axial Stresses

The results show no significant effect of S_v on displacements; however, it has a more visible effect on reinforcement axial forces. In Figure 6.40, the comparison of S_v = 0.4 m and 0.6 m are shown for Configurations 1 and 7. It can be seen that the axial force in the uppermost reinforcement in the MSE Wall model with S_v = 0.6 m configuration is higher than the reinforcement in the MSE Wall model with S_v = 0.4 m. In order to better evaluate this effect, the differences in the axial force were plotted with respect to each earthquake frequency case in Figure 6.41. The maximum difference is observed for SL= 1.5 Hz case. For all configurations, S_v versus extreme axial force (envelope) at the uppermost reinforcement is presented in Figure 6.42.

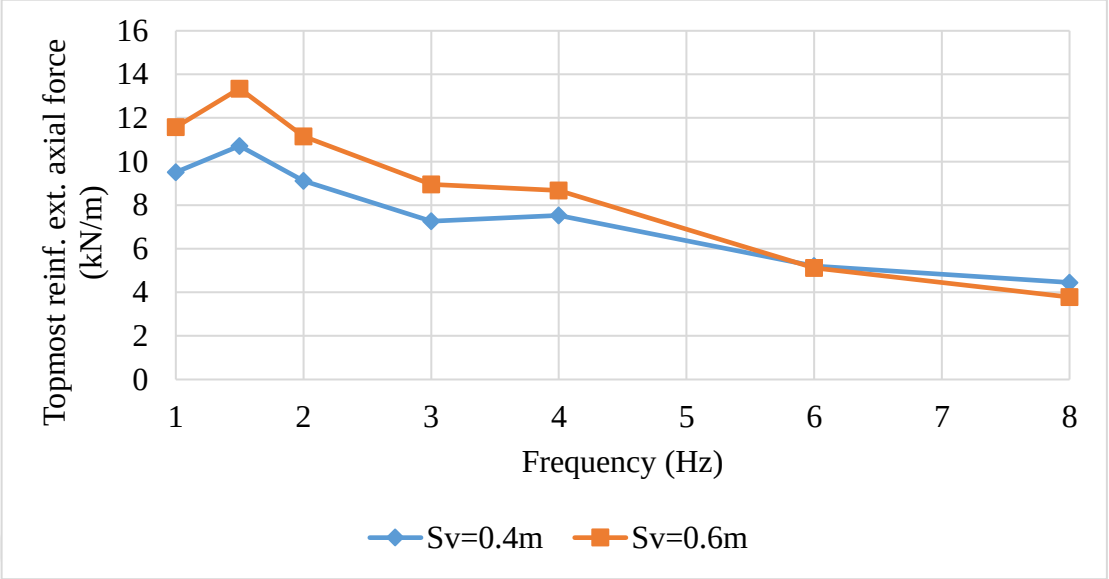


Figure 6.40. Extreme axial force (env.) at uppermost reinforcement versus frequencies: Configurations 1-7 (EA=600kN/m, L/H= 0.7).

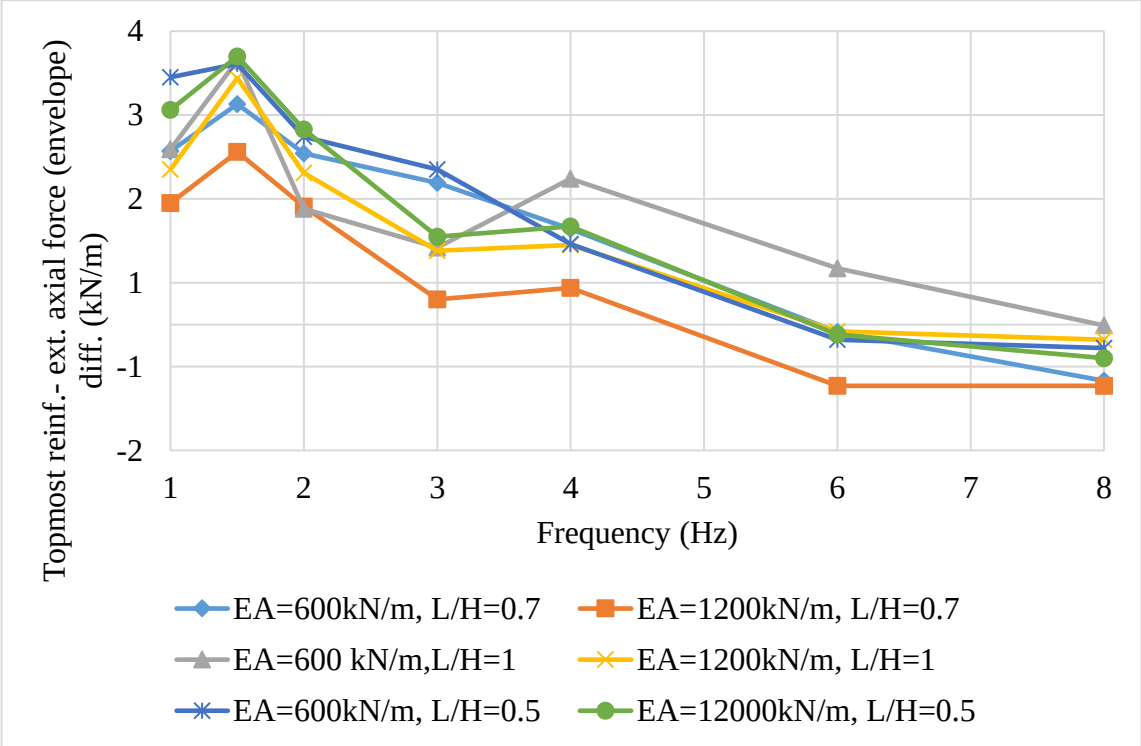


Figure 6.41. Frequency versus extreme axial force (env.) difference (from S_v=0.4 values, S_v=0.6 values subtracted) at the uppermost reinforcement.

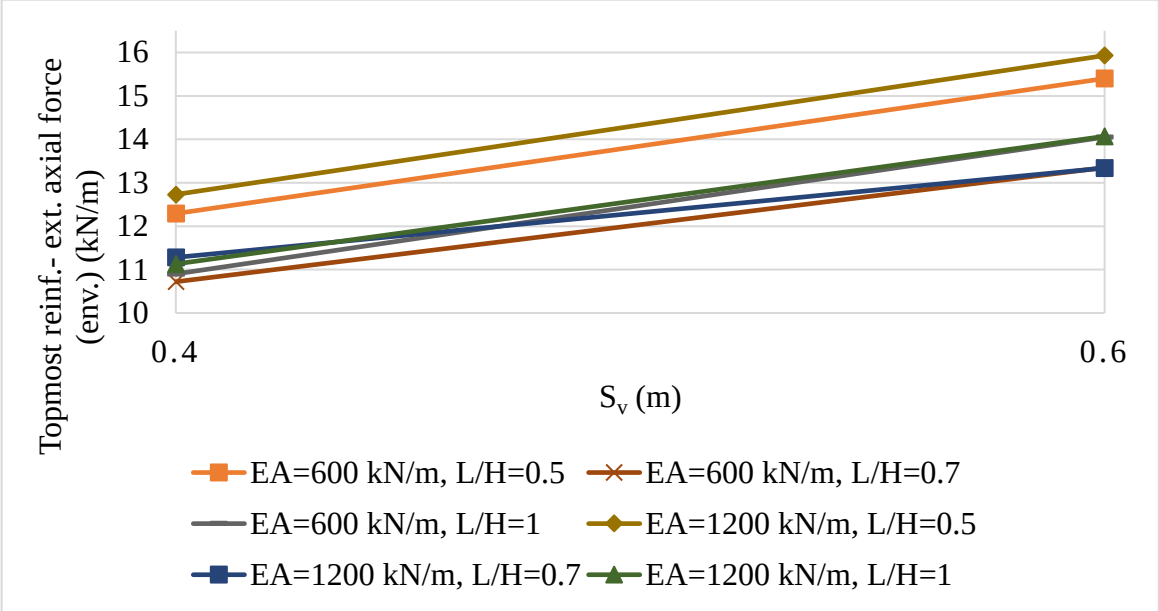


Figure 6.42. S_v versus extreme axial force (envelope) at the uppermost reinforcement, SL=1.5 Hz.

6.8. Effect of Overall Stiffness on Maximum Acceleration

The overall stiffness of the earth-reinforcement system can have an effect on the variation of accelerations in the MSE Wall. The properties of the backfill soil, which can impact the overall stiffness, is kept constant in this study. Therefore, the effect of S_v, EA, and L/H ratio on the overall stiffness of the system and hence, on the max accelerations were investigated in this section. The results indicate that the maximum acceleration at Point J is not affected significantly by the changes in S_v or EA. This may be due to the fact that the variations in these parameters are not drastic. The effect of the L/ H ratio on the overall stiffness of the system and the maximum accelerations are somewhat more obvious. Table 6.1 summarizes the max accelerations at Point J for various configurations and earthquake frequencies. When the L/H ratio is increased from 0.5 to 1.0, the difference in the acceleration values reaches close to 0.1g at Point J at various earthquake frequencies. The slope of the maximum acceleration difference at Point J is positive between 1.5 Hz and 6 Hz earthquake frequency cases. In other words, when the L/H ratio is changed from 0.5 to 1, the increase in acceleration increases with an increase in earthquake frequency (see Figure 6.43).

Table 6.1. Max. acc. (abs.) (a_x) in terms of g=10m/s^2 at Point J (for L/H= 0.5 and 1.0).

		Frequency (Hz)						
L/ H	Configuration	1	1.5	2	3	4	6	8
0.5	S_v =0.4m, EA= 600 kN/m	0.24	0.34	0.32	0.27	0.30	0.12	0.11
1		0.24	0.30	0.31	0.32	0.37	0.22	0.14
0.5	S_v =0.4m, EA= 1200 kN/m	0.24	0.33	0.32	0.29	0.31	0.13	0.12
1		0.25	0.29	0.31	0.32	0.38	0.23	0.15
0.5	S_v =0.6m, EA= 600 kN/m	0.22	0.32	0.30	0.25	0.27	0.10	0.09
1		0.25	0.31	0.30	0.29	0.33	0.18	0.12
0.5	S_v= 0.6m, EA= 1200 kN/m	0.22	0.31	0.30	0.26	0.28	0.11	0.09
1		0.24	0.29	0.29	0.29	0.34	0.19	0.13

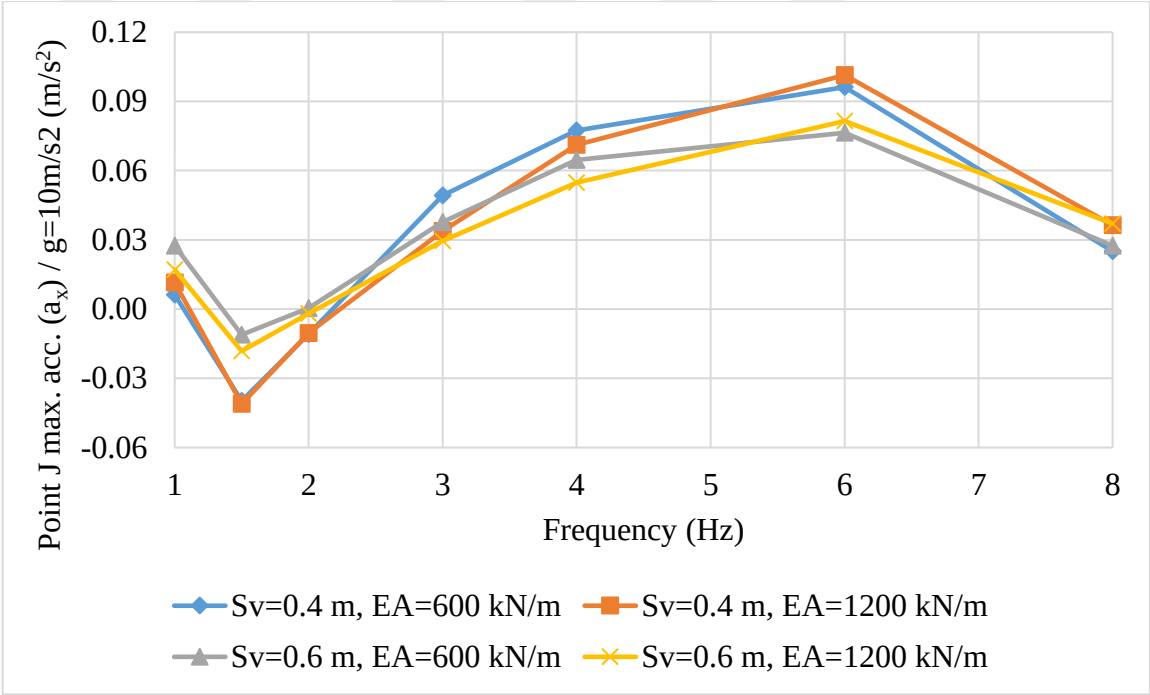


Figure 6.43. Frequency versus max. acc. difference (a_x) in terms of g=10m/s^2 at Point J (from L/H= 1.0 value, L/H= 0.5 subtracted).

6.9. Summary of Seismic Results

The results obtained from the seismic cases are gathered together to compare all configurations. In Figure 6.44, maximum acceleration values obtained at Point J are provided in terms of gravitational acceleration (g). When the plots are reviewed, two frequencies draw

attention. The acceleration at Point J makes a peak for SL=1.5 Hz and for SL=4 Hz. In Figure 6.45, shows the frequency versus corresponding (abs.) extreme horizontal displacement values at Point J. In Figure 6.46 and Figure 6.47, shows the frequency versus extreme horizontal displacement (abs.) and extreme axial force (env.) values for the uppermost reinforcement for all the configurations, respectively. When all configurations are considered, the peak displacements and axial forces are observed at the topmost reinforcement for SL= 1.5 Hz. The maximum horizontal displacements at the topmost reinforcement are in the 8.71 to 16.51 cm range for SL= 1.5 Hz and the maximum axial forces at the topmost reinforcement are in 10.72 to 15.93 kN/m range for SL= 1.5 Hz.

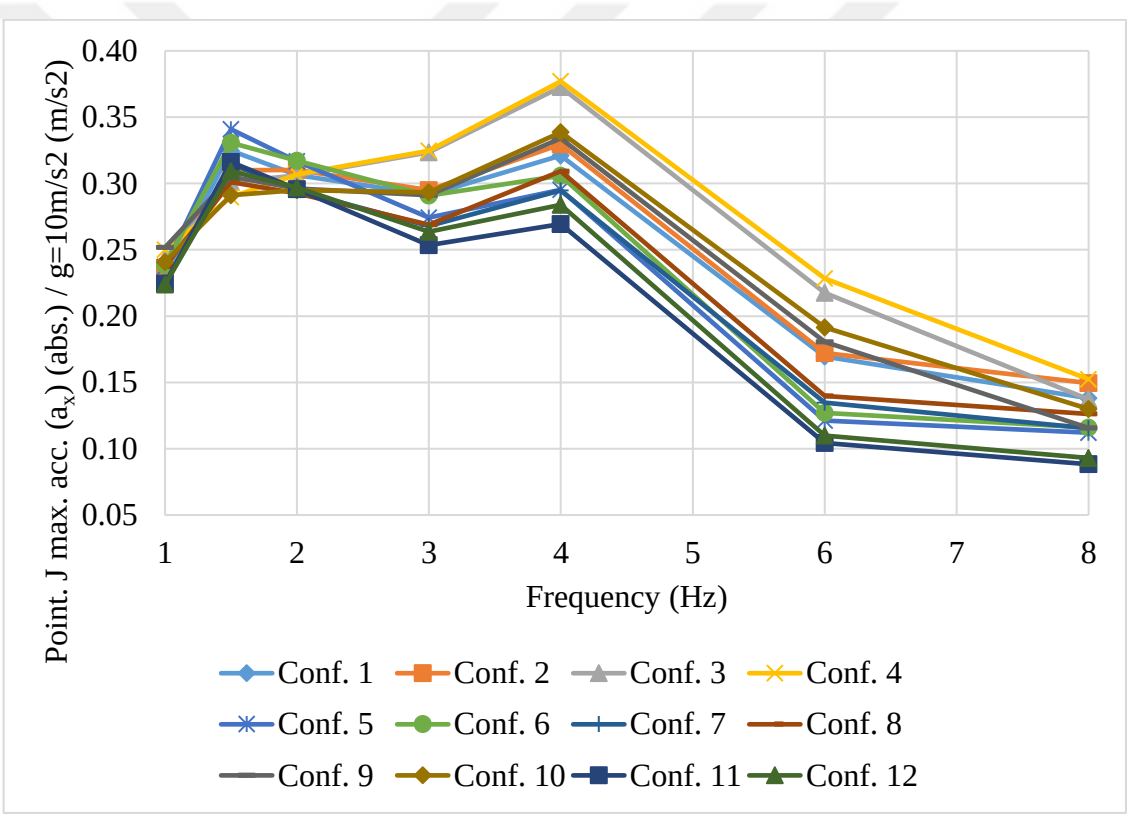


Figure 6.44. Frequency versus maximum absolute acceleration at Point J.

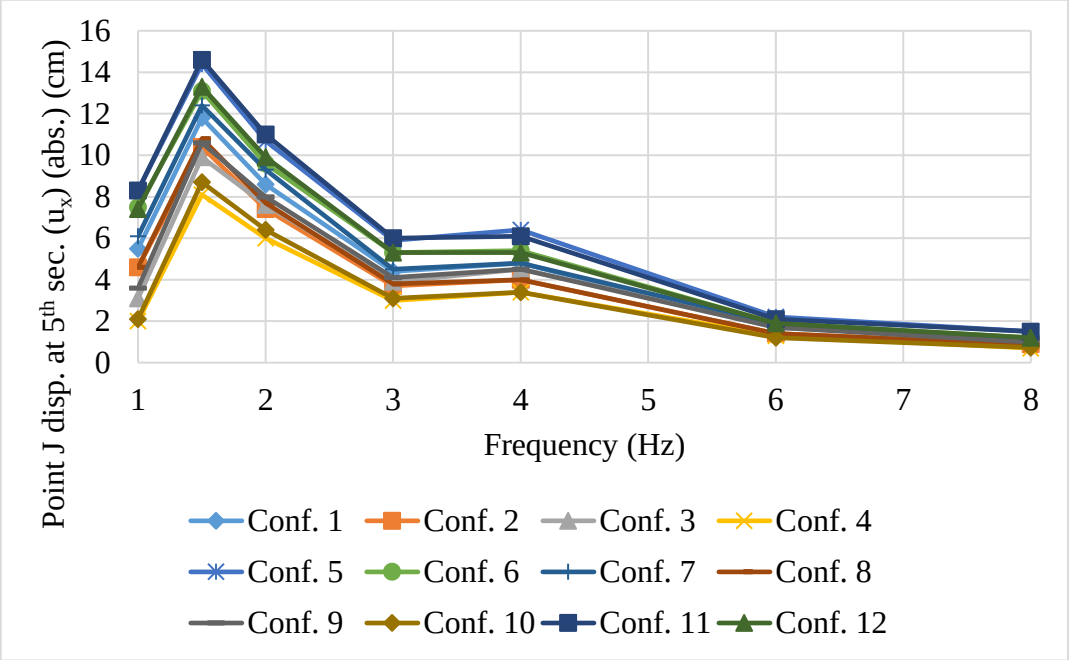


Figure 6.45. Frequency versus maximum displacements (abs.) at Point J at the end of the 5th second.

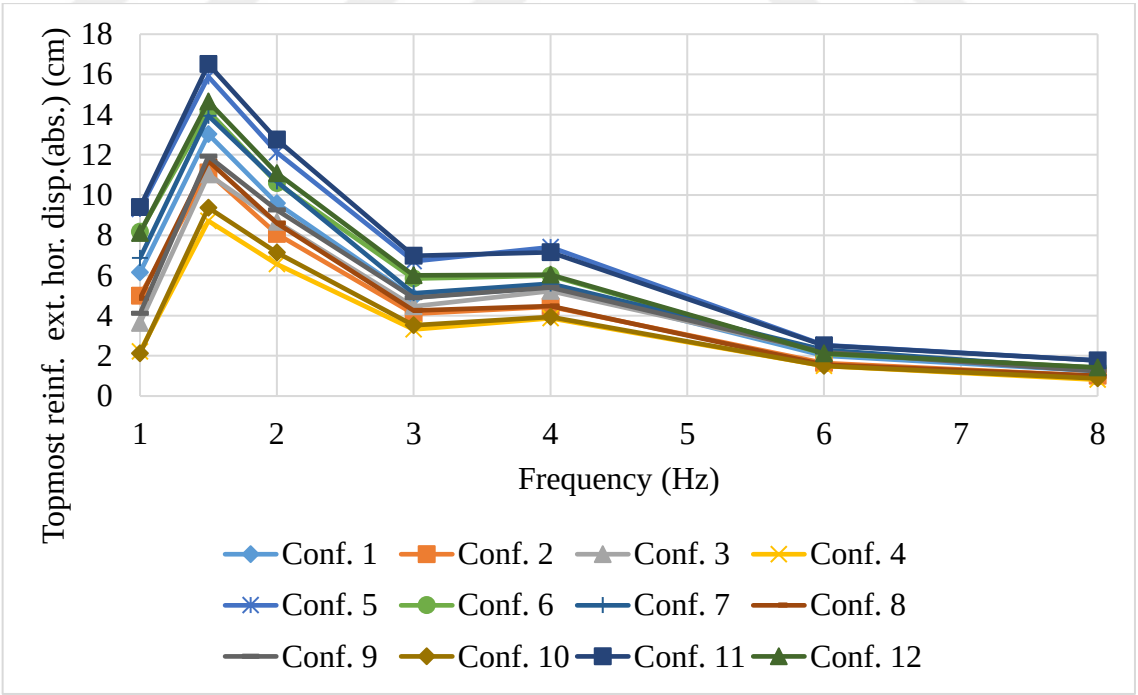


Figure 6.46. Frequency versus extreme horizontal displacement (abs.) at the uppermost reinforcement.

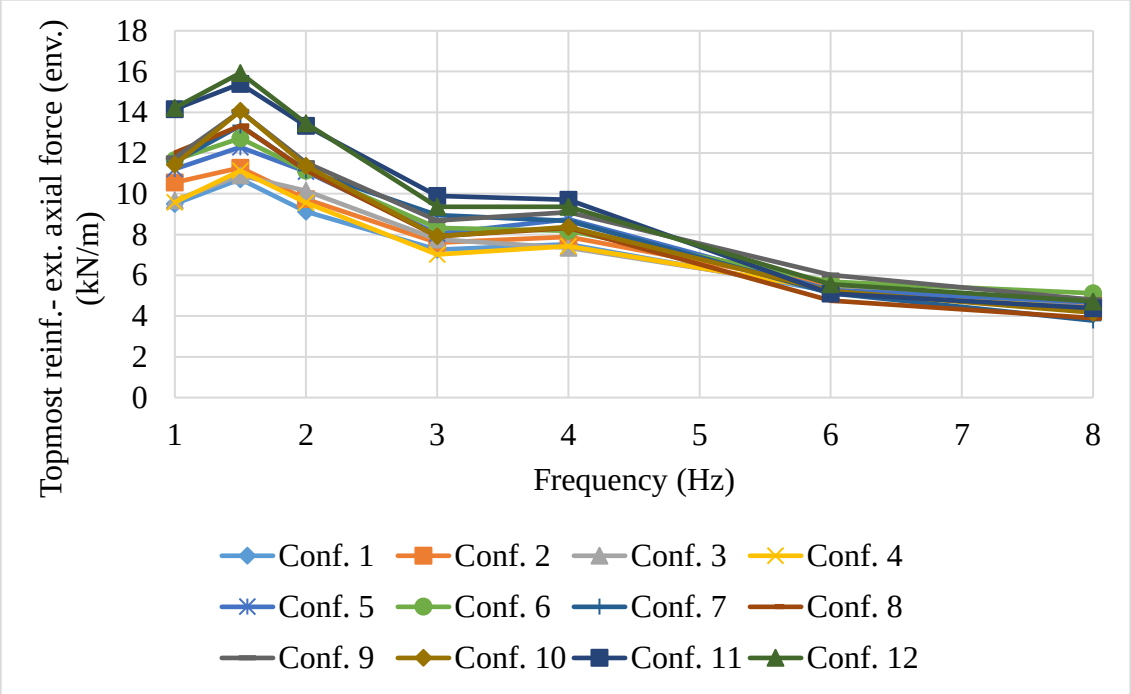


Figure 6.47. Frequency versus extreme axial force values (env.) at the uppermost reinforcement.

7. CONCLUSIONS

The main focus of this study was the investigation of the general behavior of Mechanically Stabilized Earth (MSE) Walls under static and dynamic loading using finite element analysis. Numerical analyses were conducted with a commercial computer program, PLAXIS v8.6 using Hardening-Soil model.

A parametric study was conducted to determine the effect of several reinforcement design parameters, namely reinforcement length (L), reinforcement spacing S_v and reinforcement stiffness (EA) and the frequency content of the input ground motion on the earthquake behavior of MSE Walls. Keeping the geometry, soil properties and all other parameters constant, and changing the single parameter, 8 m high MSE Walls were prepared in PLAXIS to determine the effect of that parameter on the wall behavior. In the models, reinforcement length to wall height ratios was selected as L/H = 0.5, 0.7 and 1.0. Two vertical reinforcement spacing (S_v) values used in the models were 0.4 m and 0.6 m. Reinforcement stiffness values of EA= 600 kN/m and 1200 kN/m that correspond to conventional geogrids were utilized. These three main parameters and their combination resulted in 12 MSE Wall configurations. Staged construction feature of PLAXIS program was utilized. Each one of these 12 MSE Wall configurations was excited with seven (7) different harmonic input ground motion data. Analyzing the MSE Wall configurations with each of the different earthquake data, a total of 84 cases were generated and analyzed. The behavior of the MSE Wall was evaluated for both the static case (at the end of construction) and the seismic/earthquake case (at the end of the harmonic loading).

At the end of the construction phase, center-bulging (swelling) behavior was observed in all cases analyzed. Following this behavior, axial normal stresses also increased towards the bottom of the wall, highest axial forces and horizontal displacements occurred generally at the mid-height of the wall. The horizontal displacements of the bottommost reinforcement were concentrated at their front. This indicated the effect of bulging on the shape of the reinforcement. Front displacements at the bottom were affected by the toe displacement. The horizontal displacements of the uppermost reinforcement were concentrated from its center to its rear-end. As expected, the horizontal displacement of the reinforcement was reduced

by an increase in reinforcement length, characterized by L/H ratio and reinforcement stiffness represented by EA. Naturally, the horizontal displacement of the reinforcement was reduced when the reinforcement vertical S_v spacing value decreased. Generally, the change in the reinforcement axial forces with respect to these parameters followed a similar trend with displacements. However, it is important to note that the change in axial forces was most significantly affected by the changes in S_v rather than the change in reinforcement length or stiffness.

Dynamic analyses of the MSE models were conducted by applying various varying amplitude harmonic loading records. These records were created with different frequencies of: 1 Hz, 1.5 Hz, 2 Hz, 3 Hz, 4 Hz, 6Hz, 8Hz which are around the estimated natural frequency of the MSE Wall. All harmonic loading records applied had a peak ground acceleration value of 0.2g. The analyses were performed with a constant damping ratio of 10% in order to better represent the load-strain response of the materials. On the contrary to the static case, outward movement of the top of the wall was observed with the tendency of the overturning of the wall in all configurations. Reinforcements experienced the maximum bending moment and maximum shear strains at the connection points with facings. The maximum shear strains were also observed at the rear-end of reinforcements due to the tendency of the reverse motion of the reinforced soil with respect to the retained soil.

Based on the FEM results, the acceleration of the input seismic loading (SL) applied at the bedrock was amplified at frequencies below 2 Hz and de- amplified at the frequencies above 2 Hz in the foundation soil. Regardless of the frequency of the input motion, the accelerations were all amplified in the MSE Wall which was consistent with the previous research studies. The estimated natural frequency of the 8 m high wall was around 4 Hz; and accordingly, the maximum amplification in the wall occurred for SL= 4Hz. However, the amplification in the overall system (foundation and MSE Wall) was higher for SL= 1.5 Hz. The maximum amplification factor at the top of the wall was recorded as 1.75 for SL= 1.5 Hz. This value was higher because amplification in the foundation soil was greater for SL= 1.5 Hz compared to that of SL= 4 Hz and hence, this contributed to a greater acceleration at the top of the wall. These results indicated that the fundamental frequency of the foundation soil is at about 1.5 Hz. This result can be further verified with future studies of free field site response analysis. Following these results, when all configurations were considered,

maximum horizontal displacements at the topmost reinforcement were in the 8.71 to 16.51 cm range, and the maximum axial forces at the topmost reinforcement were in 10.72 to 15.93 kN/m range for SL= 1.5 Hz. Moreover, the maximum axial forces were also observed for SL=1.5 Hz at the mid to lower reinforcements which can be attributed to normal stress and friction mechanisms.

Considering the results obtained for all configurations, for SL= 1.5 Hz, increasing the EA value from 600 kN/m to 1200 kN/m resulted in an increase in axial stresses of about 5% at the uppermost reinforcement and of about 45% of at the bottommost reinforcement. Accordingly, horizontal displacements at the topmost reinforcement decreased in 11- 21% range with the increase in EA. When L/H increased from 0.7 to 1.0 for SL= 1.5 Hz, the horizontal displacements at the topmost reinforcement decreased by about 14- 22%. Furthermore, when L/H decreased from 0.7 to 0.5 for SL= 1.5 Hz, the horizontal displacements at the uppermost reinforcement increased by about 18- 27%, and axial forces at the uppermost reinforcement increased by about 13-16%. Increasing the S_v from 0.4 m to 0.6 m, increased the axial force at the uppermost reinforcement about 18- 29% for SL=1.5 Hz. The effect of S_v on axial forces decreased towards 8 Hz, for the remaining input ground motion frequencies. On the other hand, due to the effects of S_v, the percentage changes in horizontal displacements of the reinforcements were lower than that was observed for the axial forces. Horizontal displacements at the uppermost reinforcement increased by 3-8% for SL= 1.5 Hz when S_v increased from 0.4 m to 0.6 m.

The results indicated that the natural frequency of the MSE Wall and its relationship with the frequency content of the input ground motion and its amplitude has great significance in MSE Wall seismic behavior. The results showed that the amplitude of the input ground motion with PGA of 0.2g is not a critical acceleration amplitude for this model to create plastic behavior at the soil and following this fact, no obvious internal stability problem was observed in the models.

The following future research can be suggested to further develop this study:

- Real earthquake time history data can be applied to the models for comparing them with the results obtained from this study,

- Various soil damping ratios can be considered to investigate the effect of damping on MSE Wall behavior, and
- Input ground motion data with higher PGA values can be applied to the models to investigate the effect of peak amplitude.

REFERENCES

AASHTO, 1998, *LRFD Bridge design specifications*, American Association of State Highway and Transportation Officials.

ACE Geosynthetics, 2019a, *ACEGrid GG Geogrids*, https://www.geoace.com/products/Geogrids/ACEGrid%C2%AE-GG, accessed in March, 2019.

ACE Geosynthetics, 2019b, *Demonstrations/ Reinforcement*, http://www.ace geosyntheticsecopark.com/demonstrations/1, accessed in March, 2019.

Amorosi, A., Boldini, D., & Elia, G., 2010, "Parametric Study on Seismic Ground Response by Finite Element Modelling", *Computers and Geotechnics*, 37 (4), 515-528.

Anastasopoulos, I., Georgarakos, T., Georgiannou, V., Drosos, V., & Kourkoulis, R., 2010, "Seismic Performance of Bar-Mat Reinforced-Soil Retaining Wall: Shaking Table Testing Versus Numerical Analysis with Modified Kinematic Hardening Constitutive Model", *Soil Dynamics and Earthquake Engineering*, 30 (10), 1089-1105.

Arias, A., 1970, *Measure of Earthquake Intensity*, Massachusetts Inst. of Tech., Cambridge. Univ. of Chile, Santiago de Chile.

Aslan, V. Z., 2007, *Design and Numerical Modeling of Reinforced Earth Retaining Structures*, M.S. Thesis, Bogazici University.

Barrett, R. K., & Ruckman, A. C., 2007, "GRS: A New Era in Reinforced Soil Technology", *Geosynthetics in Reinforcement and Hydraulic Applications (GSP 165)*, 153-164.

Bathurst, R. J., 2019, *Geosynthetics Functions*, https://www.geosyntheticssociety.org/wp-content/plugins/resources/documents/functions/english.pdf, accessed in March, 2019.

Bathurst, R. J., & Hatami, K., 1998, "Seismic Response Analysis of a Geosynthetic-Reinforced Soil Retaining Wall", *Geosynthetics International,* 5 (1-2), 127-166.

Berg, R. R., Christopher, B. R., & Samtani, N. C., 2009, *Design and Construction of Mechanically Stabilized Earth Walls and Reinforced Soil Slopes*, US Department of Transportation, Federal Highway Administration, National Highway Institute.

Bhattacharjee, A., & Krishna, A. M., 2015, "Strain Behavior of Backfill Soil in Rigid Faced Reinforced Soil Walls Subjected to Seismic Excitation", *International Journal of Geosynthetics and Ground Engineering,* 1 (2), 14.

Bilgin, Ö., 2009, "Failure Mechanisms Governing Reinforcement Length of Geogrid Reinforced Soil Retaining Walls", *Engineering Structures,* 31 (9), 1967-1975.

Bowles, J. E., 1996, *Foundation Analysis and Design*, The McGrawHill Companies, Singapore.

Brinkgreve, R. B. J., "PLAXIS 2D Version 8 Dynamics Manual", *Delft University of Technology and PLAXIS bv The Netherlands*.

Brinkgreve, R. B. J., "PLAXIS 2D Version 8 Reference Manual", *Delft University of Technology and PLAXIS bv The Netherlands*.

Brinkgreve, R. B. J., 2019a, "PLAXIS 2D Materials Model Manual 2019", *Delft University of Technology and PLAXIS bv The Netherlands*.

Brinkgreve, R. B. J., 2019b, "PLAXIS 2D Reference Manual 2019", *Delft University of Technology and PLAXIS bv The Netherlands*.

Brinkgreve, R. B. J., Kappert, M. H., & Bonnier, P. G., 2007, "Hysteretic Damping in a Small-Strain Stiffness Model", *Proc. of Num. Mod. in Geomech., NUMOG X, Rhodes*, 737-742.

Brinkgreve, R. B. J., Kumarswamy, S., Swolfs, W. M., Zampich, L., & Ragi Manoj, N., 2019, "PLAXIS 2D General Information", *Delft University of Technology and PLAXIS bv The Netherlands*.

Burke, C., Ling, H. I., & Liu, H., 2004, "Seismic Response Analysis of a Full-Scale Reinforced Soil Retaining Wall", *Proc. 17th ASCE Engineering Mechanics Conf.*, Newark, DE.

Burke, C. B., 2003, *Full-Scale Shaking Table Tests and Finite Element Analysis of Reinforced Soil Retaining Wall,* Ph.D. Thesis, Columbia University.

Chopra, A. K., 2001, *Dynamics of Structures: Theory and Applications to Earthquake Engineering*, 4th Edition, Prentice Hall, Upper Saddle River, NJ.

Das, B. M., 2007, *Principles of Foundation Engineering*, 6th Edition, Thomson.

Das, B. M., 2010, *Geotechnical Engineering Handbook*, J. Ross Publishing.

Dey, A., Lanzano, G., Rainieri, C., Di Tullio, M., Laorenza, C., Santucci de Magistris, F., & Fabbrocino, G., 2011, "A Full Scale Instrumented Retaining Wall: Interpretation of the Measurements Using Numerical Tools", *Proceeding of the 5th International Conference on Earthquake Geotechnical Engineering*, Santiago, Chile.

El-Emam, M. M., & Bathurst, R. J., 2007, "Influence of Reinforcement Parameters on the Seismic Response of Reduced-Scale Reinforced Soil Retaining Walls", *Geotextiles and Geomembranes,* 25 (1), 33-49.

El-Emam, M. M., Bathurst, R. J., & Hatami, K., 2004, "Numerical Modeling of Reinforced Soil Retaining Walls Subjected to Base Acceleration", *13th World Conference on Earthquake Engineering*.

El-Emam, M. M., Bathurst, R. J., Hatami, K., & Mashhour, M. M., 2001, "Shaking Table and Numerical Modelling of Reinforced Soil Walls", *Proceedings of the International Symposium on Earth Reinforcement*, IS Kyushu.

Elgamal, A.-W., Alampalli, S., & Laak, P. V., 1996, "Forced Vibration of Full-Scale Wall-Backfill System", *Journal of geotechnical engineering*, 122 (10), 849-858.

Enunlu, A. K., 2007, *Investigation of Dynamic Behavior of Geosynthetic Reinforced Soil Retaining Structures Under Earthquake Loads*, Ph.D. Thesis, Bogazici University.

Ergul, E., 2012, *Mekanik Olarak Stabilize Edilmis Zemin Duvarlarinin Statik Yukler Altindaki Davranisinin Incelenmesi,* M.S. Thesis, Istanbul Technical University.

Fakharian, K., & Attar, I. H., 2007, "Static and Seismic Numerical Modeling of Geosynthetic-Reinforced Soil Segmental Bridge Abutments", *Geosynthetics International*, 14 (4), 228-243.

Falcon, P. C., 2014, *Dynamic Calculation of Geotechnical Structures*, B.S., University of Seville.

Hatami, K., & Bathurst, R. J., 2000, "Effect of Structural Design on Fundamental Frequency of Reinforced-Soil Retaining Walls", *Soil Dynamics and Earthquake Engineering*, 19 (3), 137-157.

Hudson, M., Idriss, I. M., & Beirkae, M., 1994, "QUAD4M User's Manual", *A computer program to evaluate the seismic response of soil structures using finite element procedures and incorporating a compliant base*.

IGS, 2009, *Recommended Descriptions of Geosynthetics. Functions, Geosynthetics Terminology, Mathematical and Graphical Symbols*, IGS Secretariat Jupiter, FL, USA.

International Organization for Standardization (ISO), 2015, "ISO 10319".

Jia, J., 2018, *Soil Dynamics and Foundation Modeling*, Springer.

Jones, C. J. F. P., 1996, *Earth Reinforcement and Soil Structures*, Thomas Telford Publishing, London.

Kavazanjian, E., Wang, J. N. J., Martin, G. R., Shamsabadi, A., Lam, I., Dickenson, S. E., & Hung, C. J., 2011, "LRFD Seismic Analysis and Design of Transportation Geotechnical Features and Structural Foundations", *National Highway Institute*.

Kibria, G., Hossain, M. S., & Khan, M. S., 2013, "Influence of Soil Reinforcement on Horizontal Displacement of Mse Wall", *International Journal of Geomechanics*, 14 (1), 130-141.

Koerner, R. M., 2005, *Designing with Geosynthetics* Pearson Education, Inc, Upper Saddle River, NJ.

Koerner, R. M., 2012, *Designing with Geosynthetics*, Vol. 1, Xlibris Corporation.

Kouroussis, G., Verlinden, O., & Conti, C., 2011, "Finite-Dynamic Model for Infinite Media: Corrected Solution of Viscous Boundary Efficiency", *Journal of Engineering Mechanics*, 137 (7), 509-511.

Kramer, S., 1996, *Geotechnical Earthquake Engineering*, Prentice Hall, Upper Saddle River, New Jersey.

Krishna, A. M., & Latha, G. M., 2011, "Modeling the Dynamic Response of Wrap-Faced Reinforced Soil Retaining Walls", *International Journal of Geomechanics*, 12 (4), 439-450.

Kwok, A. O. L., Stewart, J. P., Hashash, Y. M. A., Matasovic, N., Pyke, R., Wang, Z., & Yang, Z., 2007, "Use of Exact Solutions of Wave Propagation Problems to Guide

Implementation of Nonlinear Seismic Ground Response Analysis Procedures", *Journal of Geotechnical and Geoenvironmental Engineering,* 133 (11), 1385-1398.

Laera, A., & Brinkgreve, R. B. J., 2015, "PLAXIS 2D Ground Response Analysis".

Latha, G. M., & Krishna, A. M., 2008, "Seismic Response of Reinforced Soil Retaining Wall Models: Influence of Backfill Relative Density", *Geotextiles and Geomembranes,* 26 (4), 335-349.

Latha, G. M., & Santhanakumar, P., 2015, "Seismic Response of Reduced-Scale Modular Block and Rigid Faced Reinforced Walls Through Shaking Table Tests", *Geotextiles and Geomembranes,* 43 (4), 307-316.

Ling, H. I., Liu, H., Kaliakin, V. N., & Leshchinsky, D., 2004, "Analyzing Dynamic Behavior of Geosynthetic-Reinforced Soil Retaining Walls", *Journal of Engineering Mechanics,* 130 (8), 911-920.

Ling, H. I., Liu, H., & Mohri, Y., 2005, "Parametric Studies on the Behavior of Reinforced Soil Retaining Walls Under Earthquake Loading", *Journal of Engineering Mechanics,* 131 (10), 1056-1065.

Ling, H. I., Mohri, Y., Leshchinsky, D., Burke, C., Matsushima, K., & Liu, H., 2005, "Large-Scale Shaking Table Tests on Modular-Block Reinforced Soil Retaining Walls", *Journal of Geotechnical and Geoenvironmental Engineering,* 131 (4), 465-476.

Ling, H. I., Yang, S., Leshchinsky, D., Liu, H., & Burke, C., 2010, "Finite-Element Simulations of Full-Scale Modular-Block Reinforced Soil Retaining Walls Under Earthquake Loading", *Journal of Engineering Mechanics,* 136 (5), 653-661.

Mahmood, T., 2009, *Failure Analysis of a Mechanically Stabilized Earth (MSE) Wall Using Finite Element Program PLAXIS,* M.S. Thesis, The University of Texas at Arlington.

Matsuo, H., & Ohara, S., 1960, "Lateral Earth Pressure and Stability of Quay Walls During Earthquakes", *Proc. of 2nd WCEE*.

Moradi, G., 2014, "Seismic Response Analysis of Geosynthetic Reinforced Soil Retaining Wall", *Electronic Journal of Geotechnical Engineering*, 19, 3819-3835.

National Concrete Masonry Association (NCMA), 2016, "Segmental Retaining Walls Best Practices Guide".

Panah, A. K., Yazdi, M., & Ghalandarzadeh, A., 2015, "Shaking Table Tests on Soil Retaining Walls Reinforced by Polymeric Strips", *Geotextiles and Geomembranes*, 43 (2), 148-161.

Raikar, P., 2016, *Modelling Soil Damping for Suction Pile Foundations*, M.S. Thesis, TU Delft.

Reinforced Earth, 2015, *Seatac Airport- Airports-Retaining Walls, Embankments*, http://www.terre-armee.com/ta/wterrearmee_fr.nsf/0/8EAF0FCE16B5B950C1257E1A004FEAFA/$file/REX_FC_ENGLISH%20(1).pdf, accessed in March, 2019.

Richardson, G. N., 1978, "Earthquake Resistant Reinforced Earth Walls", *Symposium on Earth Reinforcement*, ASCE.

Scott, R. F., 1973, "Earthquake-Induced Pressures on Retaining Walls", *Proceedings of the 5th World Conference on Earthquake Engineering*.

Shukla, R. P., N.S. Parihar, A.K. Gupta, 2016, "The Effect of Geotextiles on Low Plastic Sandy Clay", In: International Geosynthetics Society, *6th Asian Regional Conference on Geosynthetics - Geosynthetics for Infrastructure Development*, New Delhi.

Shukla, S. K., 2002, *Geosynthetics and Their Applications*, Thomas Telford.

Shukla, S. K., 2011, *Handbook of Geosynthetic Engineering*, ICE Publishing, London.

Shukla, S. K., & Yin, J. H., 2006, *Fundamentals of Geosynthetic Engineering*, Vol. 117, Taylor & Francis Group, London, UK.

Tensar, 2013, "Product Specification Tensar Structural Geogrid".

Tensar, 2016, *TriAx Geogrid Product Overview Brochure*, https://www.tensarcorp.com/Systems-and-Products/Tensar-Triax-geogrid, accessed in March, 2019.

Tensar, 2019a, *Ground Stabilization & Subgrade Improvement*, https://www.tensarcorp.com/Applications/Ground-Stabilization-and-Subgrade-Improvement, accessed in March, 2019.

Tensar, 2019b, *Tensar Biaxial BX Geogrids*, https://www.tensarcorp.com/Systems-and-Products/Tensar-Biaxial-BX-geogrids, accessed in March, 2019.

Tensar Earth Technologies, I., 2005, *Design Guidelines for Mesa Retaining Wall Systems*, http://nilex.com/sites/default/files/nilex-design_guidelines_for_mesa_retaining_wall_systems.pdf, accessed in March, 2019.

Tensar Earth Technologies, I., 2019, *Installation and Special Considerations Manual*, https://www.ephenry.com/wp-content/uploads/2018/01/mesa-installation-and-special-considerations-manual.pdf, accessed in March, 2019.

Tsai, C.-C., Park, D., & Chen, C.-W., 2014, "Selection of the Optimal Frequencies of Viscous Damping Formulation in Nonlinear Time-Domain Site Response Analysis", *Soil Dynamics and Earthquake Engineering*, 67, 353-358.

Vieira, C. S., 2017, "Review of Seismic Performance of Geosynthetic Reinforced Soil Retaining Walls", *6th ECCOMAS Thematic Conference on Computational Methods in*

Structural Dynamics and Earthquake Engineering, Rhodes Island, Greece, Eccomas Proceedia.

Walthall, R. M., Wang, J., Kiousis, P., & Khan, A., 2012, "Finite-Element Analyses of Mechanically Stabilized Earth Walls Subjected to Midlevel Seismic Loads", *Journal of Performance of Constructed Facilities*, 27 (2), 171-180.

Wang, L., Chen, G., & Chen, S., 2015, "Experimental Study on Seismic Response of Geogrid Reinforced Rigid Retaining Walls with Saturated Backfill Sand", *Geotextiles and Geomembranes*, 43 (1), 35-45.

Wikipedia, 2019, *Geosynthetics*, https://en.wikipedia.org/wiki/Geosynthetics, accessed in March, 2019.

Woodward, P. K., & Griffiths, D. V., 1996, "Comparison of the Pseudo-Static and Dynamic Behaviour of Gravity Retaining Walls", *Geotechnical & Geological Engineering*, 14 (4), 269-290.

Wu, G., 1994, *Dynamic Soil-Structure Interaction: Pile Foundations and Retaining Structures*, Ph.D. Thesis, University of British Columbia.

Wu, J. T. H., & Payeur, J.-B., 2015, "Connection Stability Analysis of Segmental Geosynthetic Reinforced Soil (GRS) Walls", *Transportation Infrastructure Geotechnology*, 2 (1), 1-17.

Yardimci, T., 2013, *Investigation of Geosynthetic Reinforced Tiered Retaining Walls Using Finite Element Analysis*, M.S. Thesis, Bogazici University.

Zarnani, S., El-Emam, M. M., & Bathurst, R. J., 2011, "Comparison of Numerical and Analytical Solutions for Reinforced Soil Wall Shaking Table Tests", *Geomechanics and Engineering*, 3 (4), 291-321.